

Aus dem Institut für Rechtsmedizin
der Universität München

Vorstand: Prof. Dr. med. Matthias Graw

**Some aspects of a conceptual design of an advanced electronic non-lethal
weapon**

(Ausgewählte Aspekte des Entwurfs einer fortgeschrittenen elektrischen
nichtletalen Waffe)

Dissertation

zum Erwerb des Doktorgrades der Humanbiologie

an der Medizinischen Fakultät

der Ludwig-Maximilians-Universität zu München

vorgelegt von

Yulia Aronshtam

aus Sankt Petersburg

Jahr 2013

Mit Genehmigung der Medizinischen Fakultät
der Universität München

Berichterstatter: PD Dr. med. Oliver Peschel

Mitberichterstatter: Prof. Dr. Dr. Erhard Grunwald
PD Dr. Oliver Pieske

Mitbetreuung durch den
promovierten Mitarbeiter: Dr. med. Sebastian Kunz

Dekan: Prof. Dr. med. Dr.h.c. Maximilian Reiser, FACR, FRCR

Tag der mündlichen Prüfung: 26.09.2013

Table of contents

| | |
|--|----|
| 1. Introduction | 4 |
| 2. Methods | 7 |
| 2.1 A new design procedure for an advanced NLW | 7 |
| 2.2 Modelling and simulation | 10 |
| 2.2.1 Model | 11 |
| 2.2.2 Dielectric properties of human tissues | 17 |
| 2.2.3 Simulation | 18 |
| 3. Results | 21 |
| 3.1 State of the art of EID technology | 21 |
| 3.2 Concept of an advanced EID | 24 |
| 3.2.1 Controlling the distance to the target | 25 |
| 3.2.2 Controlling EID electric output | 26 |
| 3.2.3 Controlling EID output rate | 27 |
| 3.2.4 Combined EID-Defibrillator | 30 |
| 3.3 Modelling | 30 |
| 3.3.1 Development of the model | 31 |
| 3.3.2 Verification of the model | 37 |
| 3.3.3 Simulation results | 52 |
| 3.4 Safety analysis of Taser | 56 |
| 3.4.1 Simulation of IEC thresholds for AC currents | 60 |
| 3.4.2 Evaluation of the delivered energy as a measure for damage | 62 |
| 4. Discussion | 66 |
| 5. Conclusions | 76 |
| Summary | 78 |
| Abstract | 81 |
| Zusammenfassung | 82 |
| References | 83 |
| Chapter 1 | 83 |
| Chapter 2 | 83 |
| Chapter 3 | 86 |
| Chapter 4 | 89 |
| Abbreviations | 91 |
| Acknowledgments | 92 |
| Appendix 1 Multi-simulation tool | 93 |
| Appendix 2 Measurement data for the dielectric properties of organic tissues | 94 |

1. Introduction

Non-lethal weapons (NLWs) are weapons, devices and ammunitions “which are explicitly designed and developed to incapacitate or repel personnel, with a low probability of fatality or permanent injuries, or to disable equipment with minimal undesired damage or impact on the environment” [1].

NLWs by definition are not expected to be non-lethal, i.e. to have a zero probability of causing a lethal injury or a permanent destruction [2]. Their specific purpose is to provide a significantly lower risk of lethality and irreversible damage. To reflect this aspect, NLWs are often called “less-lethal” or “less-than-lethal” weapons.

NLWs have been developed as an additional tool, a transitional option for the operations where due to legal, political, social or operational factors an employment of lethal force is undesirable or prohibited. Such situations are very frequent in the civil law enforcement, where the rules of engagement of lethal force are very strict. Nowadays military forces are called to serve in the peace-keeping and peace-enforcement operations and humanitarian missions more and more frequently, so their need for non-lethal options increases greatly [3].

NLWs can be classified by their function: counter-personnel and counter-materiel NLWs. The counter-materiel NLWs include those systems, which targets are vehicles, vessels, aerial systems, and lethal and non-lethal weaponry. Further the NLWs can be categorised by their basic technology. There are kinetic, chemical, acoustic, optic, electromagnetic, and biological NLWs [4-9].

Having been available for at least 30 years by now, the NLWs are still assessed diversely both by the armed forces and law enforcement, and by the civil society. There is a number of reasons that cause this situation. The most significant one is the NLW’s technical immaturity. The limited operational range, no scalable effects, low selectivity, weak protection from abuse, combined with weather and counter-measures susceptibility often lead to a situation, when an engagement of an NLW either is not reasonable or is ineffective, or causes an undesired damage.

Most of the available NLWs are based on a single effect, which effectiveness is naturally limited to a certain range and is influenced by environmental conditions. For example, laser dazzlers cannot be engaged at the distances less than several meters to the target due to the risk of the permanent ocular damage. Their effect is strongly influenced by fog and rain. One of the solutions of these problems is to combine several effects in one device. These effects

can be then employed separately (each in its “effective area”) or simultaneously, possibly providing a synergistic effect.

Also a logistic problem could be solved in the same way, as this could significantly decrease the amount of weapons that must be transported to the operational site.

On the other hand, an NLW is also a delivery system for its basic effect(s). Kinetic NLWs use different types of guns or canons to deliver the ammunition, grenades are used to disperse smoke or chemical irritants. A delivery system determines the range, the intensity and the degree of the impact of the NLW. Most available systems offer only one set of these properties. That means that for example the rubber bullets are shot with the same kinetic energy at any distance to the target within the range of the gun. This often leads to serious injuries of a target situated at a close distance to an operator, or, on the contrary, to a negligible effect on a person situated further from an operator. On the other hand, it creates a need for a number of delivery systems for the same effect to provide a different operational range, for instance. A delivery system, which is able to adjust the intensity (i.e. energy or power) of the effect according to the actual operational conditions, could improve the situation.

Finally, there is an operator, who controls the NLW and whose decisions can influence the outcome of the operation significantly. However, sometimes the operator has to make the decisions lacking crucial information. For example, some of the anti-materiel NLWs deactivate machines without any visible impact [6], so that the operator does not realise if there is any impact at all. There is a lack of feedback about the impact on the target, informing the operator, if there was any impact and how strong it was.

Another issue related to an operator is a poor training that can result in unintentional or intentional abuse of an NLW. Any abuse of NLW would normally lead to a lethal outcome. This indicates a need for an automated security mechanism, which prevents any attempt to use an NLW inappropriately.

Thus the demand for a new generation of NLWs that could be deployed in different and changing operational environments is obvious. An advanced NLW, based on several basic effects, would be able to analyse the situation on-the-fly and adapt its effects accordingly.

An approach for a design procedure of advanced NLWs is suggested in this study. The main aspects of its implementation are discussed on the example of electric incapacitating devices (EIDs) with the focus on the safety of these devices. A great part of the research was devoted to the development of a simulation model for EID-human-interaction. The purpose of the

model is the ability to investigate the effects of the EID on human tissues and organs. This provides a powerful tool in the design process, on the stage of operational employment, and in the post-employment investigations, for example, for forensic purposes.

2. Methods

2.1 A new design procedure for an advanced NLW

An advanced non-lethal weapon provides a precise demanded outcome in a given operational scenario, ensuring the minimal risk of causing any residual damage.

A design of such a weapon is a complicated conceptual procedure, which consolidates the knowledge and experience from different fields: engineering, military science, law, artificial intelligence, medicine etc. In this study an approach for organisation of such a procedure is suggested (see fig. 2-1).

The initial point of the procedure is an analysis of the operational scenarios, where NLWs can be employed. A thorough study of the field and training reports, and expert knowledge, immediately shows:

- What non-lethal effects are needed in certain situations;
- Which effects can be combined;
- What are the parameters, that can influence the efficiency of the NLW;
- What precautions should be taken in order to prevent undesired health effects or materiel damage (adaptive effects, measures against abuse, after-treatment planning).

An operational scenario contains the following information [2, 3]:

Operational context

Operational context defines general environmental and legal conditions. For instance, military operations can take place in the frame of peace support operations, which include preventive peace keeping, building, and law enforcement, or under application of international resolutions. The situations of terrorist or organized criminal activity, religious or ethnic violence, and non-conventional warfare are united under the asymmetric threats and are treated differently from a legal point of view. The operations in an urban environment represent a special case: a complex terrain with a very dense infrastructure, presence of civilians, and actions in the close spaces create additional challenges and restrictions for the collateral damage.

Origin of danger

Origin of danger is defined as a person or a group of persons holding any kind of weapon, or controlling a possible dangerous machine (vehicle, mechanism, or weapon).

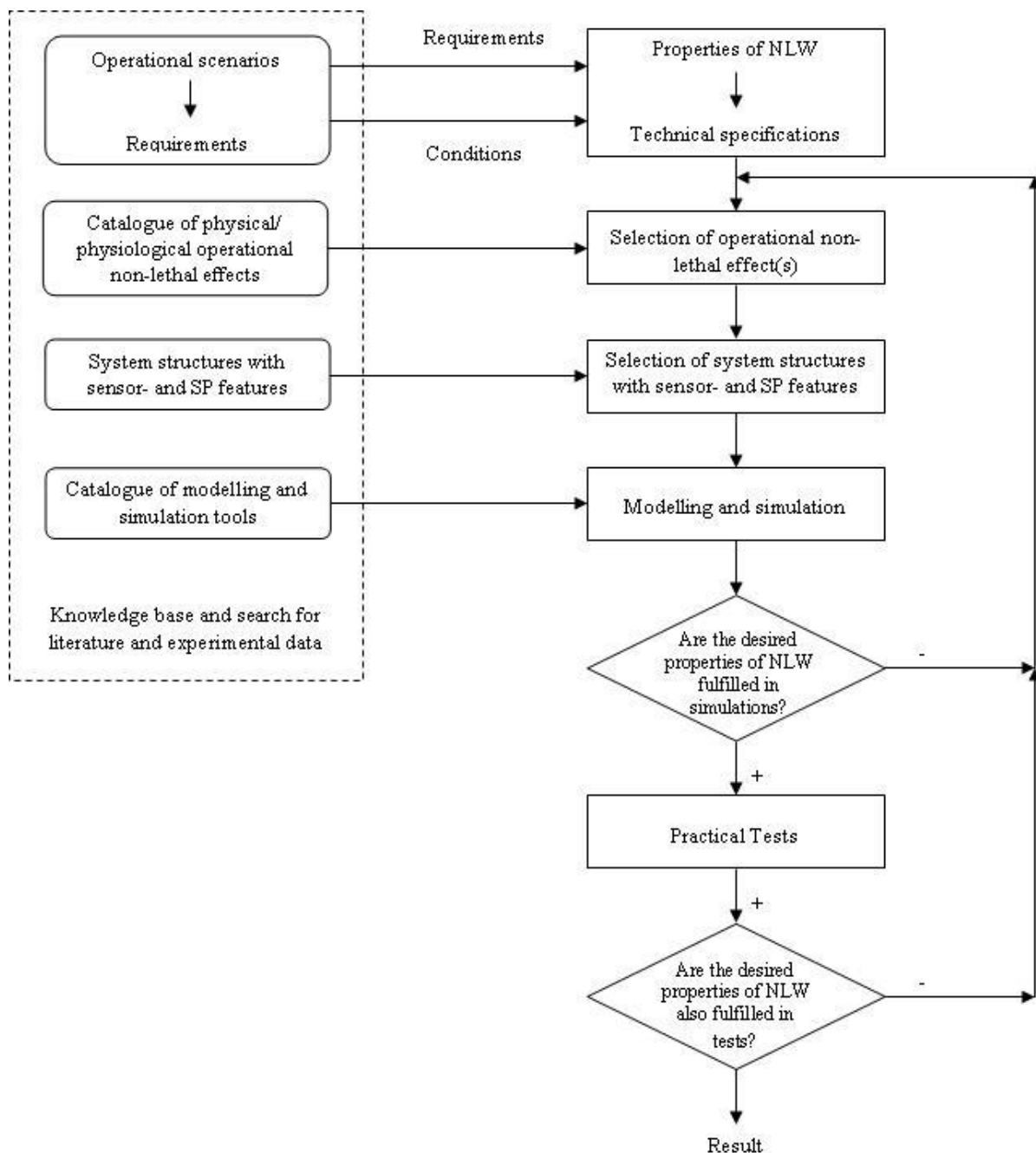


Figure 2-1 Development process of an advanced NLW [1]

Tactic aims

Tactic aim is the final goal of the operation.

Restrictions

The restrictions can be of legal or political nature and are the factors that limit the set of applicable options: they can be caused by the targets (in case of a person: gender, nationality,

religion, state of health etc) that affect the selection of actions and weapons that can be used against them, or by the environment.

Tasks

The major tasks in the operations are neutralisation (incapacitation) of individuals or groups; control, channeling or dispersion of crowds; separating groups or collecting individuals together; removing individuals from a crowd; marking individuals in a crowd; area access denial for individuals or groups; neutralisation of infrastructure, vehicles and facilities; and protection of facilities and equipment.

Specification of the needed non-lethal capabilities

An operational scenario defines the following requirements for an NLW: the range (distance to the target), time to the activation (onset time), duration of the effect, the reactions of the targets (immobilisation, compliance, escape etc.)

Based on the operational scenarios a technical specification of an NLW is identified. On the following two steps the base non-lethal effects are selected and the requirements for the NLW's adaptability are determined.

The capability to adapt itself to different operational situations is the main characteristic of an intelligent non-lethal weapon. This capability secures both efficient and safe use of an NLW. The requirement for adaptability refers both to the active agents of an NLW (projectiles, chemicals, electrodes delivering electric impulses etc.) and to the delivery systems.

The ability to recognise the parameters of the real operational conditions, to evaluate their deviation from the pre-set values, and to change the NLW's output accordingly is provided by sensor systems, which include sensing elements and signal-processing features.

Sensors enable the recognition, localisation and tracking of the targets. Also, they serve the identification of targets' properties. Thus the output of an NLW can be customized for every target according to its peculiarities.

Sensors that are placed proximately to the target deliver the information about the impact of an NLW, which is used to control the NLW's output in the real-time. For instance the gas pressure in a kinetic NLW can be controlled by the distance to the target, so to keep the impact energy constant.

Sensors used in the NLWs should fulfil a number of requirements, e.g. small size, robustness, insensibility to certain environmental influences, short response time etc.

The combination of the parameters of the selected non-lethal effects, the delivery system and the sensor system makes an NLW's concept. On the next step, the plausibility of the concept has to be verified. The verification process consists of two phases: first in the model, and second in the real experiments.

In the first phase the two critical requirements – safety and efficiency – are checked for fulfillment. A simulation model is designed to investigate the impact of the selected non-lethal effects on the human body or on the target devices.

The characteristics of the NLW are iteratively controlled and redefined until the requirements for safety and efficiency are fulfilled. At that point a prototype of an NLW is built.

On the final step the NLW's prototype is validated in the practical test. As soon as the test employment shows an expected outcome, the NLW's production may start.

The procedure is an iterative process, where selected non-lethal effects, system structures including sensors and signal processing features, models and simulation tools, are varied until the required NLW properties and outcome are achieved.

2.2 Modelling and simulation

An advanced antipersonnel NLW is characterized first of all by a low risk of undesired injures. Therefore, a modelling is the essential part of its development, as it provides for the crucial information about the possible pathophysiological impacts of an NLW on a person. A well-established model allows to analyse the sensitivity of the impact to individual peculiarities of a person (e.g. body constitution, medical preconditions, presence of illegal substances in blood). This is used for a further development of a target feedback system, which enables the adaptability of the impact to a certain target person.

Additionally, such a model may be applied as a retrospective investigation tool in forensic practice for cases, when a fatal role of an NLW cannot be ruled out.

A development of an accurate model for investigation of impacts on humans is often a challenging task. There is no universal approach for such a modelling, as effects of different nature influence specific target organs in different ways. A great part of this research was

devoted to a study of a modelling process. Further a method for a model development for an investigation of an EID-human-interaction will be described.

2.2.1 Model

Modelling is the essential process in any scientific activity. Its aim is to represent objects or phenomena in a form convenient to study, to analyse or to predict their parameters. A model is a limited reconstruction of an object or a phenomenon, which is valid only for a given task. This means, the purpose of a scientist determines which properties of an object or a process must be reflected in the model, and which ones can be neglected due to their irrelevancy.

The purpose of an EID-human-interaction model was to create a tool for investigation of physiological effects of the EID's specific electric impulses on the human organs and tissues, and for analysis of the factors influencing these effects.

A research showed that a number of different models had been designed for a similar task.

Biomechanical models of muscle contraction

Various biomechanical models for muscle contraction can be found in the literature [e.g. 4, 5]. They reproduce the processes on different levels and usually consist of two parts: an activation model, which describes the chemical process of the contraction excitation, and a mechanical part describing the process of the physical changes in the muscle tissue.

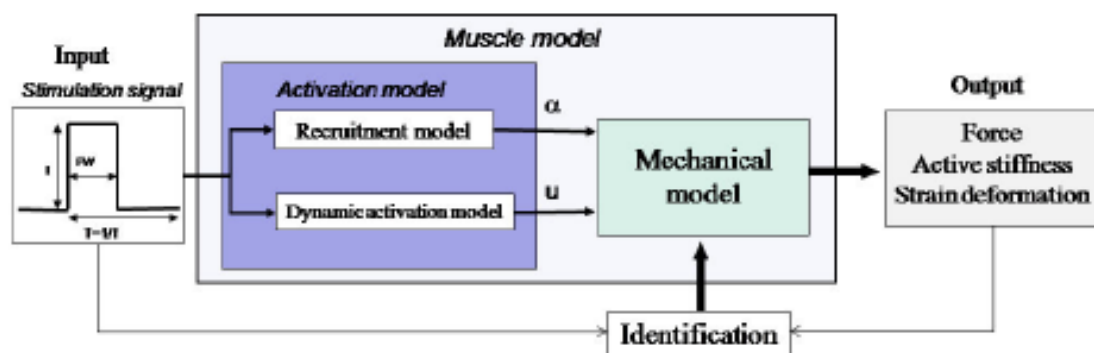


Figure 2-2 Diagram for a dynamic muscle model [5]

These models are usually represented [4-6] as a set of differential equations of visco-elasto-plastic type that reflects the relation in the myofibril between stress and strain.

There are similar models for different types of muscles.

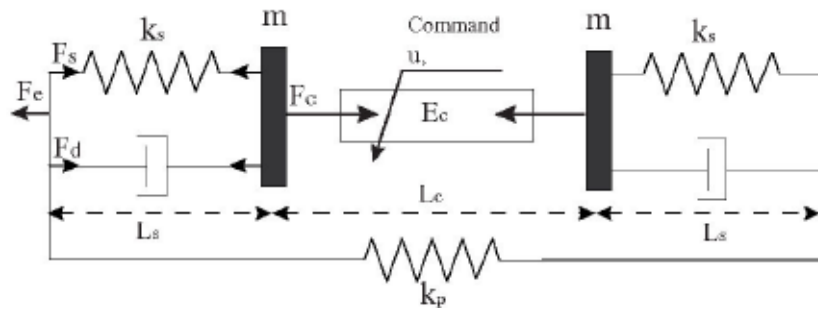


Figure 2-3 Structure of the heart muscle mechanical model [3]

A Teledeltos paper model

Teledeltos paper is a resistive paper that has uniform resistance [7, 8]. It can be cut to the scaled shape of the body region, which has to be investigated. Electrodes painted with conductive ink allow connection to current or voltage sources. It is possible to introduce inhomogeneities by means of perforations or silver spots (e.g. pinhole regions simulating lungs). Field intensity values are read with sharp-tipped voltmeter probes (see fig. 2-4).

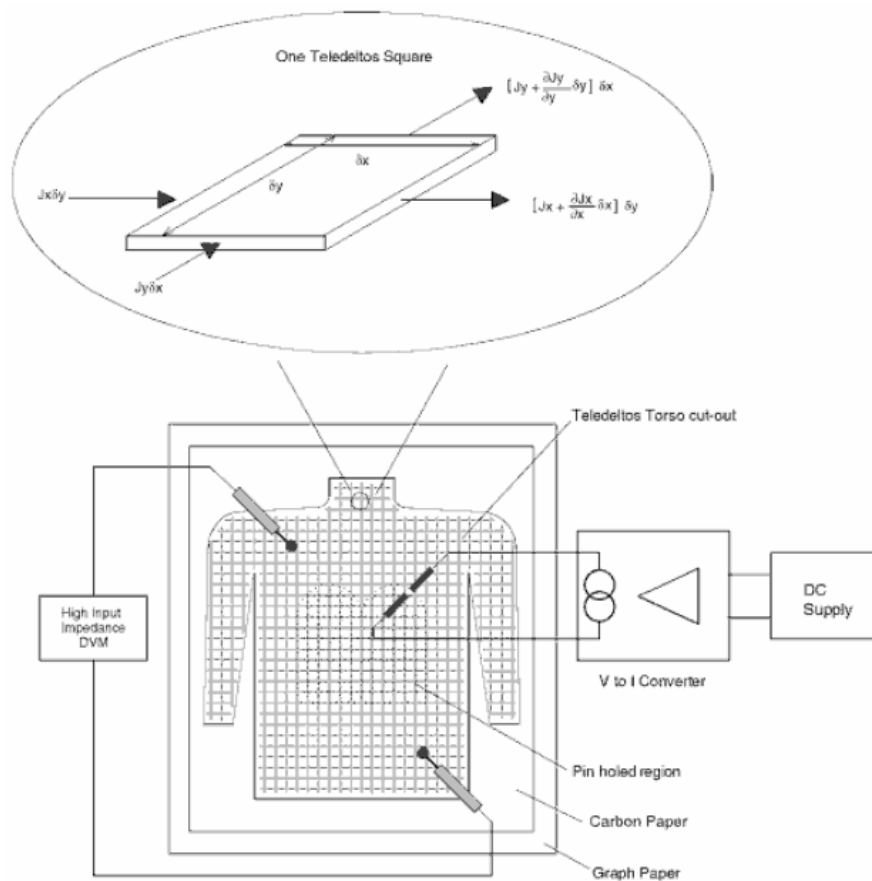


Figure 2-4 Modelling with the Teledeltos paper [9]

Phantoms

In the radio-safety analysis different tissue-mimicking phantoms are used. There are models of high-water-content [10] and low-water-content [11] biological tissues. The phantoms are fabricated from various substances: gelling agents and polyethylene powder [10, 12], polyester resins and aluminium powder [11, 12], polyacrylamide gel [13, 14], silicone rubber with carbon fibre [20], gelatines [17] or a mixture of flour, oil and saline [18].

The composition and the proportion of the ingredients determine both physical properties of the phantom and the radiation frequency range, for which the model can be employed. Normally models are designed for a narrowband spectrum [22 - 24]. However, there are models that successfully cover the frequency range between MHz and GHz [15, 20] and the range from Hz to MHz [21].



Figure 2-5 The available solid phantom of a lower arm [24]

The selection of a certain material depends on its properties. For example, the polyacrylamide gel-based models have very limited shelf life (up to several hours exposed to air). On the other hand, they provide optical transparency and gel-like mechanical properties. Gelatine-based materials are widely used because of their stable mechanical properties and ease of fabrication. However, it is problematic to fabricate a heterogeneous model, because of diffusion of two neighbour gelatine layers of different concentrations. The models based on silicone rubber can reproduce a number of tissues: by varying the relative amounts of the different types of carbon fibres a wide range of dielectric properties can be achieved.

Computer models

Modern technologies allow to combine all mentioned approaches, i.e. the mathematics of the physical and chemical models, the optic representation of the phantoms and the visualisation possibilities of the Teledeltos paper models, in a computer model.

Using of computer models in human studies provides a number of benefits. First of all, the accuracy of a geometrical representation of the tissues and organs is very high thanks to the modern imaging techniques. The computer tomography (CT) and the magnetic resonance imaging (MRI) allow to create a model based on a real anatomical data. A computer model can be arbitrarily customized for a given application with much less effort than in a case of a solid phantom. Finally, a computer model can combine any number of physical models, represented as systems of equations.

In the last 30 years anthropomorphic computer phantoms have obtained an important place in many scientific applications, e.g. ionising radiation dosimetry [25] or microwave cancer therapy [26]. Thus a decision was made to use the experience from these areas in this research.

Several anthropomorphic computer models of a human body, which have been used for electromagnetic applications, were analysed in this study (see tables 2-1 and 2-2).

The models presented in the table 2-1 are voxel-based phantoms. The tissues in these phantoms are divided into numerous volume elements (voxels) of an end size. The size of the voxel is defined during the model design and cannot be changed afterwards.

The VIP-Man (VIsible Photography-Man) [27], MEETman (Models for Simulation of Electromagnetic, Elastomechanic and Thermic Behavior of MAN) [28] and RVH (reduced visible human) [29] models are based on the Visible Human project. The Visible Human Male data set was released in 1994 and consists of MRI, CT, and anatomical images [36]. The disadvantage of this model is that it does not represent an average person. The weight and height of the Visible Human Male do not refer to the standard parameters of a male person. However, some software product do allow for scaling of the model [37].

Table 2-1 Characteristics of some anthropomorphic voxel phantoms used for ionizing radiation dosimetry

| Name | Gender | Age | Height, cm | Weight, kg | Source | Body section | Voxel size (min), mm ³ |
|--------------------|--------|-------|---------------|---------------|---------------|-------------------|--------------------------------------|
| VIP-Man [27] | male | 38 | 186 | 103 | photos | whole body | 0.33x0.33x1 |
| MEETman [28] | male | 38 | 186 | 103 | photos, CT | | 1x1x1 |
| RVH-male [29] | male | 38 | 186 | 103 | CT | head- midthigh | -- |
| Golem [30] | male | 38 | 176 | 69 | | | 2.08x2.08x8 |
| Voxelman [31] | male | 35 | 178 | 70 | | | 4x4x4 |
| Norman [32] | male | adult | 170 | 70 | IRM | | 2x2x2 |
| Otoko [33] | male | adult | 170 | 65 | | | 0.98x0.98x10 |
| RVH-female [29] | female | 59 | 167 | -- | | whole body | -- |
| Donna [34] | female | 40 | 176 | 79 | | | 0.98x0.98x10 |
| Adelaide [35] | female | 14 | 157 | 48 | CT | thorax | 2.5x2.5x10 |

The Voxelman [31] model and the Golem [30] model were developed from the whole-body medical image data of living male humans. In both cases the modeled persons agreed well with the ICRP Reference Man [38], which is a standardized male elaborated by the International Commission on Radiological Protection.

Norman is a male model, developed using MRI data. The dimensions of the model do not correspond to the standard man [38], however there is a modified Norman model designed by Dymbilov [39], which was rescaled to have the standard height and weight.

Otoko is the first Asian voxel phantom, which represents an average Japanese adult male. The model consists of more than 100 tissues and organs.

Donna [34], Adelaide [35] and RVH-female [29] are models of a female body. Donna was developed from CT images of a 40-years-old female person. Adelaide is a CT-based model of a 14-year-old female torso. Adelaide has dimensions that are close to the Australian average

female of this age. RVH-female is based on the CT images of a female cadaver.

Table 2-2 Characteristics of the Virtual Family models

| Name | Gender | Age | Height, cm | Weight, kg |
|------------|--------|-----|------------|------------|
| Duke | male | 34 | 174 | 70 |
| Ella | female | 26 | 160 | 58 |
| Billie | female | 11 | 146 | 35.6 |
| Thelonious | male | 6 | 117 | 19.5 |

Another type of computer phantoms uses an unstructured representation of the tissues. This enhances the accuracy of the thin layers and small organs modelling. The examples of such models are the phantoms from the Virtual Family and the Virtual Classroom, developed by IT'IS Foundation [40]. The models were designed based on the high-resolution MR-imaging data of volunteers of an average weight and height. The phantoms contain up to 80 different tissues and organs, depending on the represented gender and age.

Based on the analysis of the phantoms it was decided to use one voxel phantom (similar to the MEETMan) and the Virtual Family models in this research.

2.2.2 Dielectric properties of human tissues

The geometry of the phantoms must be supplied with the relevant physical properties for the model to be completed. A simulation of the electromagnetic fields effects in a human body requires that the modeled human tissues are supplied with their electromagnetic properties: the dielectric conductivity σ and permittivity ϵ .

These parameters are frequency dependent (see fig. 2-6) and their acquisition is a complicated task.

The dielectric properties can be measured with the help of the following principles: A piece of a tissue (a probe) is characterized by its capacitance C and conductance G . These parameters are functions of the physical dimension of the probe and can be measured with an impedance analyser. The parameters of the probe are measured under different environmental conditions, e.g. in air and in a salt solution of a known conductivity. Thus the dielectric properties – the permittivity ϵ' and the conductivity σ – of the probe can be calculated using the following relationships:

$$\begin{aligned}\epsilon' &= C / K \\ \sigma &= G \epsilon_0 / K\end{aligned}$$

where ϵ_0 is the permittivity of vacuum.

Such factors as the measurement electrodes form or tissues polarisation significantly influence the quality of the measurements.

There are several sets of the dielectric data of the body tissues available [41-47]. The results published in three parts of “The dielectric properties of biological tissues” [41-45], obtained by Camelia Gabriel (PhD) and Semi Gabriel (MSc), are considered as the most satisfactory and are widely used in bioelectricity research [e.g. 48, 49].

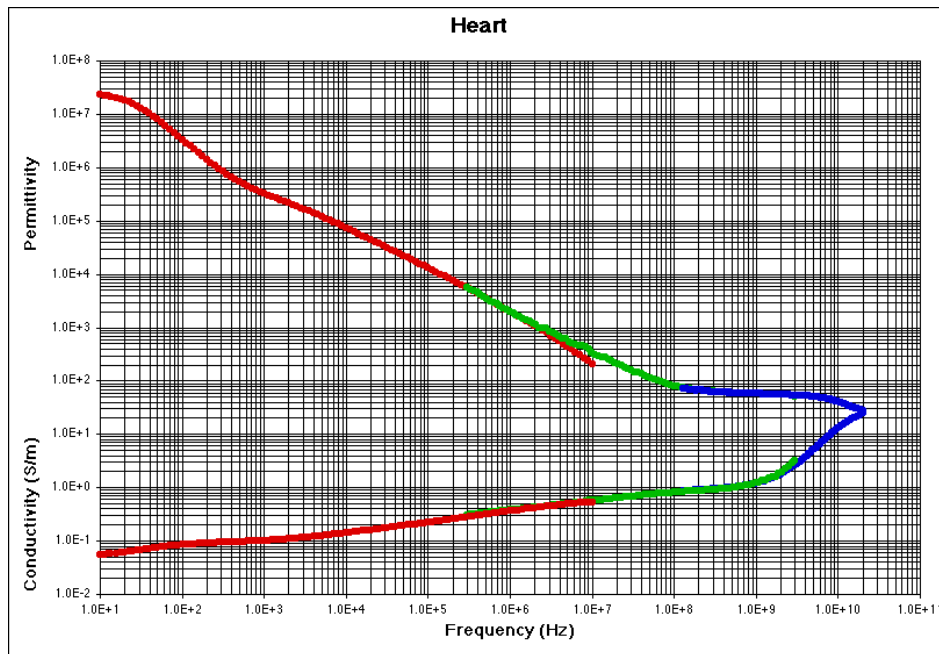


Figure 2-6 Heart muscle conductivity and permittivity versus frequency [46]

They measured dielectric properties of organic tissues in the frequency range 10 Hz to 20 GHz, using excised animal tissue (mostly ovine, from freshly killed sheep) and human autopsy materials, and human skin and tongue in vivo, and applying different techniques. The results were compared with the different dielectric data published in the last 50 years and it was found that the data obtained in the course of the study fell well within the reported data. At the moment the library contains dielectric properties of more than 60 human tissues and is available for free online at <http://niremf.ifac.cnr.it/tissprop/>.

In this research the Gabriels dataset was used as the reference data for the dielectric parameters of the tissues and organs.

2.2.3 Simulation

A reconstruction of object behaviour with the help of its model is defined as a simulation. In a simulation an object interaction with other objects or its changes in time or space are reproduced. Thus, a simulation model provides a tool for objects investigation, testing and predicting of their parameters or behavioural changes, and serves for training purposes.

A computer simulation model needs a computational method. Two computational methods - Finite Element Method (FEM) and Finite Difference Time Domain (FDTD) method - were considered in this research.

Both of the methods are widely used for the simulation of the electromagnetic effects in an inhomogeneous volume.

FEM works with objects that are represented as an unstructured grid of geometrically similar linked discrete regions of a simple form (e.g. triangle), i.e. finite elements. When applied for an electromagnetic problem, a system of Maxwell's equations in a partial differential form is formulated for every element. The system is solved simultaneously for every element in the computational domain using standard methods, e.g. finite differences. The main problem for solving the system of the partial differential equations is the numerical stability, as the system only approximates the domain and the accumulation of error can occur. One of the existing FEM-based software is COMSOL (formerly FEMLAB) [50].

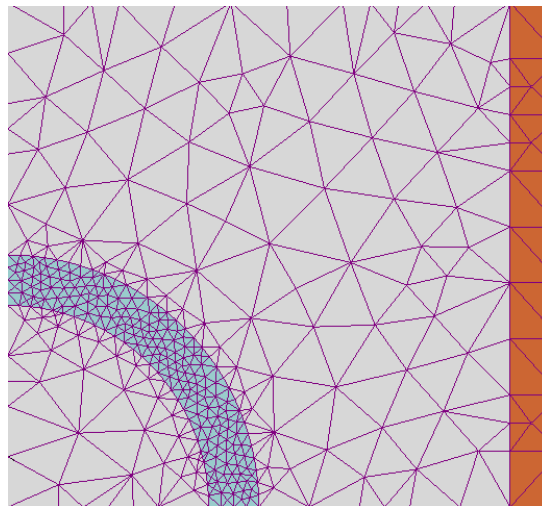


Figure 2-7 An object with a triangle-finite-element mesh [51]

The FDTD method operates with a structured Cartesian grid of elements and a system of central partial differential equations.

$$\nabla \times \mathbf{H} = \frac{\partial}{\partial t} \varepsilon \mathbf{E} + \sigma_E \mathbf{E}$$

$$\nabla \times \mathbf{E} = -\frac{\partial}{\partial t} \mu \mathbf{H} + \sigma_H \mathbf{H}$$

The equations are solved in a cycle, in time for electric field, and in space for magnetic field. The problem is formulated in the time domain, which allows a fast solution for multi-frequency complex fields.

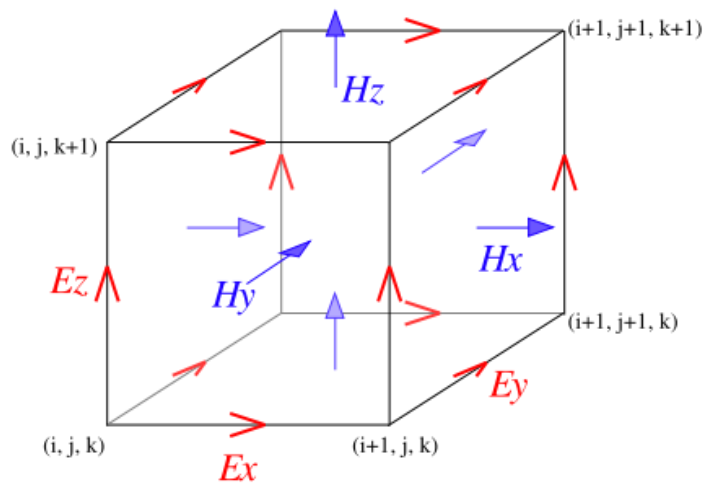


Figure 2-8 3D Yee-cell showing the electric (E) and magnetic (H) fields components in the staggered grid [52]

The EID impulses have a complex waveform, therefore the FDTD method was selected for the developed simulation model.

There are various commercial and non-commercial FDTD-based simulation software tools, where the building of a model, the definition of the physical properties, the simulation itself and the visualisation of the results are integrated in one environment. SEMCAD (SPEAG AG, Zurich) was used in this project, as it is compatible with the mentioned anthropomorphic phantoms.

3. Results

3.1 State of the art of EID technology

The electronic incapacitating devices, also known as conducted energy weapon (CEW) or electroshock devices (ESD), are based on the electric stimulation of a person by short high-voltage impulses. The impulses cause a painful sensation and an uncontrolled contraction of skeletal muscles, and thus temporarily incapacitate a person during the stimulation.

An EID delivers electric current through its electrodes: either in a drive-stun mode – in the same manner as stun-guns for self defense (see fig. 3-1), or via wired darts, which are shot into a person (see fig. 3-2).



Figure 3-1 Stun-gun Power200 PTB [1]

There have been various non-lethal concepts employing the incapacitating electric current: electric-charged nets [2], electrified water cannons [3, 4], and electro-shocking rounds for 12 calibre guns (XREP incl. a special gun [5], Sticky Shocker [3]). However, these systems could not show yet the stable and precise stimulating effect. So, the EIDs are seen as dependable alternative weapons among law enforcement and armed forces.

The devices produced by Taser International Inc. [6] are the most used EIDs today. Taser X26, X2, and X3 are hand-held pistol-like devices, equipped respectively with one, two or three cartridges. The cartridge contains the power circuit and two wired darts (electrodes). The operational range of the Tasers is limited by the length of the wires, which varies between 4.5 m and 10.6 m.



Figure 3-2 Taser X26 [7]

The company states that the impulses (see fig. 3-3) are specially designed to stimulate the alpha motor neurons that control movement. This causes temporarily contraction of major muscle groups regardless of the size or pain-tolerance of the target [7].

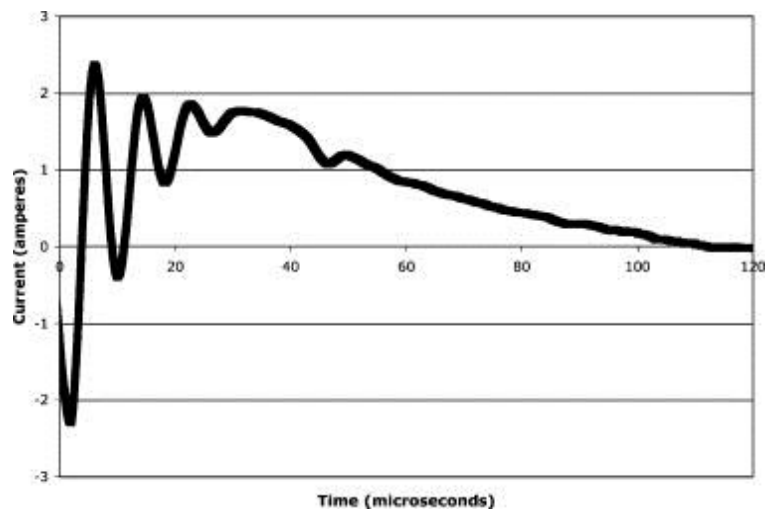


Figure 3-3 Taser X26 impulse waveform [8]

The electric current is transmitted via electrodes that penetrate or touch a person's skin. However, if an electrode gets stuck in the clothing, an electric arc is realized, and thus the current is transmitted through the air to the body.

When the electrodes hit the target, a 5 s stimulating cycle begins. The short (approx. 100 mcs) impulses are delivered at a rate of 19 pulses per second.

Table 3-1 Specification of TASER X26 output [9]

| Electrical Output Characteristic | Comments |
|--|--|
| Waveform | Complex (a single cycle 100 kHz arcing phase followed by monophasic 100 μ s stimulation phase, 48 μ s decay time constant) |
| Waveform and stimulation capability with typical 400 Ω (ohm) load | 1 A average current during the 100 μ s pulse |
| Pulse Rate | 19 pulses per second crystal controlled |
| Pulse Duration | 100 μ s |
| Total per second discharge time (“on” time) | 0.0019 seconds |
| Voltage (peak open circuit arcing) | 50 000 V |
| Voltage (peak loaded) | 1 200 V |
| Avg. voltage over duration of main phase | 400 V |
| Avg. voltage over duration of full pulse | 350 V |
| Voltage – average (one second baseline) | 0.76 V |
| Current – average (one second baseline) | 0.0021 A (average rectified current) 0.0019 A current from main phase (a better estimate of stimulation capacity) |
| Energy per pulse – at main capacitor | 0.36 J |
| Energy per pulse – delivered into load | 0.07 J |
| Delivered charge – main phase | 100 μ C, 88 μ C net |
| Power delivered to main capacitor | 7 W nominal |
| Power output – delivered into load | 1.3 W |

The Tasers are being employed by the police agencies in several countries, e.g. USA, Canada, Australia, UK and France. The USA statistics shows that the use of Tasers resulted in a decrease of both officers and criminals injures [10]. In more than 5% of cases of Tasers employment in the USA the lethal force was not necessary according to the field statistics of Taser International Inc [11].

However, the use of Tasers is not uncontroversial. Amnesty International reported recently [12] about 500 deaths following Taser use since 2001, in more than 60 cases Taser was listed as a cause or contributing factor [13]. A prolonged or multiple use of a Taser, an induced state of an excited delirium or a triggered ventricular fibrillation are considered as the most probable causes of death in those cases. As a result, the U.S. Army Center for Health Promotion and Preventive Medicine recognises a Taser as an effective non-lethal weapon, but does not recommend using them in training due to the potential risk [14].

Thus, although the rate of the lethality compared to the total number of Tasers uses is comparably low, the uncertainty about the Tasers safety has some dramatic consequences. Often the use of EIDs is seen as unsafe, and is therefore prohibited, which means no non-lethal option for the police or military forces.

There is such a situation in Germany: the use of Tasers is only restricted to some selected special response units (Sondereinsatzkommandos) [15], the German Armed Forces (Bundeswehr) allows neither operational nor training use of the Tasers [16].

Additionally there are several structural shortages in the Taser design.

An absence of an auto-stop mechanism makes it “inherently open to abuse” [17]. This, especially in conjunction with an insufficient training may lead to an intentional or unintentional misuse of the EID [18].

A short range limited by maximum 10 m and an inflexible wired structure prevent from an effective military use of Tasers.

Therefore there is a need for a new advanced EID: with a flexible construction, adaptable dosage rate and an anti-abuse mechanism. In the following chapters the basic concepts for an “intelligent” EID are presented.

3.2 Concept of an advanced EID

A direct contact between EID and a target person predefines the possibility to realise a feedback from a person to the device. Thus, valuable information about the person can be obtained before or during the electric impulses are sent. This information is the key factor for an efficient and safe use of an EID: it allows to control the darts-spread on the target depending on the distance to the target, to adapt an EID output (voltage/ current/ power) corresponding to the target’s bioimpedance, and to control the output rate according to the

person's ECG.

Further, there is a need for an automatic stop-mechanism, which would prevent an operator from misuse or abuse of the device. In the lethal cases reported by Amnesty International [19] already 5 cycles (or 25 s) of uninterrupted tasering could be a contributory factor for a lethal outcome. Therefore, it would be reasonable to limit the continuous operational time to 15 seconds. A break of at least 10 s, when it is impossible to activate the device, should follow, after which the device could be activated for the second time for 15 seconds, if necessary. The necessity for the subsequent 15 seconds-series should be investigated.

Additional advantages could be achieved combining an EID with other non-lethal effects, e.g. chemicals. Dexmedetomidin [20] is known to increase the electric conductivity of organic tissues, i.e. an infusion of such a solution could allow for decrease of the electric impulses amplitude. It could be possible to use special electrodes with a hollow needle on the tip (see fig. 3-4) with special openings for administration of a chemical solution.

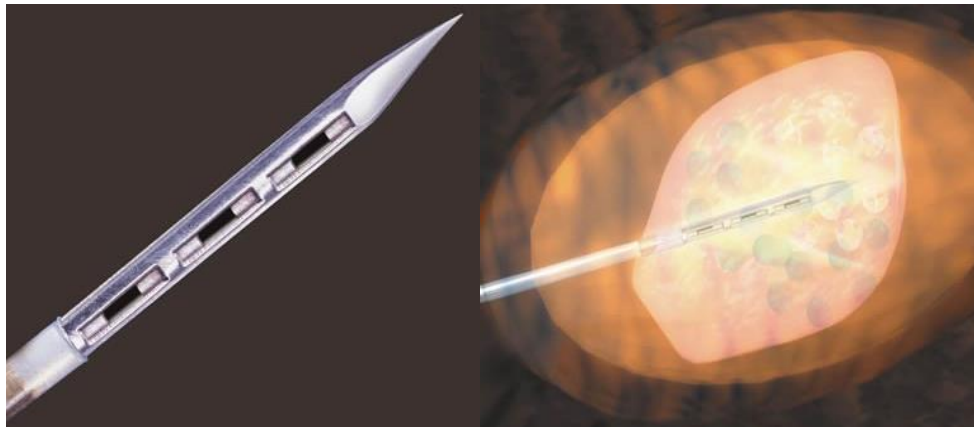


Figure 3-4 A needle electrode with openings for infusion of chemical solutions [21]

Further, the risk of EID in combination with other factors to cause a cardiac failure has to be considered. A possibility to convert an EID energy to a defibrillation energy will be discussed in the following chapters.

3.2.1 Controlling the distance to the target

Measuring the distance to the target with a help of a laser or ultrasonic sensor enriches the device in two ways: first, it helps an operator to stay in the range of the device; and second, it ensures an effective darts-spread (min. 11 cm [22]) on the target body both for short (up to 1

m) and long (over 4 m) operator-to-target distances.

The Taser electrodes are shot out with a constant 8° angle between them (see fig. 3-5). Assumed that the electrodes are shot perpendicular to the target, the spread between the electrodes on the target's body S is equivalent to the distance from the Taser to the target D multiplied by the tangent of the angle α between the electrodes $tg\alpha$. For a small angle its tangent can be replaced by the angle value in radians:

$$S = D \cdot tg\alpha \approx D \cdot \alpha^\circ \cdot (\pi / 180^\circ).$$

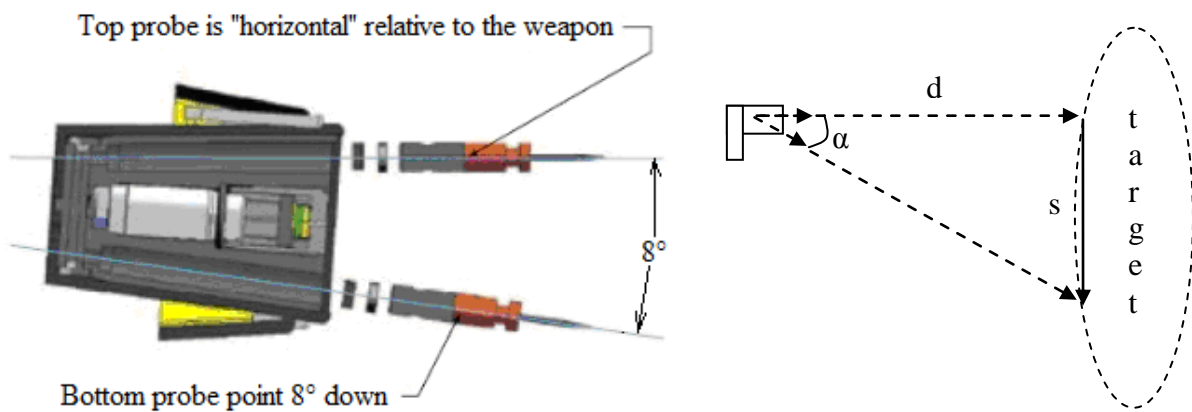


Figure 3-5 Taser 15' Cartridge [22] and the projection of the electrodes on the target

Thus the measured distance to the target can be used to set a necessary angle between the darts, in order to provide an effective spread of the electrodes on the target:

$$\alpha^\circ = \frac{S}{D \cdot (\pi / 180^\circ)}.$$

The standard Taser is equipped with a laser vizier, which can probably be integrated into the distance-measurement circuit, providing accurate measurements for long distances. However, ultrasonic sensors have an advantage versus laser sensors: they operate with targets of any colour and almost any material.

3.2.2 Controlling EID electric output

The modern Taser devices (X2 and X3) have a current metering feature, which is based on "The pulse calibration system" [23]. The technology is said to provide a delivery of an

optimal charge to safely incapacitate a person at any moment by a constant control and adjustment of the electrical output of the device. Taser International states that this technology provides “margin of safety up to 40% greater than previous ECD technology” [23]. The company does not explain how the technology is realised in the device.

In order to provide a safe and effective dose of electricity for any target, the EID’s output has to be adapted to the target’s bioimpedance. The measurement of a bioimpedance is possible to realise with modified electrodes, e.g. bipolar coaxial or needle electrodes, that provide a simultaneous excitation and signal registration. The direct contact of the electrodes and the device allows for allocation of the signal-processing hardware and software within the device. There are experimental data from the Taser International training trials, which includes measurements of the impedances, voltages and currents in the tasered persons [24]. These data could be used to develop the impedance-output-patterns, which would be applied for adjusting an EID’s output.

3.2.3 Controlling EID output rate

There is a serious concern about the Taser, that under some circumstances it can cause a ventricular fibrillation (VF) in an effected person. A number of studies were performed in order to estimate this risk [25 – 40].

Walter et al [36] could detect a ventricular fibrillation pattern in a pig heart. However these results were not found in human experiments [40].

Most of the investigation used an adapted VF threshold for 50/60 Hz current defined by the International Electrical Committee [41] in order to estimate the risk of VF induced by Taser. A safety analysis performed in this study showed a 500% safety margin for a single Taser impulse based on this threshold.

There are two prerequisites for an electric impulse to be able to trigger VF. According to IEC [41] and other sources [42 – 44], an electric stimulus of the threshold strength must be delivered during the vulnerable period of a heart cycle, to be able to induce VF.

The ventricular vulnerable period is a period of repolarisation of cells (relative refractory period), which corresponds to the first part of the T-apex (see fig. 3-6) on the electrocardiogram (ECG). During this period the cells are highly inhomogeneous and hyper-excitable [44], so that an electric stimulus of a sufficient amplitude is probable to trigger an abnormal activity of the heart (tachycardia, fibrillation of ventricles etc.).

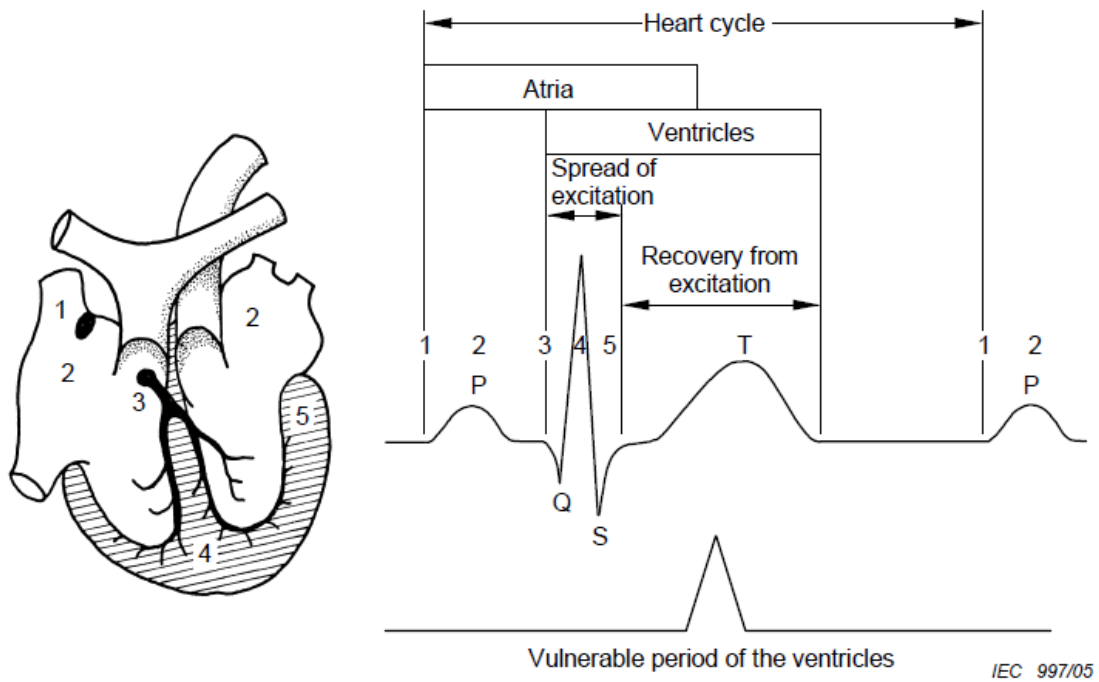


Figure 3-6 ECG of a heart cycle [41]

The probability that an impulse of Taser X26 can coincide with the vulnerable period of a person's heart is evidently not a zero (see fig. 3-7). Taser delivers impulses at the rate of 19 pulses per second that means that a normal person with a heart rate of 50 – 100 beats per minute inevitably gets the whole 19 impulses-series between two heart beats, and consequently at least one of the impulses can also be delivered during the vulnerable phase.

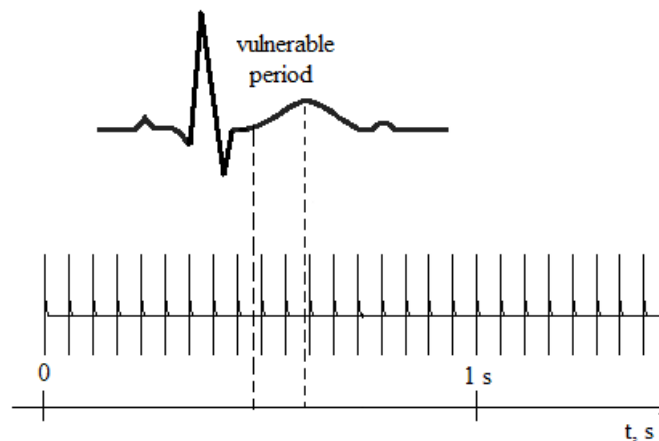


Figure 3-7 Normal heart beats and a series of Taser impulses within 1 second

Furthermore, it was found that certain medical preconditions and use of illegal substances [45] may decrease the electrical VF threshold. Therefore it is reasonable to eliminate the

probability that a shock can be delivered during the dangerous vulnerable phase.

Supplying an EID with heart-beat sensor and programming it in a proper way could accomplish this task. On the occurrence of a heart-beat a special impulse is produced to block the shock-impulses of the EID for the next 300 – 350 ms (see fig. 3-8). The heart-beat sensor allows controlling the emission of the impulses during the heart cycle, truncating the series during the vulnerable period and, consequently lowering the probability of inducing the ventricular fibrillation.

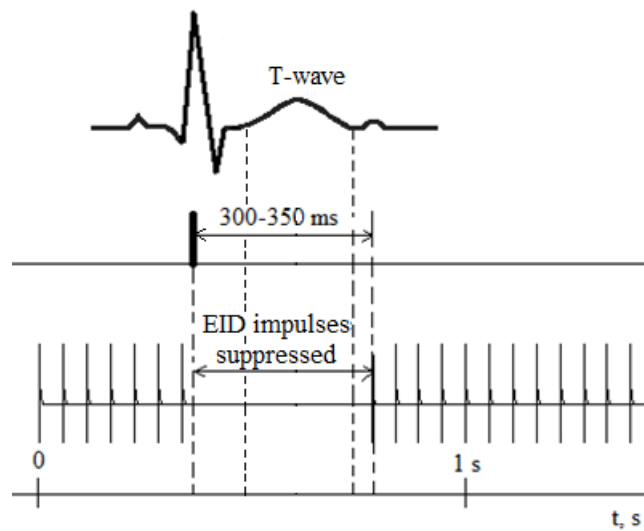


Figure 3-8 Suppression of EID's impulses by the signal from a hear-beat sensor

3.2.4 Combined EID-Defibrillator

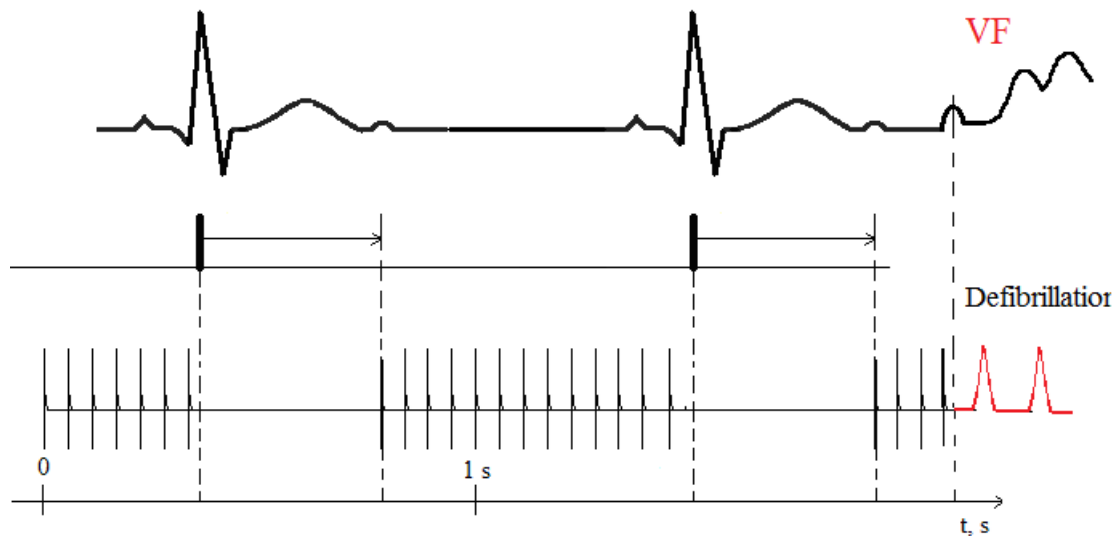


Figure 3-9 Combined EID-Defibrillator in action

The first medical measure in a case of VF is a heart defibrillation. Defibrillation is an external electric excitation of the heart muscle with short direct current shocks of high energy 120 – 200 J [46]. The defibrillation has to take place within several seconds on the onset of VF for a successful outcome. Therefore it is necessary to have a defibrillating device at the operational site.

A possible solution could be to implement the defibrillation functions in the EID's structure. On the detection of the failure heartbeat by a sensor, an EID could be switched from the incapacitating mode to the defibrillation mode (see fig. 3-9).

The feasibility of such a device has to be investigated.

3.3 Modelling

In order to develop a new advanced EID, which would be safer and more efficient, it is necessary to understand the basic mechanism of the incapacitation and to define the influencing factors.

The nature of Taser total body incapacitation is not yet completely understood. A study by Despa et al. [47] discusses the possibility of a central mechanism of the initiated muscle

contraction, i.e. the Taser impulses stimulate the spinal nerves that then activate the skeletal muscles in the whole body.

The influence of such factors as body constitution, age, fitness etc on the Taser's efficiency also still remains unclear.

In this study an attempt was made, to develop a model for a reliable and accurate representation for an EID-person interaction, which could contribute to the investigation of the open points.

3.3.1 Development of the model

A specialized simulation software (SEMCAD by SPEAG AG) and a set of three-dimensional computer based phantoms of the human body were used to perform the modelling and simulations.

The phantom set consisted of one voxel phantom based on the Visible Human model, and four non-voxel models of the Virtual Family (IT'IS) - two adults, one youth and one child.

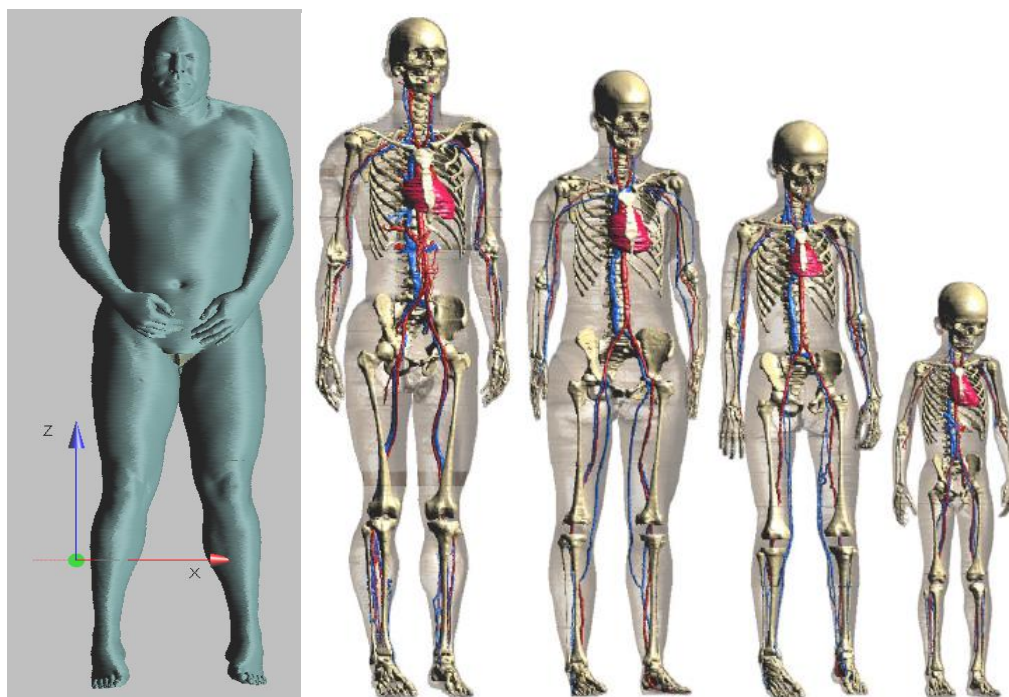


Figure 3-10 SEMCAD voxel phantom and the Virtual Family models [48]

It was decided not to develop an own phantom due to the complexity of the task. These models were selected because of their anatomical fullness and accuracy, and the high resolution.

The model of the EID-human interaction was developed under a number of assumptions.

Assumptions

1. It was assumed that the lack of the barb and tip in the dart geometry did not affect the results. The electric current density is sensitive to dart geometry but the current density far away from the dart tip does not change much [49].
2. It was assumed that all firings were perpendicular to the skin.
3. Due to the computational restrictions it was not possible to model the arcing mode, i.e. when electrodes do not penetrate the skin and the electric current is transmitted via electric arc. So the electrodes penetrate the body in the developed model.
4. Thick clothing was modeled as a skin layer with manipulated dielectric properties.
5. The displacement of the electrodes on the skin was modelled based on the training report by HOSDB [50]. The following cases were considered:
 - a) Electrodes wires on torso and on back, with an electrode separation of 225 mm;
 - b) Barb electrodes on torso and on back, with an electrode separation of 378 mm;
 - c) Electrodes on wires on torso and on back, with an electrode separation of 601 mm;

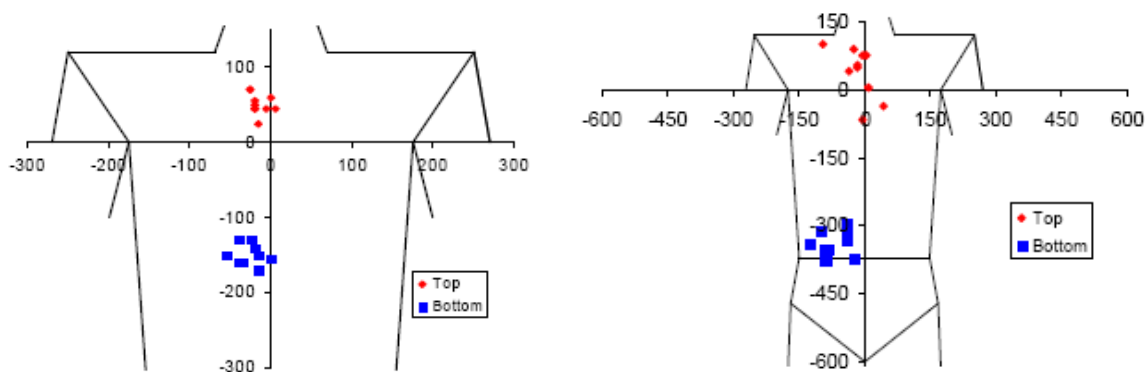


Figure 3-11 Electrodes displacement for the firing distances of 1.5 and 4 m [50]

6. Due to restrictions of the simulation software only a single impulse discharge was considered.
7. It was assumed that the state of the lung during the EID discharge does not affect the results.
8. The output of the EID was not changed for different models, which presumably should have different impedances. Considering the technical data of Taser X26, it was

assumed that it can be replaced as a current source, which output does not depend on the load (for the loads below some tens of kOhms).

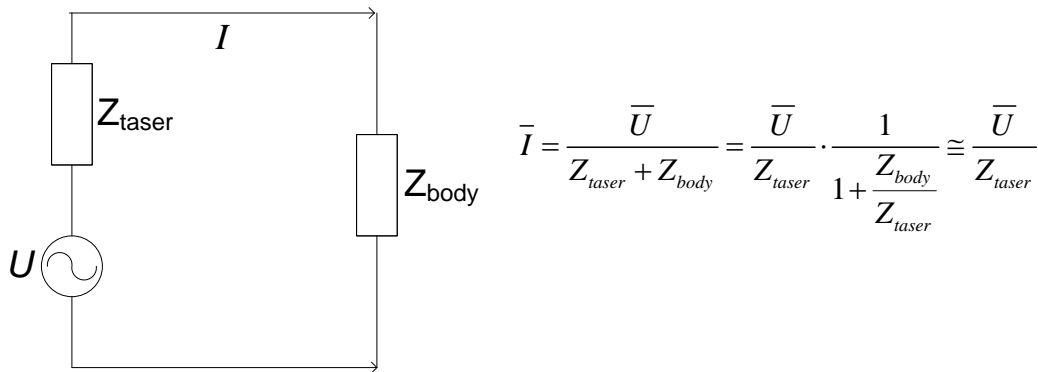


Figure 3-12 Taser X26-load circuit.

9. The conditions such as temperature and respiratory performance were not considered.
10. The EID discharge was approximated as a compound electrostatic problem in the operating spectrum of Taser X26.

Geometry

The selected phantoms included originally more than 80 different tissues and organs. The average resolution of the voxel phantom was $0.2 \times 0.2 \times 0.2 \text{ mm}^3$. The target resolution for the non-voxel models was 1 mm^3 . Thus it was necessary to reduce the number of tissues in order to lower the computation domain and decrease the simulation time. Therefore the tissues of the head and lower the knees were excluded from the simulation area. There were not relevant for the simulation, so this did not affect the result.



Figure 3-13 Taser X26 electrode.

The Taser electrodes have a complicated shape, having a fishing-hook on the tip. However, as stated in the assumptions, it was concluded that it was possible to use simple cylinders to model them. The cylinders dimensions were set in respect to the real size of the darts: 9 mm in length and 0.8 mm in diameter.

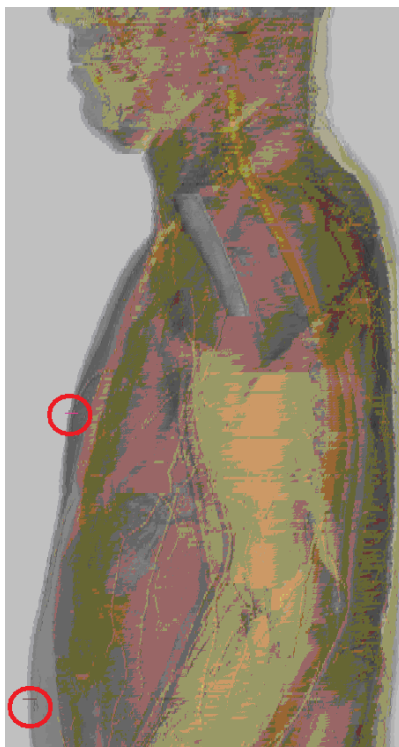


Figure 3-14 The electrodes penetrating the skin

Gridding and voxeling

The FDTD method used in these simulations requires that all the objects in the computational domain are spatially divided into elements (or voxels). The size of the voxels is determined by the grid. The grid settings directly influence the accuracy of the simulation.

Normally, when solving a problem with FDTD, the grid settings depend on the wavelength. However, for applications in the low frequency domain there are different criteria for gridding: the geometry of the objects should be resolved and the grid should provide the large enough padding, so that the field does not reflect within the computational domain.

In the present case the air that surrounds the human body served as the natural boundary, within which the electric field was eliminated.

SEMCAD allows for non-uniform gridding that enables the resolving of both the geometry and the physics of the objects.

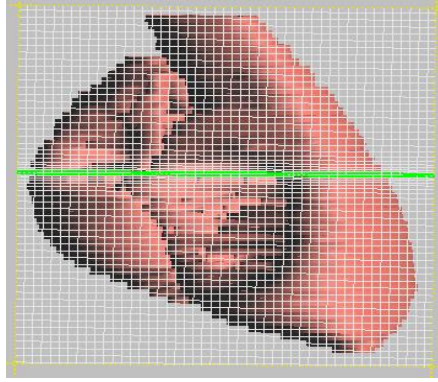


Figure 3-15 Gridding of the heart-muscle

While considering the darts, the aim was to resolve their geometry, as it influences the electric excitation distribution.

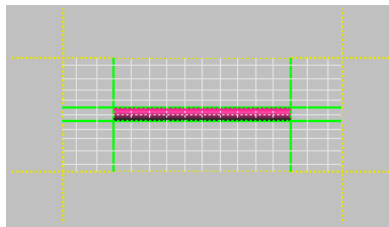


Figure 3-16 Gridding of the dart

In order to lower the size of the computation, and consequently the demanded resources, it was decided not to use the fine grid everywhere throughout the model. 2 mm baseline resolution with maximum step of 10 mm was used almost everywhere except several objects, e.g. the darts, skin and fat layers, and heart tissues. A resolution of 0.2 mm with 1 mm maximum step was used there.

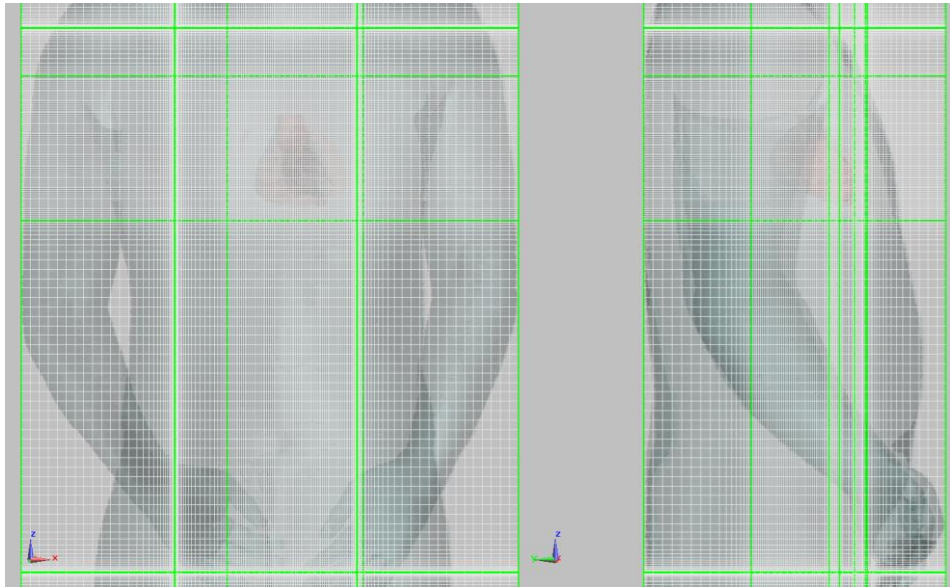


Figure 3-17 Non-uniform grid, front and right side view

The generated grid was then applied for the voxeling.

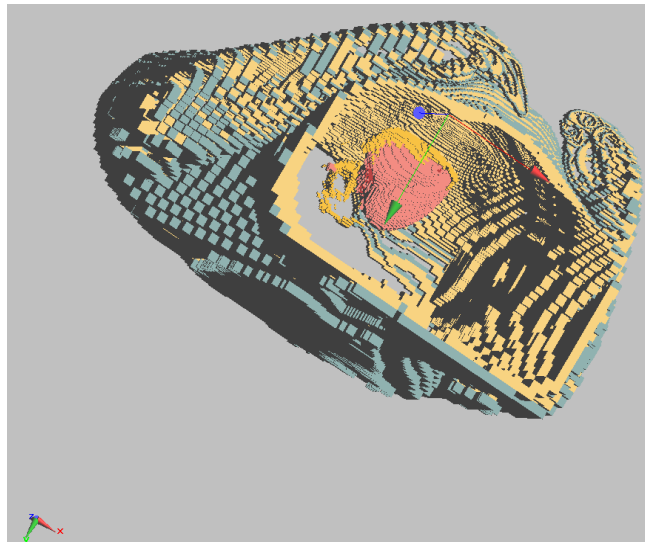


Figure 3-18 Voxeling of the body (skin, fat and heart are represented)

Simulation process

The simulating process is the computation of electric field distribution in the tissues after the EID impulse has been ejected.

We used a simplified Taser X26 impulse in the simulations. The Taser X26 impulse has a complicated shape, i.e. it is a multi-frequency harmonic signal, which we converted into

frequency domain. A number of simulations for each extracted frequency were performed and then all the results were superposed in one combined field.

MATLAB 7.4.0 (R2007a) was used to perform the normal Fourier transformation, which resulted in the array of coefficients for 60 frequencies from 8.3 kHz to 500 kHz.

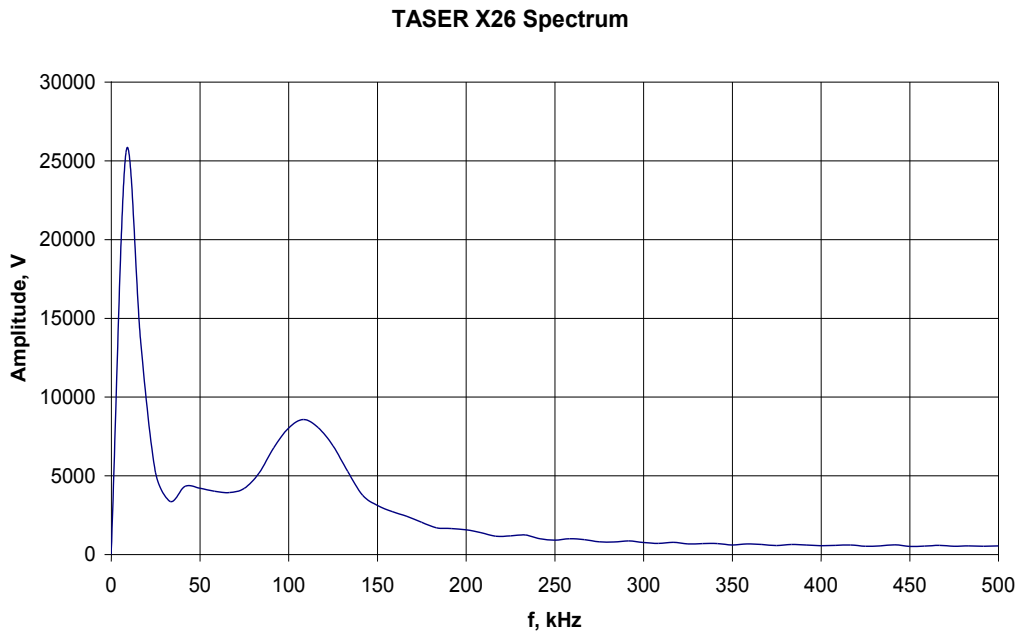


Figure 3-19 Taser X26 impulse transformed into frequency domain

The darts represented the electric sources. All of the body tissues were treated as dielectric solids. The dielectric properties of the tissues like permittivity, permeability, electric and magnetic losses and density were assigned according to the Gabriels' material properties library corresponding to the frequency of a simulation.

The simulation process for all of the frequencies was automated with the help of specially developed script. The final superposition of the simulations results was also performed with a special script, which was available with the software.

3.3.2 Verification of the model

A number of tests were developed in order to validate the modelling approaches. There were two series of experiments.

The first one was focused on checking the correctness of some of the assumptions and on verification of the computational method. These experiments were performed on freshly

exercised swine tissues (muscles, skin, fat, liver, lungs and heart) and on human autopsy material (muscle, liver, heart).

The second series was devoted to the validation of the dielectric properties of the organic tissues. These measurements were performed both on fresh and aged swine material in vitro and on the human autopsy material. The experiments with animal tissues were held partly in Baierbrunn slaughter house, and partly at the Institute of Forensic Medicine, LMU.

The general experimental set-up is presented on the fig. 3-20. We used a specially designed bioimpedance measurement device, which was developed in the cooperation with Mr. Marek Rist from Eliko Tehnoloogia Arenduskeskus OÜ (Estonia).

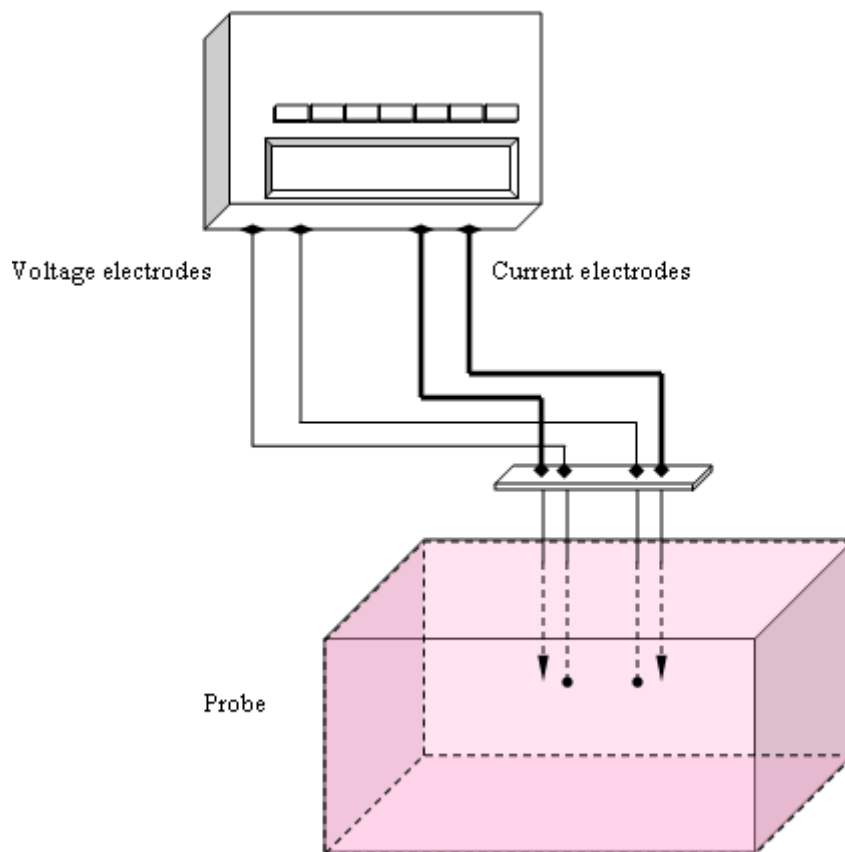


Figure 3-20 Measurement set-up

Bioimpedance measurement device

There was a need to perform measurement of currents and voltages across the probes (animal and human tissues in-vitro) at different types of excitation with variable frequencies, as well as impedance measurement. So a specialised measurement unit was designed. The unit based

on the data acquisition module Agilent U2531A [51] provided a high sampling rate up to 2 MSa/s, 14-bit channel resolution and 24-bit digital programmable input and output. Labview was used to perform the computational transformation of the measured signals and to visualize the results.

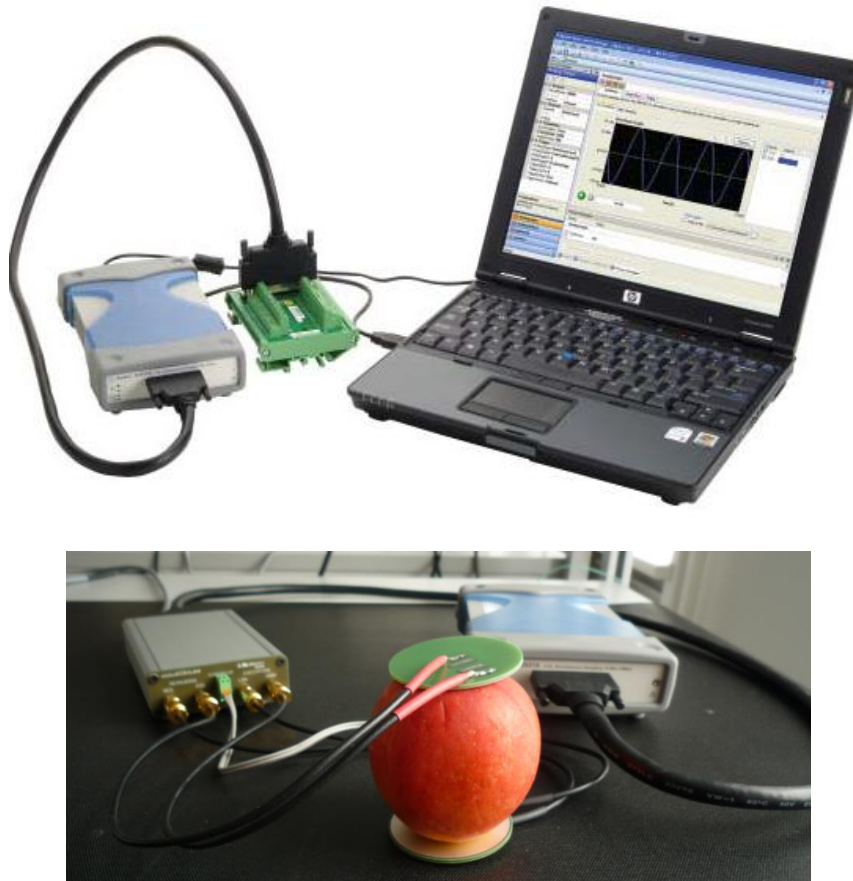


Figure 3-21 Measurement unit [52]

The measurements were performed in two modes. A constant current mode was used to measure the impedances between 1 mOhm and 1 kOhm and at excitation signal frequencies up to 100 kHz. The measurements in the voltage divider mode were performed for higher frequencies of the excitation signals and higher impedances.

In the constant current mode the measured sample is the feedback loop of the excitation current generation amplifier.

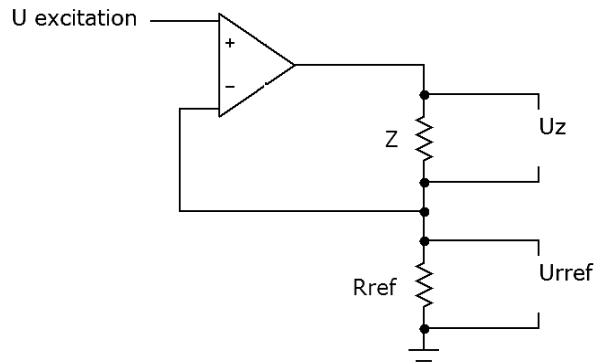


Figure 3-22 Inner circuit in constant current mode [52]

In this mode the impedance of the object can be calculated as:

$$Z = \frac{U_Z}{U_{exc}/R_{ref}},$$

or

$$Z = \frac{U_Z}{U_{rref}/R_{ref}}$$

Voltage on the sample is measured using instrumentation amplifier and current through the sample can be measured as a voltage on reference resistor R_{ref} or be calculated

$$I = \frac{U_{osc}}{R_{ref}}.$$

The designed measurement device directly measured the current through the sample too. This provided us with a protection from destroying the delicate measured object.

When working with higher impedances and frequencies higher than 100 kHz it is advisable to use voltage divider method. In this mode the measured object is outside the feedback loop, so that the oscillation and instabilities that occur at higher frequencies do not influence the measurements.

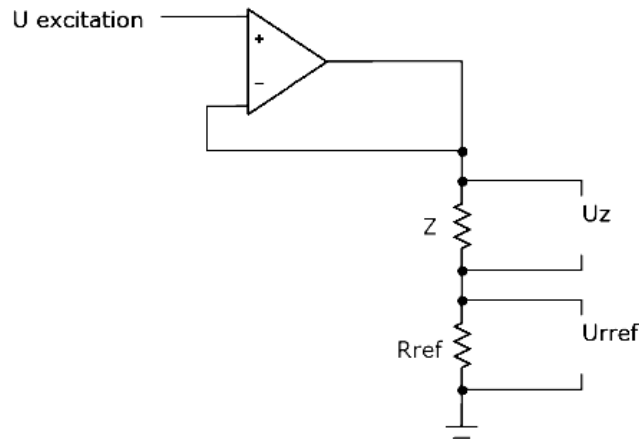


Figure 3-23 Inner circuit in voltage divider mode [52]

In this mode the impedance of the object can be calculated as:

$$Z = \frac{U_Z}{U_{ref} / R_{ref}} .$$

Electrodes

The measurements were performed using 3 set ups of electrodes.

Type 1: 4 aligned electrodes set up with 100 mm distance between excitation electrodes and 60 mm distance between measuring electrodes, electrodes diameter 2 mm;

Type 2: 4 aligned electrodes set up with 100 mm distance between excitation electrodes and resettable distance between measuring electrodes (20 mm, 40 mm, 60 mm and 80 mm), electrodes diameter 0.5 mm, connected to the measuring device via adaptor;

Type 3: set up as in Type 2 connected directly to the measurement unit.

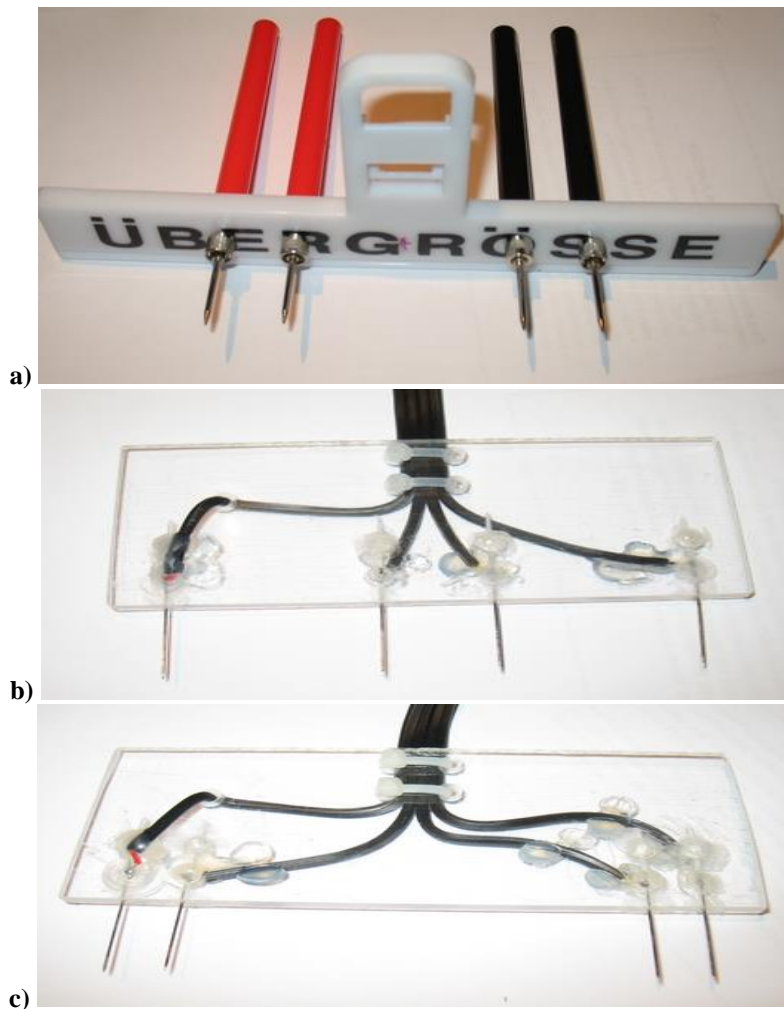


Figure 3-24 Electrodes
a) Type 1; b) Type 2/3 20mm inter-electrode distance; c) Type 2/3 80 mm inter-electrode distance

Calibration

The measurement unit and the electrodes were calibrated before the experiments. For the calibrations a conductive solution and a dummy-model were used:

a) Conductive solution $\sigma = 0.1413 \text{ S/m} @ 25^\circ\text{C}$

The gel was chosen considering the properties of the tissues under measurement: liver, conductivity in the range of 0.038130 – 0.10519 S/m, lungs 0.20588 – 0.28349 S/m, heart 0.093565 – 0.23824 S/m, tongue 0.27211 – 0.29653 S/m, muscle 0.26671 – 0.38408 S/m [54].

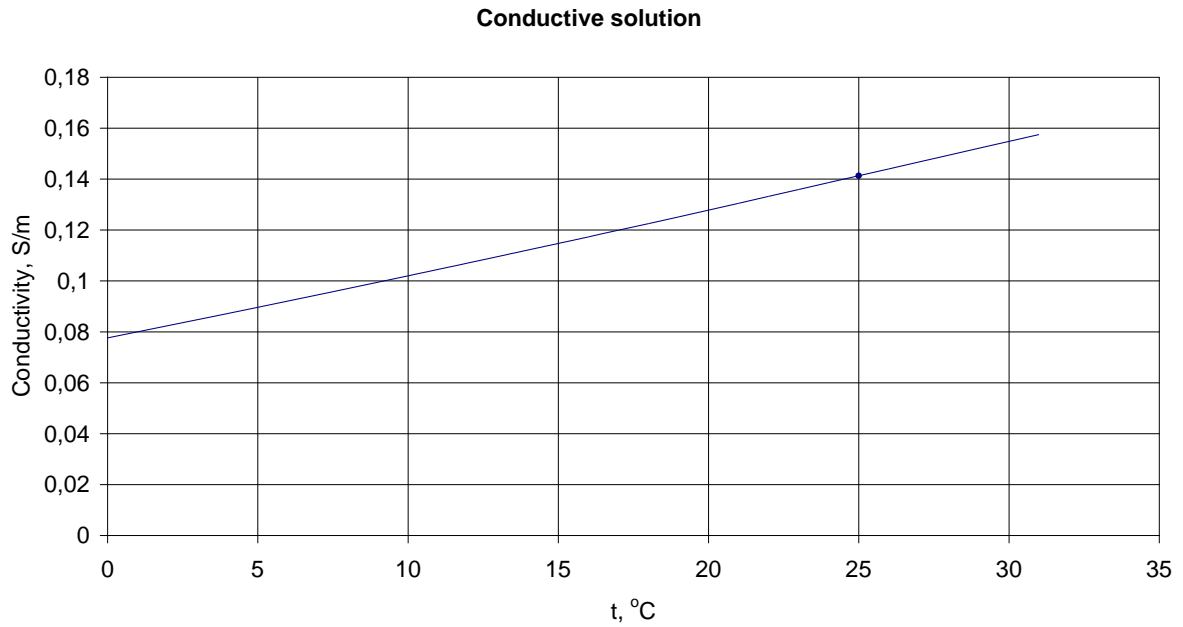


Figure 3-25 Conductivity-temperature curve for the conductive solution [53]

b) Dummy model

A simple resistive-capacitive dummy model was designed, in order to perform the electrodes calibration, and therefore to diminish the contribution to the measurement error from this side. The correspondent systematic error caused by the electrodes was corrected for every type of electrodes.

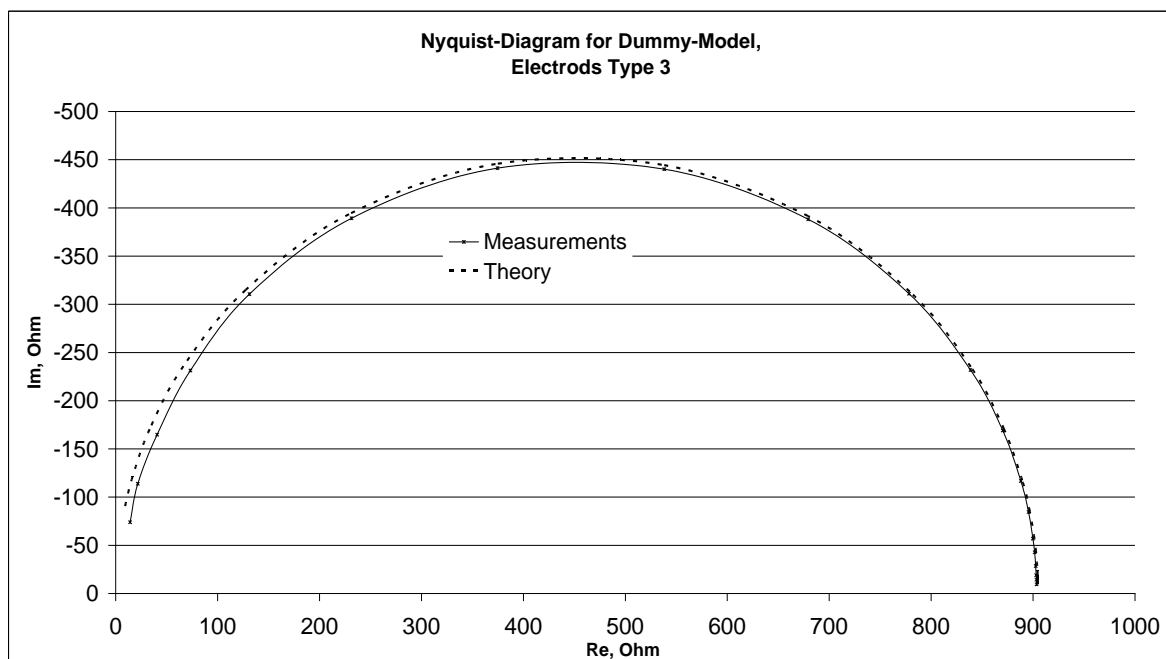


Figure 3-26 Experimental and theoretical Nyquist diagrams for the dummy model

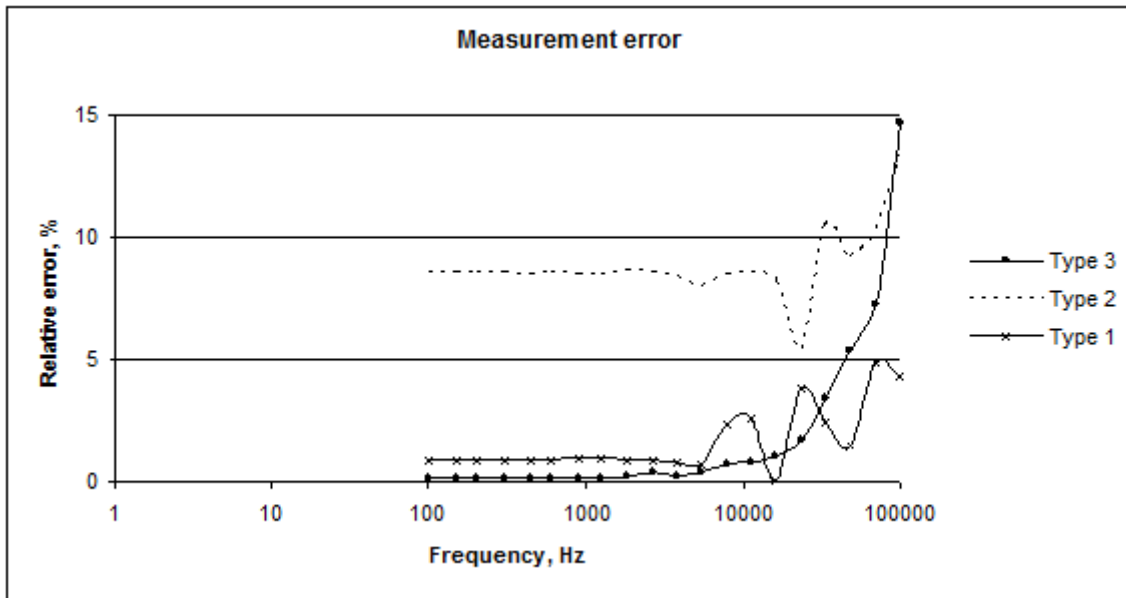


Figure 3-27 Measurement error for different electrodes set-ups

Measurements of dielectric properties of the organic tissues

The measurements were performed on site directly in the slaughterhouse or in the dissection room, so that to provide the better quality of used organs.



Figure 3-28 Freshly slaughtered swine

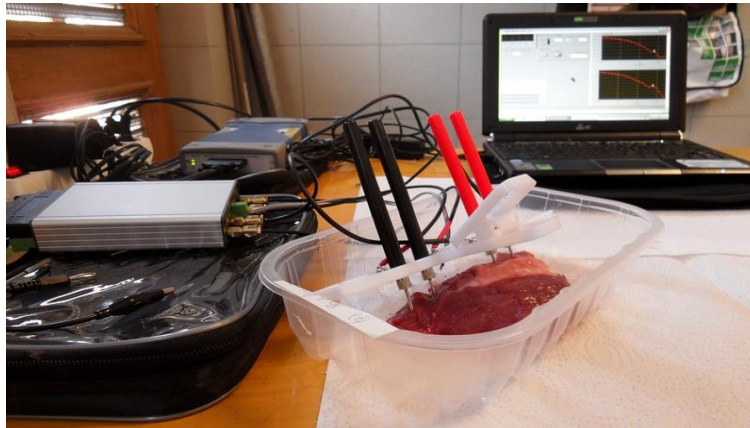


Figure 3-29 Measurement set-up with Type-1 electrodes at the slaughterhouse

First the measurements to define the dielectric properties of the organic tissues were performed. A constant voltage with the amplitude of 1.2 V in the frequency range 100 Hz – 200 kHz was applied. The complete measurements data are given in the Appendix 2.

The Nyquist diagrams for the measured data were reconstructed and compared with the theoretical ones based on the data by the Gabriels (at the same temperature).

The figures below show the Nyquist diagrams for the experiments with the freshly exercised swine tissues (ca. 1.5 hours after animal's death).

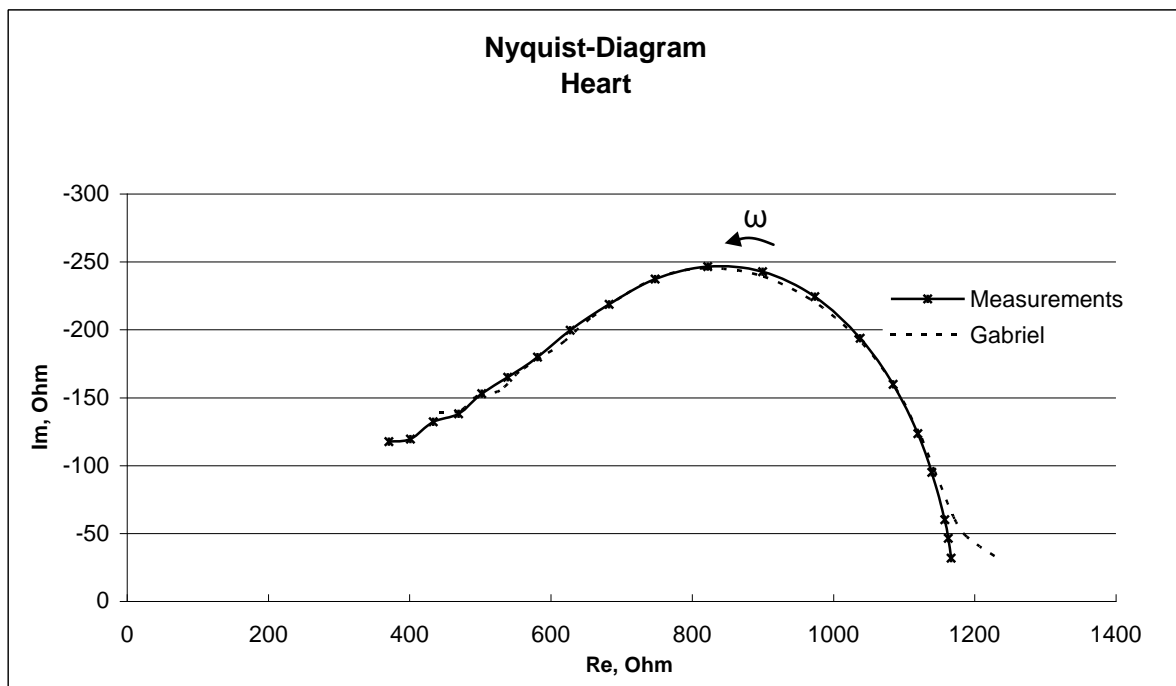


Figure 3-30 Experimental (Type-1 electrodes) and theoretical Nyquist diagrams for a swine heart tissue

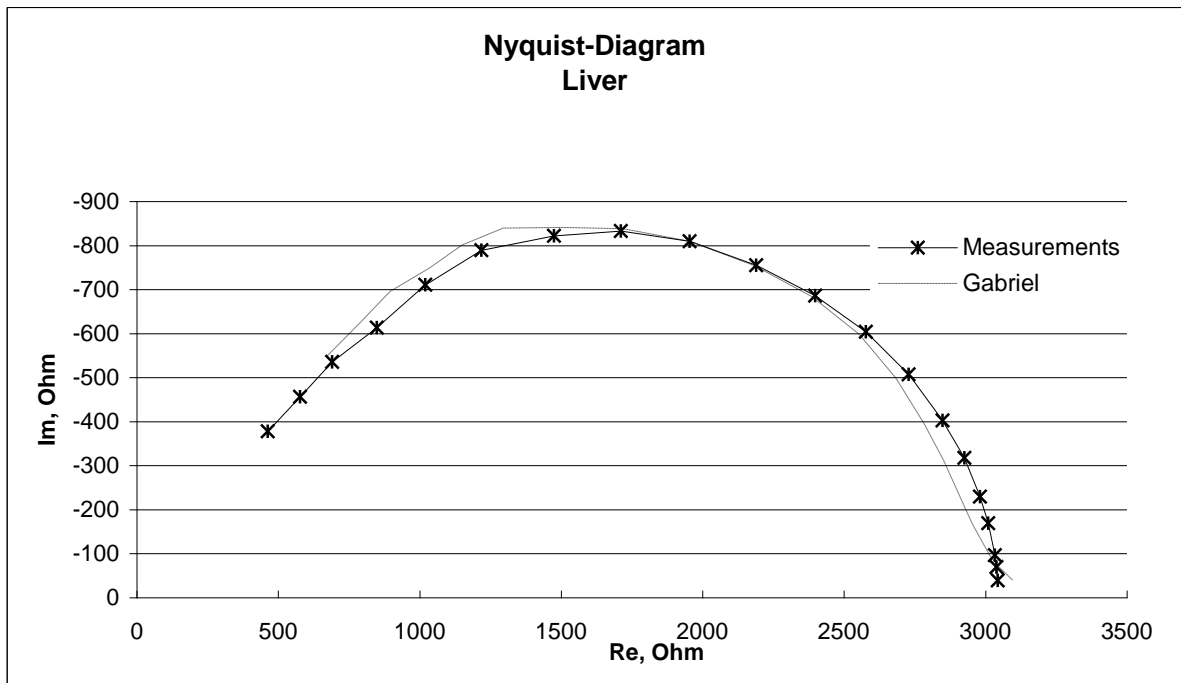


Figure 3-31 Experimental (Type-1 electrodes) and theoretical Nyquist diagrams for a swine liver tissue

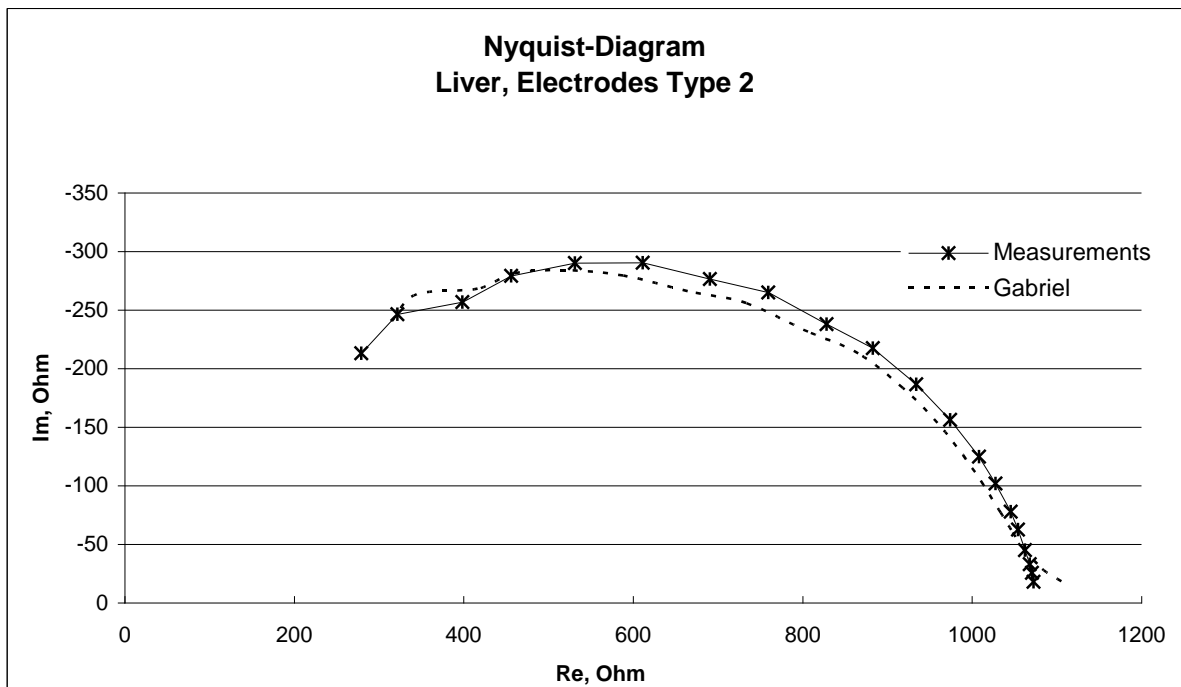


Figure 3-32 Experimental (Type-2 electrodes) and theoretical Nyquist diagrams for a swine liver tissue

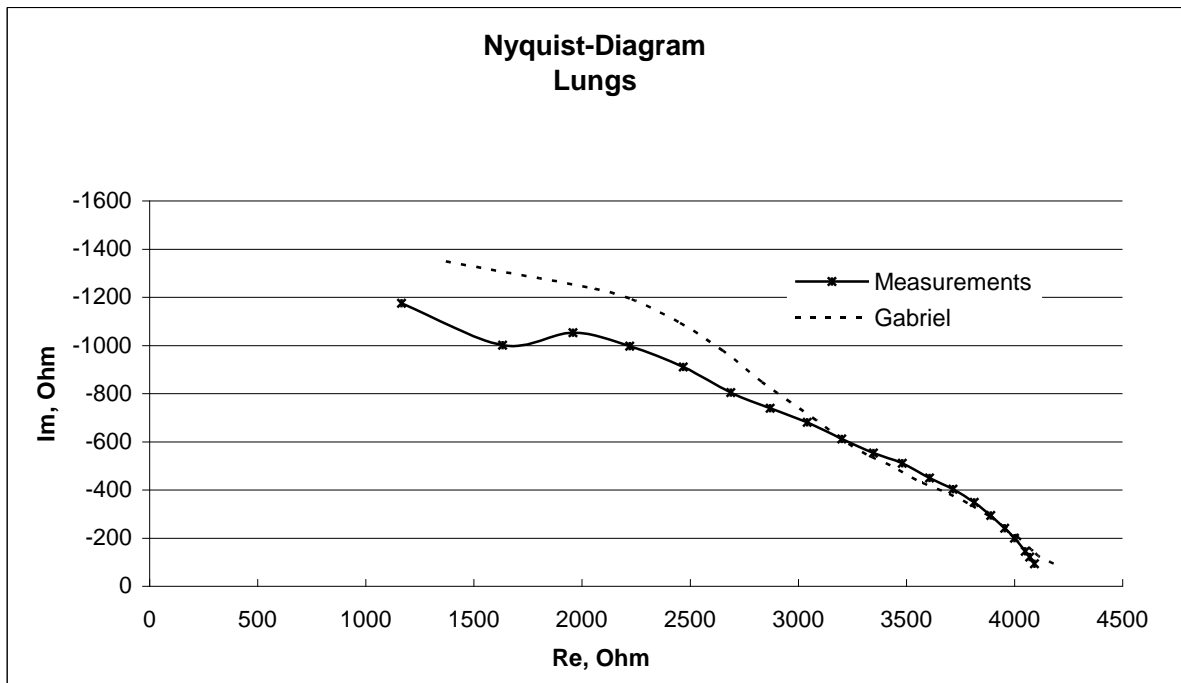


Figure 3-33 Experimental (Type-1 electrodes) and theoretical Nyquist diagrams for a swine lung tissue

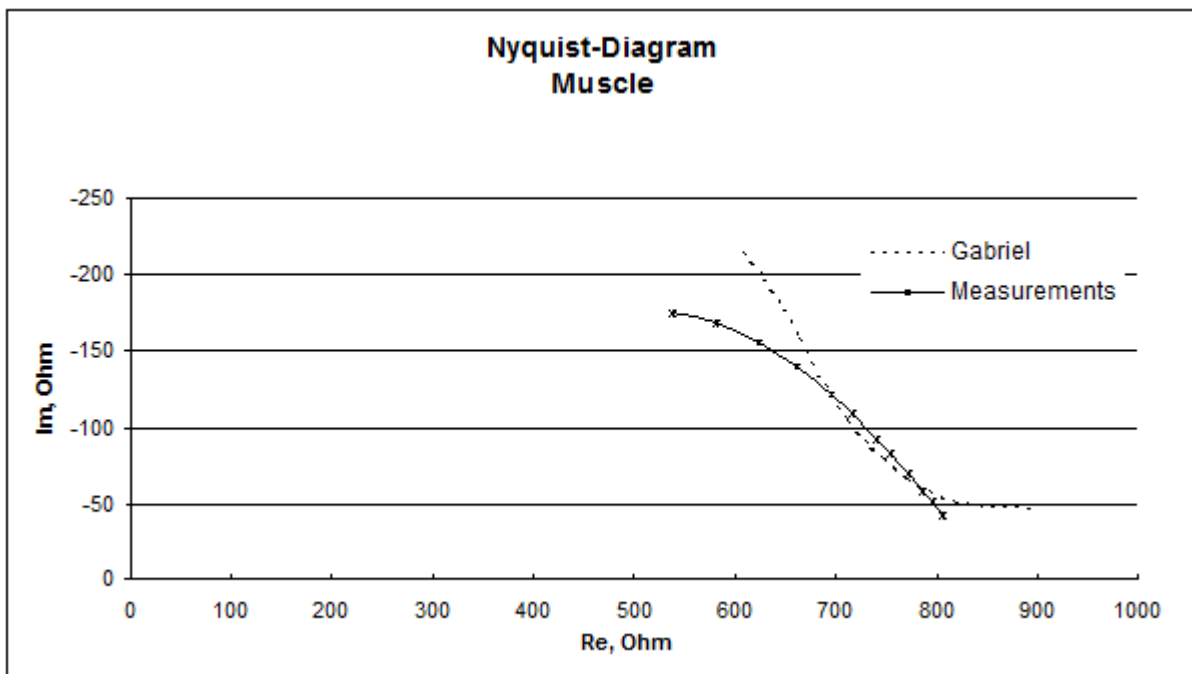


Figure 3-34 Experimental (Type-1 electrodes) and theoretical Nyquist diagrams for a swine muscle tissue

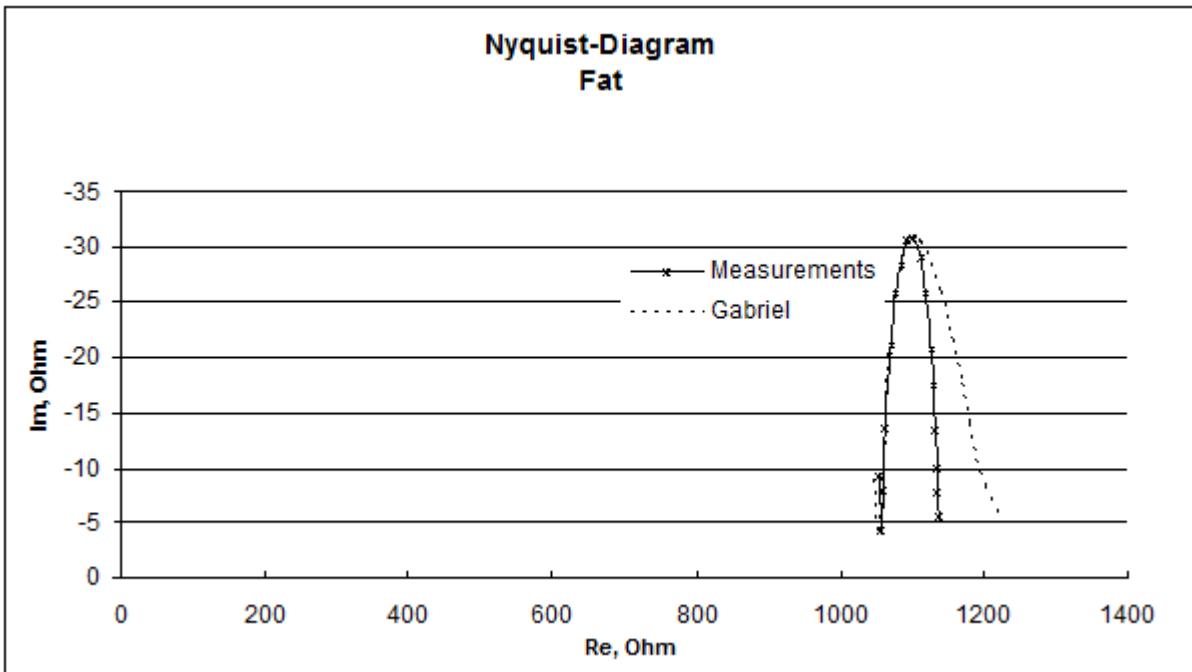


Figure 3-35 Experimental (Type-1 electrodes) and theoretical Nyquist diagrams for a swine fat

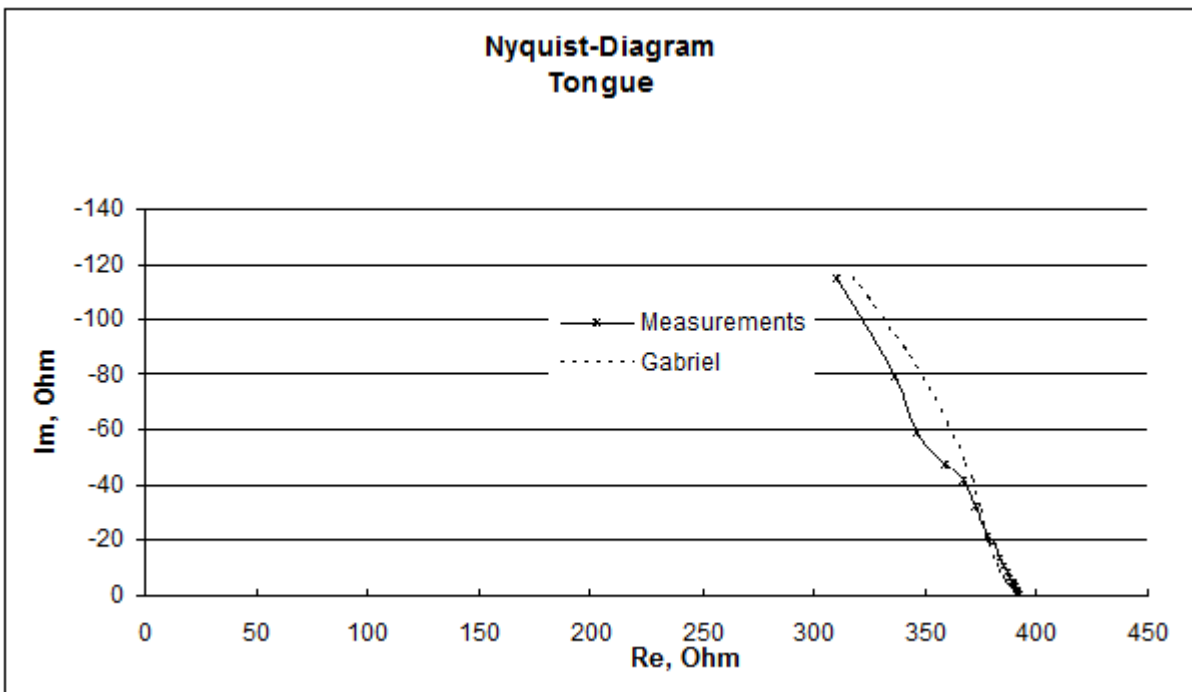


Figure 3-36 Experimental (Type-1 electrodes) and theoretical Nyquist diagrams for a swine tongue tissue

The following figures show the Nyquist-diagrams both for measured and theoretical (i.e. the Gabriels' data) for the experiments with the human autopsy tissues (24 – 48 hours post mortem).

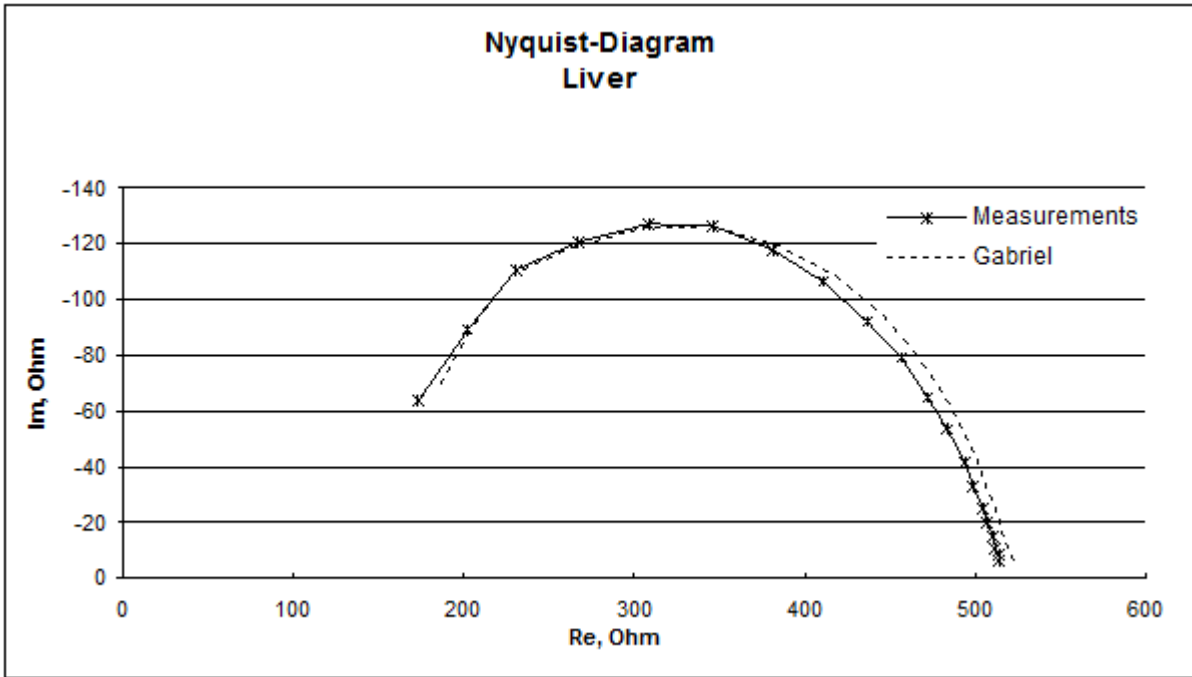


Figure 3-37 Experimental (Type-2/ 80mm electrodes) and theoretical Nyquist diagrams for a liver tissue of an adult

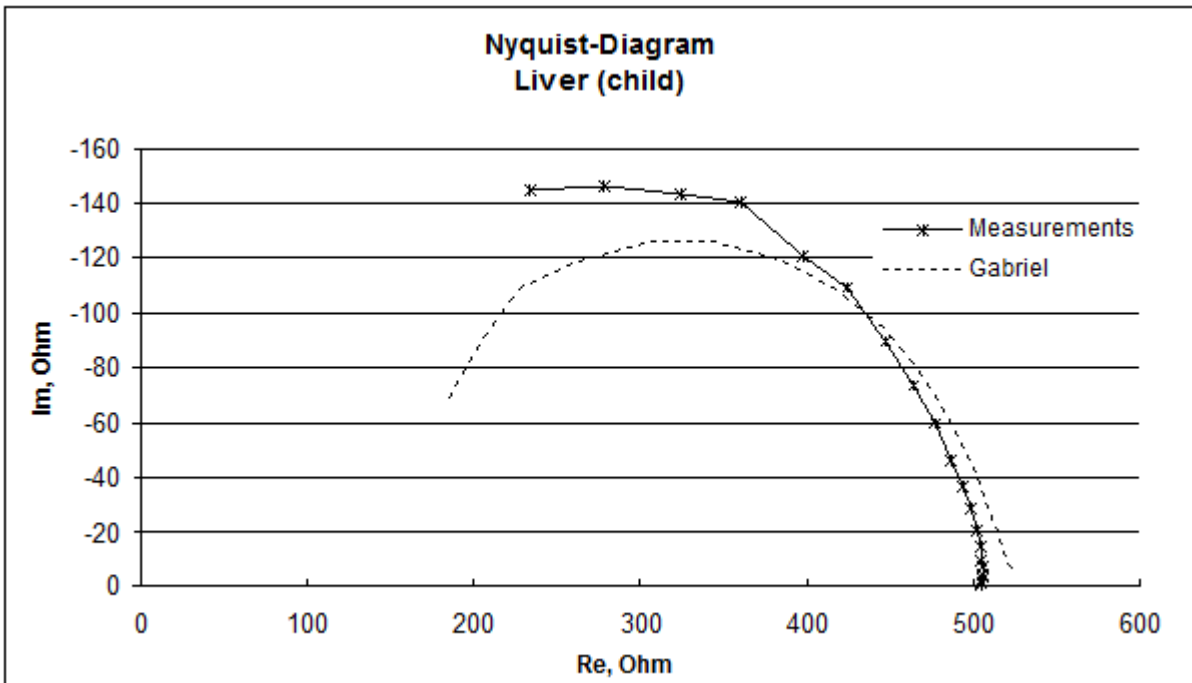


Figure 3-38 Experimental (Type-2/ 80mm electrodes) and theoretical Nyquist diagrams for a liver tissue of a child

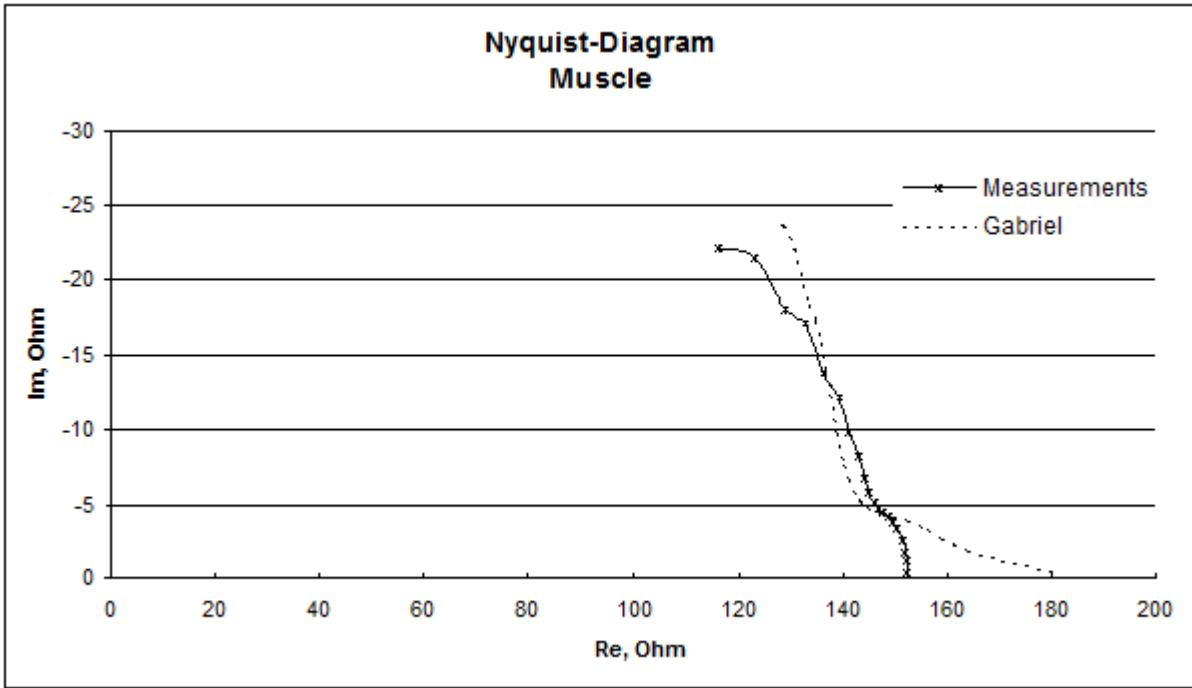


Figure 3-39 Experimental (Type-2/ 80mm electrodes) and theoretical Nyquist diagrams for a muscle tissue of an adult man

Validation of the simulation

The results of measurements on liver appeared to be the closest to the Gabriel data. Therefore it was decided to perform the simulation validation using a liver model.

The geometry of the model designed in SEMCAD is presented on the figure 3-40. The figure shows also the displacement of 2 measuring and 2 excitation electrodes.

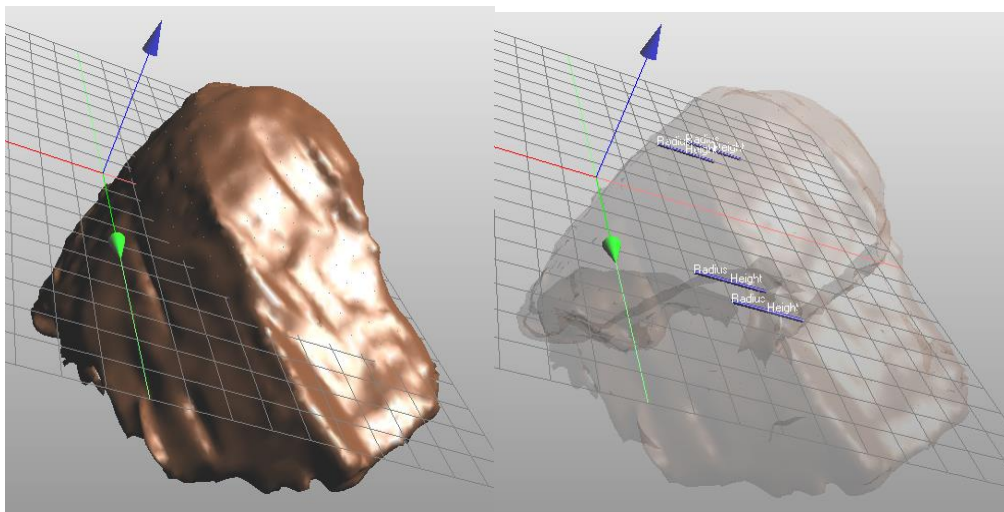


Figure 3-40 SEMCAD model: liver with the electrodes set-up

Figures 3-41 and 3-42 demonstrate the result of the simulation in SEMCAD for an excitation signal of 1.2 V.

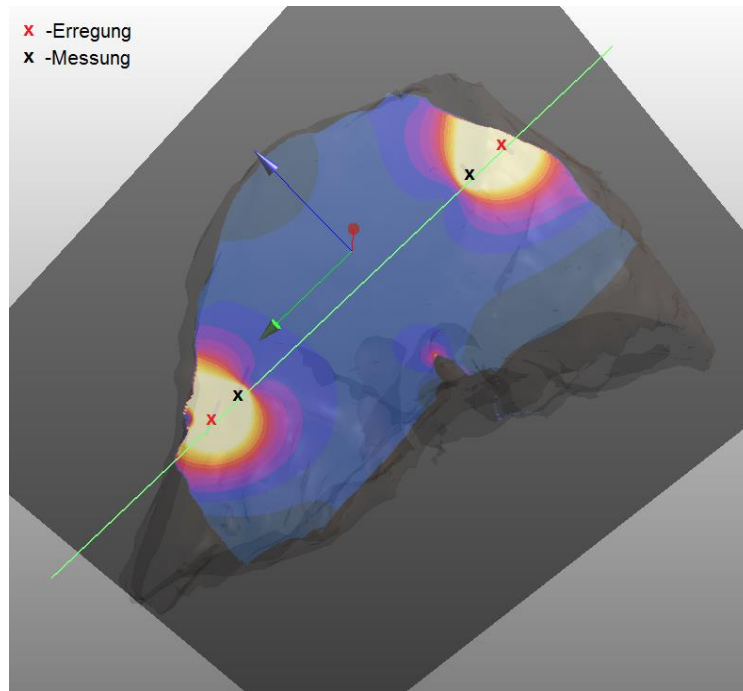


Figure 3-41 Electric field distribution simulated in SEMCAD

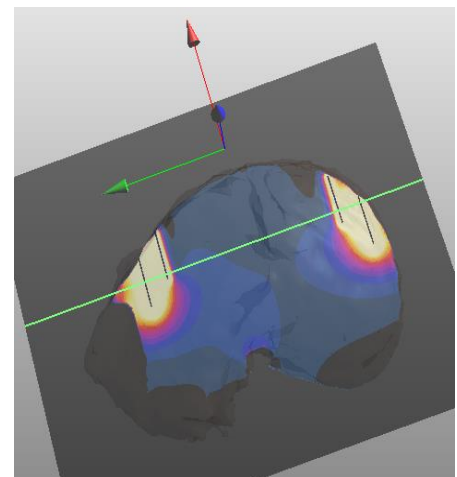
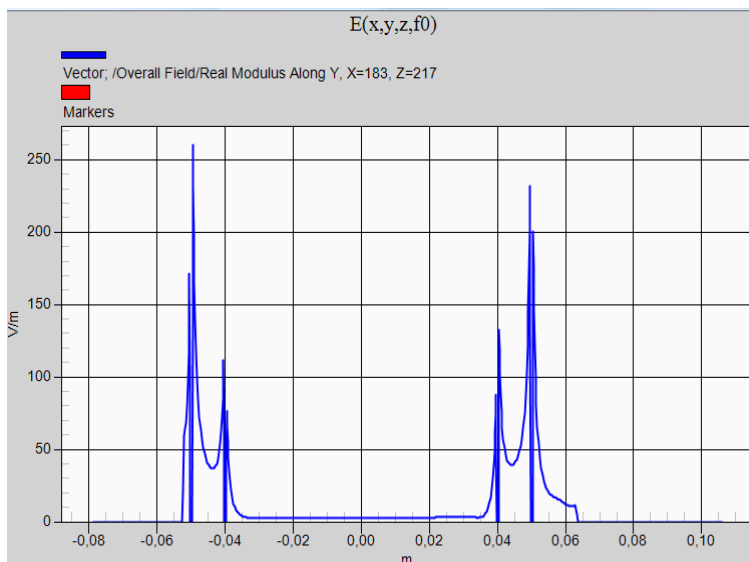


Figure 3-42 Electric field distribution between the electrodes in the simulation at 11.3 kHz

As it can be seen on the diagram the strength of the electric field around the measurement electrodes was calculated as $E = 70 \div 75 \text{ V/m}$.

This result was compared with the measured value:

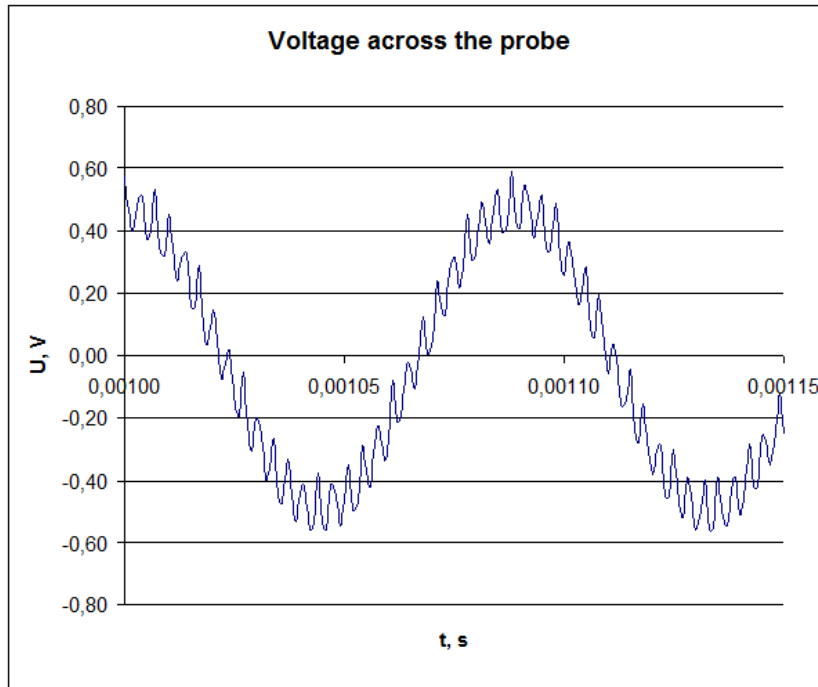


Figure 3-43 Measured voltage across the probe at 11.3 kHz

The maximal measured voltage was $U_{MAX} = 0.56V$. It was assumed that the liver is a homogeneous medium and therefore the electric field is distributed uniformly. This allowed calculating the electric field strength near to the measurement electrodes separated by 80 mm from each other as following

$$E = \frac{U}{l} = 70 V/m .$$

The divergence between the simulated and measured values for the strength of electric field between the electrodes is less than 8%. That allowed us to conclude that the model and the simulation method are accurate.

3.3.3 Simulation results

The aim of the simulations was to investigate the effects of EID impulses in a human body. The influence on the heart was of a special interest. Additionally the influence of different factors was analysed. Such factors like electrodes position on the body and their displacement, the penetration depth of the electrodes, and thick clothing (modelled as increased resistivity of the skin layer) were considered.

Penetration depth appeared to be a significant parameter: depending on how deep a dart goes

and consequently which tissues are being damaged, the conductivity of the current path can change a lot. However, it appeared to be less relevant for the lower dart, if it lands on the lower abdomen area or beyond the chest area. Depending on the displacement of the darts relative to the heart (see table 3-2 and 3-3), the deeper penetrating (3 mm) darts can deliver up to 5 times more charge than the darts that stay within the skin layer (1 mm).

The effects on the heart for front and back shots differed a lot: the values of the electric field were approximately 2.5 (male) and 3.8 (female) lower for dorsal applications (see table 3-4).

Table 3-2 Electric field strength E in the muscle layer for different darts' penetration depth (PD)

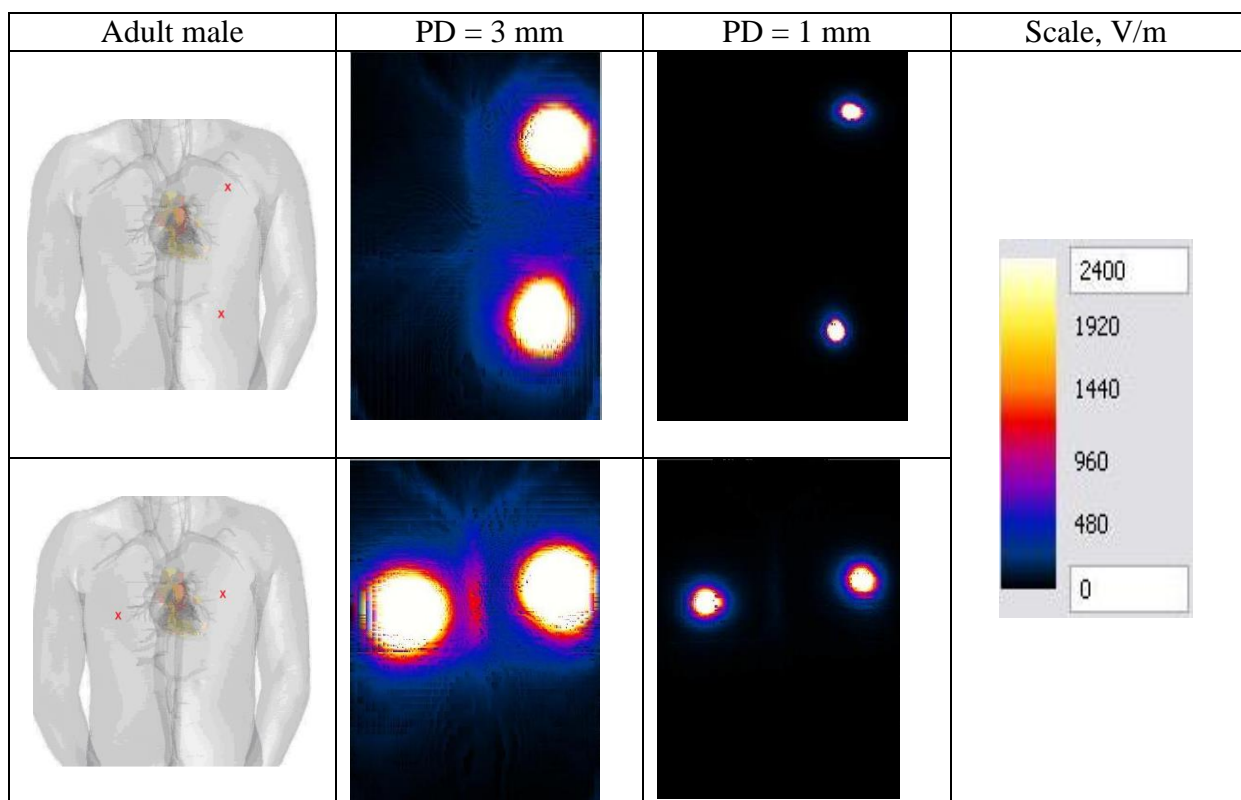
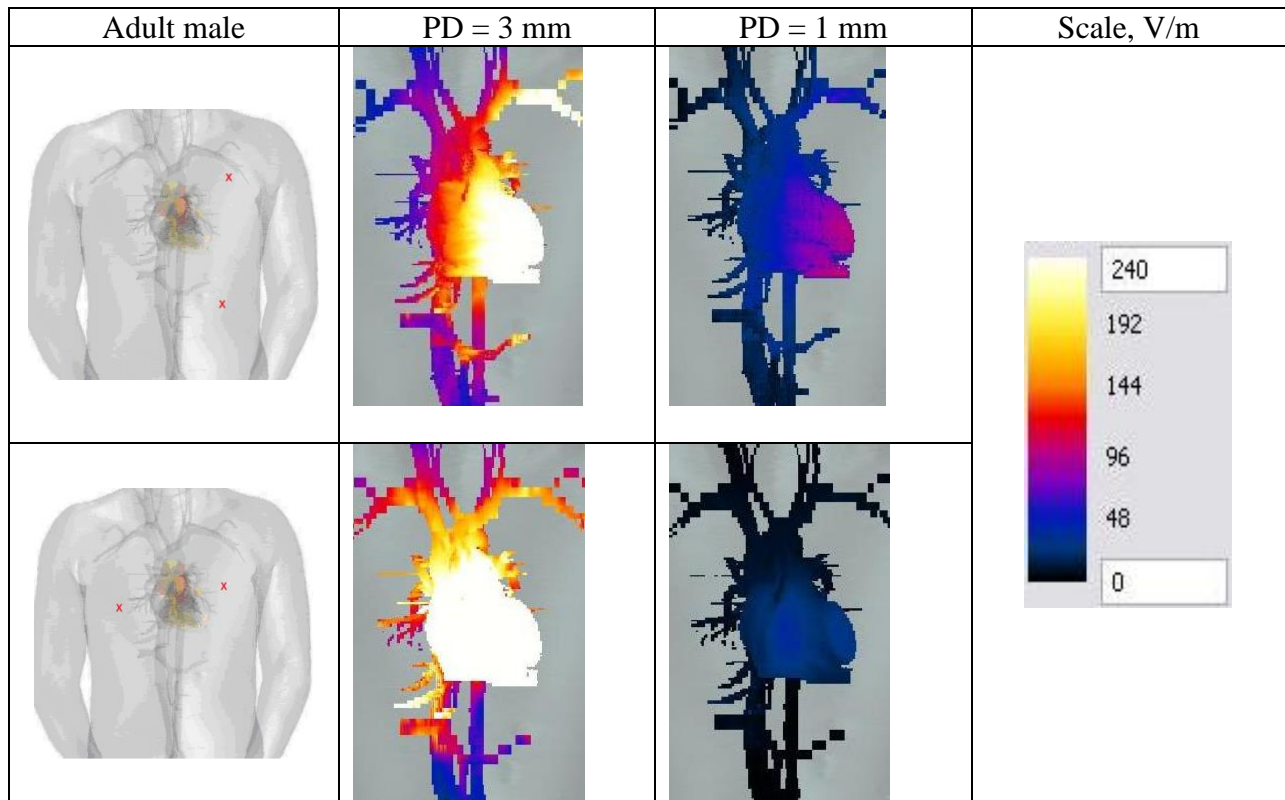


Table 3-3 Electric field strength E on the heart surface for different darts' penetration depth (PD)



The influence of the body constitution was investigated using the Virtual Family models. The simulation results showed the highest values in the youth female model: The thin inner layers of skin and fat let the electrical field get deeper and deliver higher current and charge to the heart surface. In case, when the upper dart lands on the breast area, the heart of an adult female was not very exposed presumably because of the additional fat mass in the breast area. So the heart of an adult woman was less exposed than the heart of an adult man (see table 3-5).

Table 3-4 Characteristics of the electric field (E , J , D) in different tissues for front and back shots in male and female models

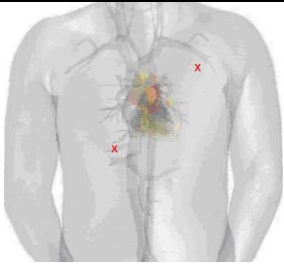
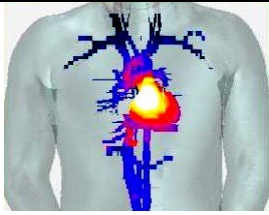
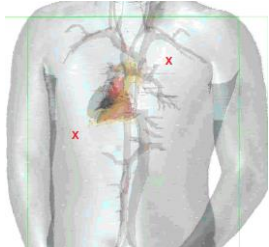
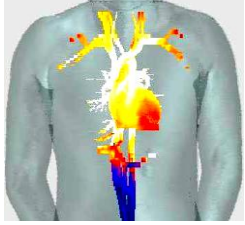
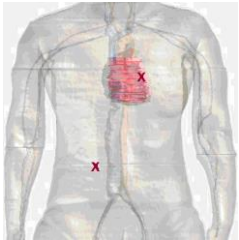
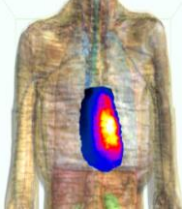
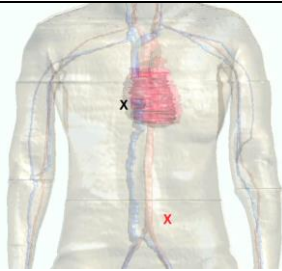
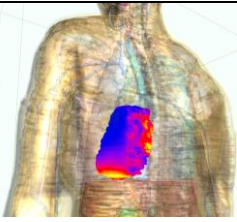
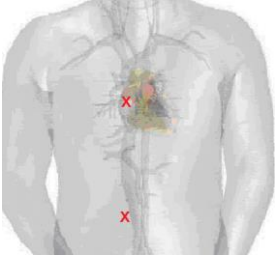
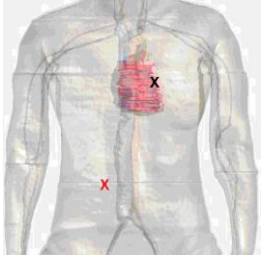
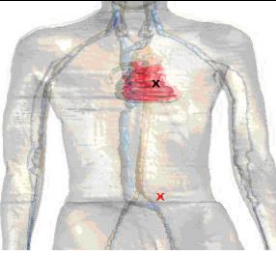
| Model | Tissue | E , V/m | J , A/m ² | D , As/m ² | Field propagation on the heart surface |
|---|--------|-----------|------------------------|-------------------------|---|
|  Front Male (M27) | Skin | 2100 | 100 | 0,005 |  Scale max. 650 V/m |
| | Muscle | 1350 | 550 | 0,0025 | |
| | Heart | 650 | 250 | 0,001 | |
|  Back Male (M06) | Skin | 1000 | 300 | 0,0002 |  Scale max. 200 V/m |
| | Muscle | 800 | 450 | 0,004 | |
| | Heart | 200 | 150 | 0,0004 | |
|  Front Female (F01) | Skin | 7000 | 400 | 0,005 |  Scale max. 300 V/m |
| | Muscle | 7000 | 700 | 0,05 | |
| | Heart | 300 | 150 | 0,0046 | |
|  Back Female (F03) | Skin | 2000 | 400 | 0,0003 |  Scale max. 300 V/m |
| | Muscle | 1200 | 300 | 0,004 | |
| | Heart | 150 | 50 | 0,0012 | |

Table 3-5 The characteristics of an electric field (E, J, D) induced by EID in the heart tissues versus body constitution

| Model | $E, V/m$ | $J, A/m^2$ | $D, As/m^2$ |
|---|----------|------------|-------------|
|  Male | 1200 | 600 | 0,006 |
|  Female | 250 | 160 | 0,0046 |
|  Youth | 1200 | 2000 | 0,015 |

The results showed that the most significant parameter while considering the effect on the heart is the proximity of the darts to the heart surface. When both darts are not on the area directly above the heart, their location is not relevant. The lowest impact on the heart occurs when Taser is applied on the back of the target.

3.4 Safety analysis of Taser

A potential health harm that an EID can cause is the main concern about the EIDs use by the police. An EID as a source of electric current is hypothetically capable of causing the fibrillation of the heart ventricles. The reports of Taser fatal casualties show a high mortality rate in cases of multiple or prolonged Taser application on the target [19, 55]. Amnesty International [19] reports 334 lethal cases of Taser use in the period from June 2001 to

August 2008, 60 of them occurred when a target was tasered more than 5 times, in 12 cases among these 60 (at 20% of Taser abuse) no further contributory factors (drugs or alcohol intoxication) or underlying health conditions (heart abnormalities, psychophysical state) were present.

Several researches [56] show that there is a correlation between the duration of the electric current flowing through the human body and the mortality probability (see 3-44). The probit model shows a linear dependency between the mortality probability and the duration of the current for both high and low voltage currents.

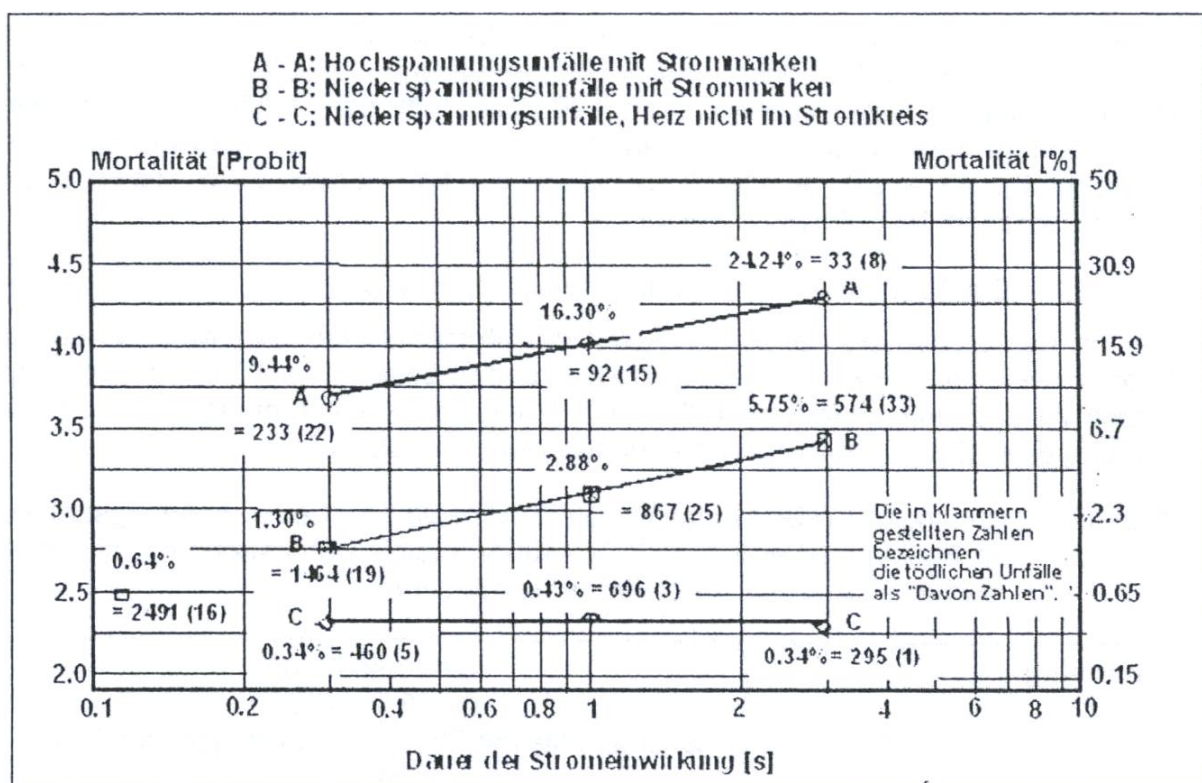
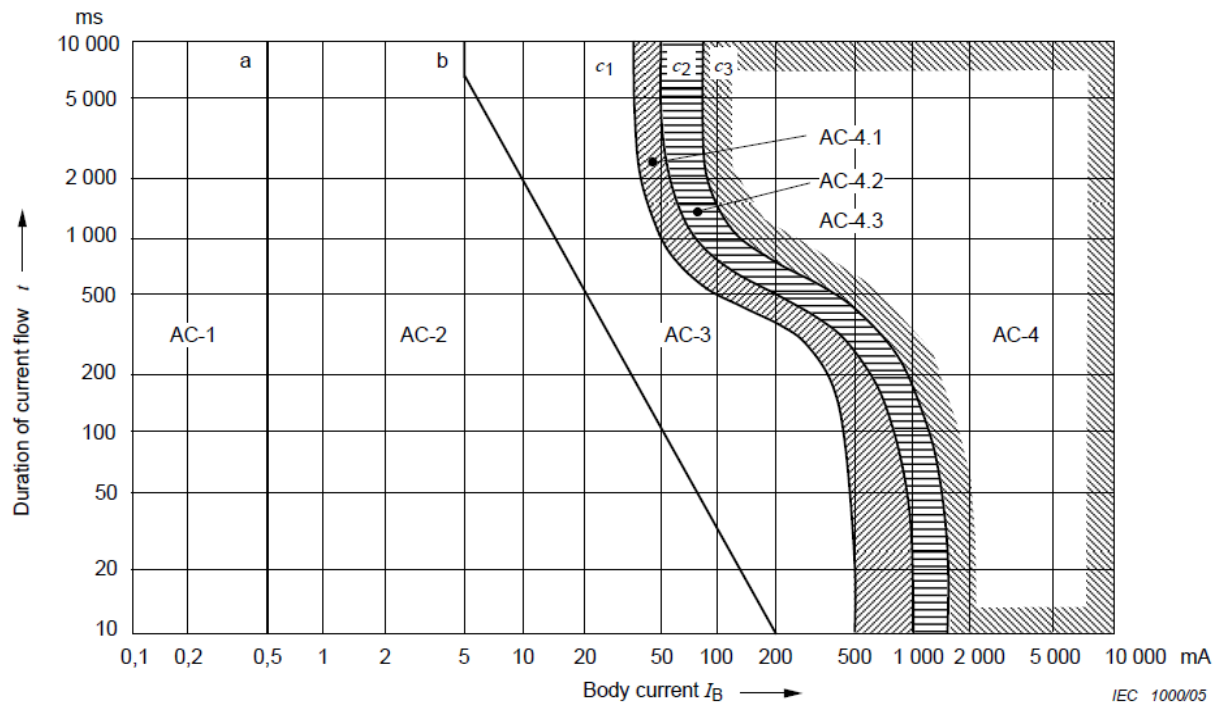


Figure 3-44 Mortality depending on the flowing current's duration – electrical accidents caused by the flowing current's duration and intensity [56]

Triggering of a ventricular fibrillation is one of the main lethal effects of electric current. VF is a "turbulent, disorganized electrical activity of the heart" [57]. Such an activity prevents an effective blood circulation and can lead to a sudden cardiac death, which when not treated within ca. 5 min will lead to cerebral hypoxia and irreversible brain damage. A death can occur within 90 seconds after VF, if the rhythm transforms into asystole. Therefore VF is an emergency and must be treated rapidly in order to save the person's life.

The International Electrotechnical Commission developed and published safety standards

IEC 60479 “Effects of current on human beings and livestock”. In this document 4 zones are defined to describe the effect of electric current depending on its amplitude and duration [41] including the thresholds for ventricular fibrillation.



AC-1: perception possible but usually no “startled” reaction

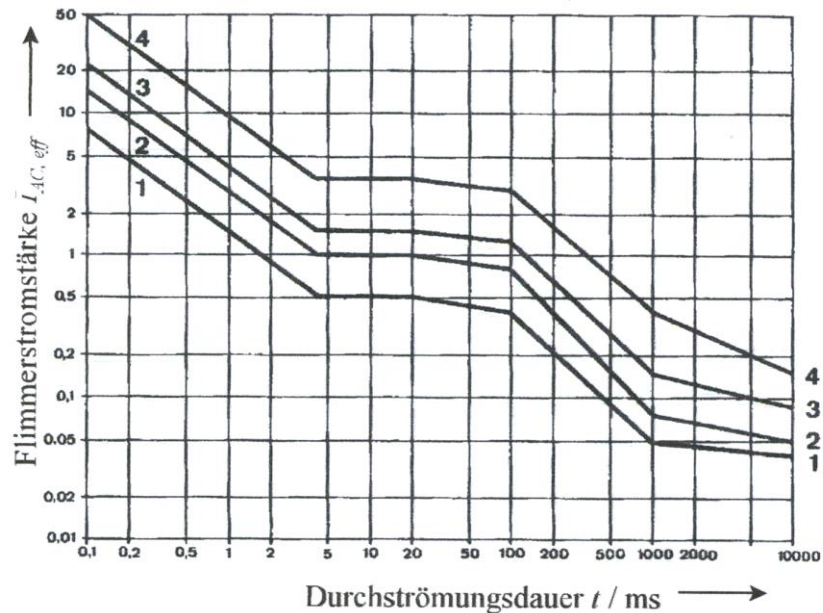
AC-2: perception and involuntary muscular contraction likely but usually no harmful electrical physiological effects

AC-3: strong involuntary muscular contractions; difficulty in breathing; reversible disturbances of heart function; immobilization can occur; effects increasing with current magnitude; usually no organic damage to be expected

AC-4: patho-physiological effects may occur such as cardiac arrest, breathing arrest, and burns or other cellular damage; probability of ventricular fibrillation increasing with current magnitude and time (4.1. 5% probability, 4.2. 50% probability, 4.3. above 50% probability).

Figure 3-45 Conventional time/current zones of effects of AC current (15 - 100 Hz) on persons for a current path corresponding from left hand to feet [41]

Biegelmeier [58] presents in his diagram (see Fig. 3-46) a non-linear dependence between ventricular fibrillation threshold for the current amplitude and the duration of the current flow.



1 – Safe threshold by IEC, 2 – 5% probability of VF,
 3 – 50% probability of VF, 4 - 95% probability of VF.

Figure 3-45 Thresholds for ventricular fibrillation for humans with normal state of health [58]

The diagram shows, that the safe amplitude (not causing ventricular fibrillation) of an electrical current, which flows through a body, is approximately 300 times higher for currents flowing for very short time (up to 1 millisecond) comparing to the ones flowing much longer (over 100 milliseconds).

Thus there is a hypothesis that the effect of the electric current can be evaluated by the delivered charge [59]. The charge delivered by a current is an integral of this current in time, therefore a high short current delivers the same amount of charge as a current proportionally smaller and longer.

A limited safety analysis of the EID was performed with two different approaches.

In the first attempt the developed 3D CAD model for a human-EID interaction was used to evaluate the safety of an EID. The effects of the electric current, which corresponds to the safe IEC threshold for VF, were simulated and compared with the results obtained in the earlier simulations for EID.

The second approach was based on the hypothesis that electric charge and energy can measure the effect of electric current on humans.

3.4.1 Simulation of IEC thresholds for AC currents

The first approach to evaluate the safety of Taser was to simulate the effects of the currents and voltages given as ventricular thresholds by IEC to obtain the values of current and charge densities. The duration of one Taser impulse is about 120 mcs. The IEC ventricular fibrillation threshold for the shortest duration, which is 0.5 A, was employed.

This value corresponds to the left hand to feet current path. However, according to the results of our simulation, one of the most critical situations was when one of the darts was placed on the chest. So the current path through the body is different.

The IEC standard determines heart current factors for different currents paths through the body. They permit the calculation of currents I_h through paths other than left hand to feet, which represents the same danger of ventricular fibrillation as that corresponding to I_{ref} left hand to feet shown on the fig. 3-45:

$$I_h = \frac{I_{ref}}{F},$$

where

I_{ref} – the body current for the path left hand to feet given in the fig. 3-45,

I_h – the body current for other path,

F – the heart-current factor.

There are several examples of different current paths and corresponding values of heart current factor and body currents, represented in the table 3-6 [41].

For example, a current of 225 mA (I_h) hand to hand has the same likelihood of producing ventricular fibrillation as a current of 90 mA (I_{ref}) left hand to both feet.

Table 3-6 Heart current factor F for different current paths

| Current path | Heart current factor F |
|--|------------------------|
| left hand to left foot, right foot or both feet | 1.0 |
| both hands to both feet | 1.0 |
| left hand to right hand | 0.4 |
| right hand to left foot, right foot or both feet | 0.8 |
| back to right hand | 0.3 |
| back to left hand | 0.7 |
| chest to right hand | 1.3 |
| chest to left hand | 1.5 |
| seat to left hand, right hand or both hands | 0.7 |
| left foot to right foot | 0.04 |

Thus, the standard value had to be corrected by dividing it by the current-path factor of 1.3. This resulted in 0.4 A. In the simulation the voltage of 240 V, calculated for an average chest resistance of 600 Ohm, was applied.

A 50 Hz signal of 240 V amplitude and 120 mcs duration was simulated. The table 3-7 represents the effect of this current on the heart surface.

Table 3-7 Results of simulation of IEC-threshold currents on the heart surface

| Parameter | Ella | | Duke | |
|----------------------|-------|-------|------|-------|
| | front | back | font | back |
| E, V/m | 65 | 10 | 100 | 30 |
| J, A/m ² | 7 | 1 | 20 | 3 |
| D, As/m ² | 0.015 | 0.003 | 0.04 | 0.008 |

Following the hypothesis that charge is a measure for the electric current effects on human, only the charge density was considered. The values of electric field strength and current density were 10-20 times less than predicted by the simulations for Taser impulse. That would mean that Taser is lethal.

The values of charge densities on the heart surface produced by house-hold current with the amplitude at which VF could occur provided the safety margins up to fold 10 for a single Taser series both for male and female models.

3.4.2 Evaluation of the delivered energy as a measure for damage

This approach searches for a measure that could evaluate the “damage” of electric current to a person using an analogy for a mechanical damage.

There is a so-called ISO-damage model [60] based on the mechanical model of damage that correlates the maximum overpressure and specific damage impulse, and defines this as a damage number:

$$DN_{mech} = (p - p_{critical})(I - I_{critical}),$$

where p represents the pressure and I stands for mechanical impulse.

The formula reflects the energy transformation, which occurs when two objects interact. Therefore if one draws an analogy for a damage of other nature, e.g. caused by electrical field, one can get the following equation:

$$DN_{electical} = (U - U_{critical}) \cdot (Q - Q_{critical}),$$

where U stands for voltage and Q represents the charge.

In order to reveal the effects of frequency and amplitude of the electric current, it can be reformulated as follows:

$$DN_{electical} = (U - U_{critical}) \cdot \left(\frac{1}{\omega} \cdot I_{avg} - \frac{1}{\omega} \cdot I_{critical} \right).$$

These equations show that the alteration of the energy in the system stands for the measure of the damage.

This concept is supported by several scientists in the field of applied biomedicine. There are suggestions to use power of the electric current or its energy as the measure of the effect of electric current on humans [59, 61], especially while considering pain sensation [59].

Therefore, it was decided to calculate the energy delivered by the EID and to compare it with the energy, delivered by IEC VF threshold current during the same time period.

This approach allowed us to consider the effect of multiple impulses during the full operation cycle of Taser X26 (5 seconds).

Single Taser X26 cycle

a) The energy delivered by Taser within its 1 cycle (5 seconds) was calculated as shown on the fig.3-47. The resulting energy delivered by Taser X26 within its cycle $W_{TASER1} = 6.02 \text{ J}$.

b) Ventricular fibrillation (VF) thresholds (fig. 3-46) were calculated for two curves: the safe threshold curve (marked as 1 on the fig. 3-46) and the curve for the 95%-probability of VF (marked as 4 on the fig. 3-46).

On the safe threshold curve the effective amplitude of current $I_{eff} = 0.04 \text{ A}$ corresponds the current duration of 5 seconds. The energy delivered during the 5 seconds-period by the given current was estimated with the help of the following formula:

$$W = \int_0^5 \left(\sqrt{2} I_{eff} \sin(2\pi ft) \right)^2 R dt ,$$

where $I(t) = \sqrt{2} I_{eff} \sin(2\pi ft)$ is the AC current with frequency $f = 50 \text{ Hz}$ (see fig. 3-48), $R = 1 \text{ k}\Omega$ is the assumed bioimpedance.

The safe energy threshold for 50 Hz AC current was calculated as $W_{VF \text{ Safe}} = 9.36 \text{ J}$.

The effective current of 0.2 A corresponds to the 5s current duration on the curve for the 95%-probability of VF. This results in the energy threshold of $W_{VF 95\%} = 234.2 \text{ J}$.

The obtained results show, that 1 cycle of Taser impulses delivers 35% less energy than it is supposed to be safe: $W_{TASER1} = 6.02 \text{ J}$ versus $W_{VF \text{ Safe}} = 9.36 \text{ J}$.

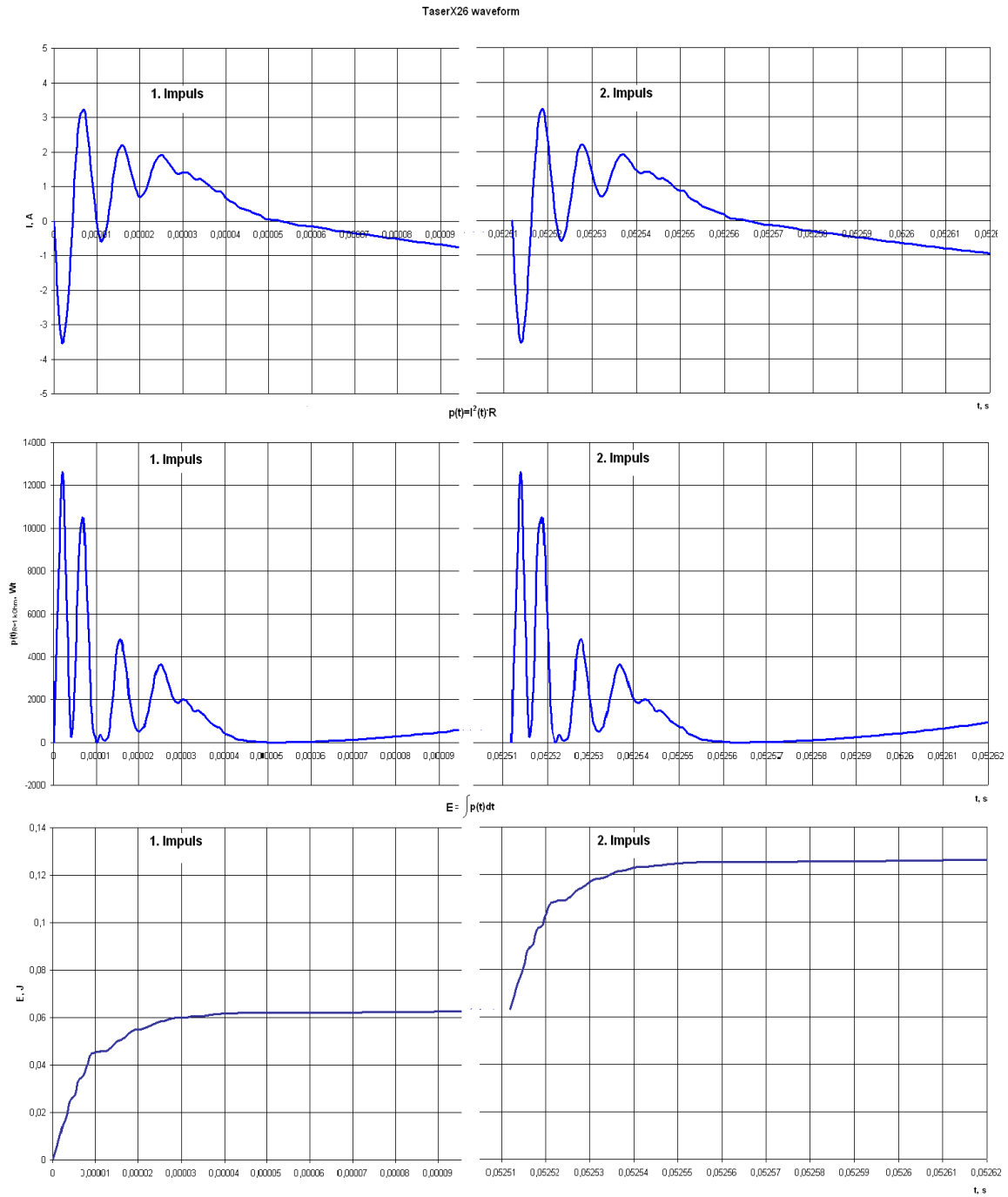


Figure 3-47 Taser X26 waveforms for signal current, power and energy

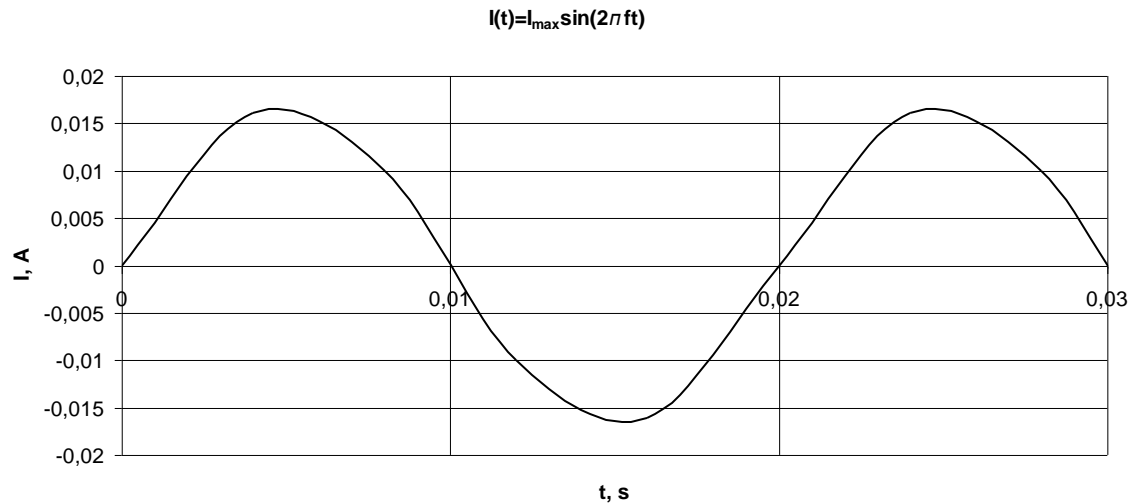


Figure 3-48 AC current waveform, 50 Hz, $I_{\max}=0.016$ A

Prolonged action of Taser X26

Earlier the statistics of the lethal accidents following Taser use was presented. It was concluded that there was a significant percentage of mortalities occurring after more than 5 Taser shots. Therefore the duration of 5 cycles was assumed as a prolonged Taser use.

The energy delivered by Taser within 5 cycles, assuming that it is fully accumulated, is then equal to $W_{TASER5} = 30.1$ J.

To obtain the VF threshold values corresponding to the duration of 25 seconds the interpolated curves was used. The forecasted values were 0.035 A for the IEC safe curve and 0.075 A for the curve for the 95%-probability of VF.

The energy levels were calculated as previously described:

$$W_{VF\ Safe\ 5} = 35.9\text{ J}$$

$$W_{VF\ 95\%\ 5} = 164.6\text{ J.}$$

Thus the prolonged use of Taser appeared to be safe with the 16% safety margin.

4. Discussion

The described implementation of the new design procedure for an advanced EID showed both the benefits of the systematical approach and the weak points.

The main advantage of the procedure is the use of the structured knowledge relevant to a given stage of the developmental process.

Analysis of the operational scenarios and the previous experience (with no non-lethal options or different NLWs) allows to define the needs and requirements for the non-lethal impacts, taking into account the real environmental and operational conditions and the possible side effects. Additionally it enables the analysis of the needed feed-back features and of the possibility to combine several non-lethal effects.

Simulation of the effects provides essential information for a safety and efficiency analysis of a designed NLW, and also shows its sensitive sides.

However there is a weak point in the procedure – the availability of the information, which completes the knowledge base. The lack of the operational data decreases the efficiency of the very first stage of the procedure. The lack of technical and medical data, the thresholds and norms for a certain effect complicates the modelling and simulation process and the safety analysis of the future NLW.

Therefore, in order to perform the development according to the procedure, it is important to complete it with the following research activities:

- a) Search for and accumulation of the NLWs-relevant information from scientific and industrial sources, expert knowledge, operational and training reports;
- b) Classification and processing of the information, in order to recognize operational patterns;
- c) Matching the available NLWs to the operational scenarios and patterns;
- d) Accumulation of available knowledge about incapacitating effects, especially in respect of their health effects;
- e) Search for novel efficient and low risk effects;
- f) Broadening the palette of employed simulation-tools for modelling of the effects of NLWs and their combinations;
- g) Development of the standards and norms for the non-lethal effects.

The latter is a critical point for a successful safety and efficiency analysis of non-lethal effect

at the stage of modelling and simulation. The impact of an NLW depends on the intensity or dosage of the basic effect. The low dosage leads to a safe but inefficient deployment. The high dosage may lead to an efficient but dangerous and even lethal outcome. The standards and norms define the thresholds for inefficient and dangerous intensities of an effect. Applying those standards in a model prevents a developer from crucial mistakes.

The lack of the recognised standards is obvious in case of EIDs. Whereas the norms for household and industrial current sources are well established and are available internationally, there is no consensus on the safety thresholds for short high voltage impulses as those of Taser.

In this research the ventricular fibrillation (VF) thresholds for a 50/60 Hz current were adopted. However, there are a number of studies, where different approaches were used.

Sun et al [1] were among the pioneers to perform modelling of neuromuscular stimulation by Taser and to evaluate the probability of VF after a Taser application. In a multistep process the maximum probability of VF induced by Taser was estimated as 0.0008 with a standard deviation of 0.002.

The initial point of those studies was a calculation of the threshold charge and current densities, which would produce a VF of a heart, for 1 A excitation current. Following these values were applied in the computer finite-element (FE) models in order to find the threshold dart-to-heart distance.

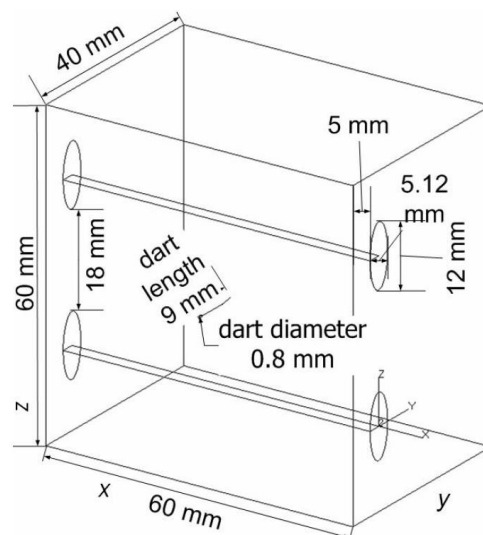


Figure 4-1 Cuboid model of torso representing muscle tissue pierced by two elliptical ribs [1]

Two models of a human torso were used for this purpose. The first one was a cuboid model of torso with the dimensions of 60 x 40 x 60 mm (see fig. 4-1). Two different tissues were created: muscle and ribs. A single 9 mm long dart penetrated the muscle. The conductivities of the tissues were set for the frequency of 5 kHz according to the Gabriels' data. A source voltage (+5 V) was assigned to the dart surface, a sink voltage (-5 V) was assigned to the skin without the dart.

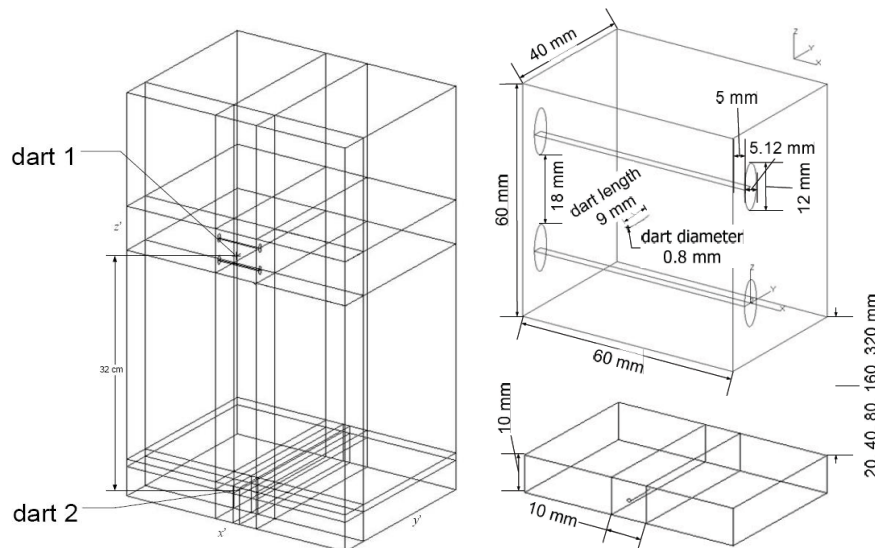


Figure 4-2 Cuboid torso model with two darts [2]

The second model was similar to the first one. It was a cuboid torso with the dimensions of 320 x 240 x 550 mm. However in this model two darts were represented: one dart inserted on the torso surface over the heart and the second dart placed 32 cm lower (see fig. 4-2). The conductivities of the muscle and ribs were set for the frequency of 5 kHz. The stimulating current of 1 A DC was set for the darts.

The values of the dart-to-heart distance were then used in the pig experiments [2], where real Taser X26 impulses were applied, in order to find the threshold current and charge densities for a single Taser X26 impulse.

Finally the obtained values were used in the third model of a human torso (see fig. 4-3), in order to evaluate the probability of VF after a Taser application. The third model was based on the three-dimensional realistic model of human torso developed by Utah University [3].

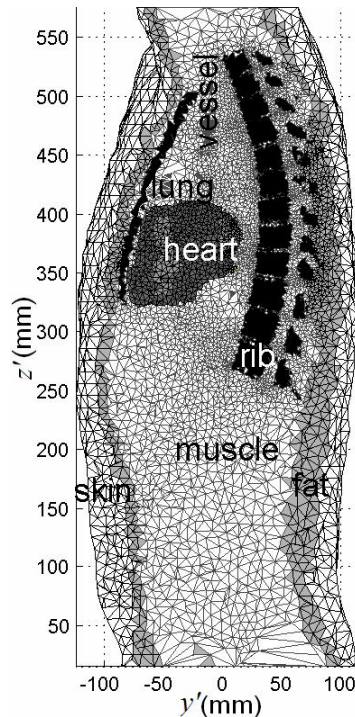


Figure 4-3 Utah model of a human torso [1]

The model included nine tissues: skin, fat, muscle, lung, heart muscle, heart chamber, fat pad, vessel, rib. However, the properties of skin, fat and fat pad were all considered to have the same properties of fat. The conductivities of the tissues were set for 5 kHz. The darts were assigned as a DC current source with an amplitude of 1 A. Therefore, in those studies a real Taser impulse was never modeled, but substituted with a 1 A DC current.

Stratbucker et al [4] used a VF threshold current density developed by Sun et al [16] to compare it with the simulation results.

They used 3D FE cone model (see fig. 4-4), which included several tissues: muscle (neck, shoulder, limbs), bone (spine, ribcage), heart, lungs, skin (fat) and abdomen.

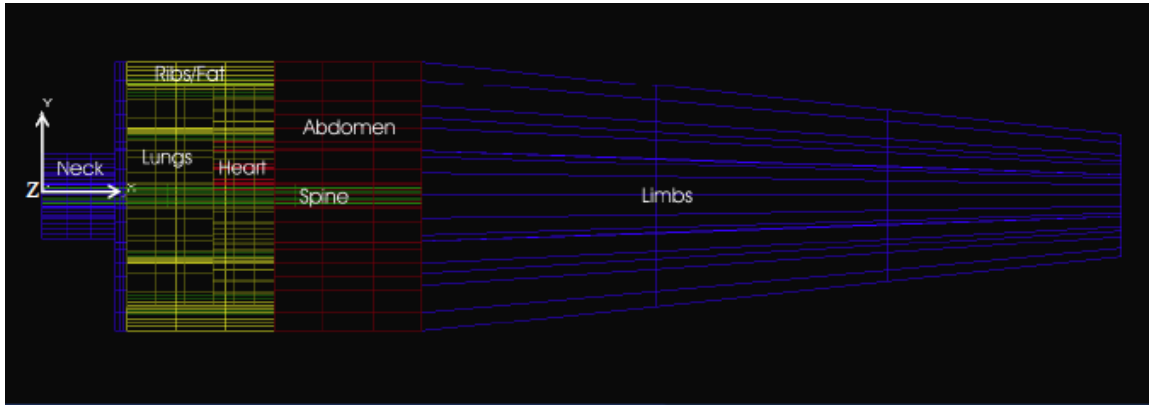


Figure 4-4 Three-dimensional FE model by Stratbucker [4]

Two Taser darts were modeled as a voltage source and placed approximately 70 mm apart. The voltage boundary conditions were used for the darts and the value of voltage was set at 100 V. Tissues properties were set as the following: muscle – 0.667 S/m (long) and 0.05 S/m (trans.), bone – 0.006 S/m, heart – 0.5 S/m (long) and 0.25 S/m (trans.), lungs – 0.083 S/m, skin (fat) – 0.05 S/m, abdomen – 0.167 S/m.

As a result, the distribution of the excited electric field was obtained. The maximum electric field strength was calculated as 12 V/m. The corresponding maximum current density was calculated as 0.0027 mA/mm^2 (assuming the heart resistivity as $450 \text{ Ohm}\cdot\text{m}$). This current density was 500 times lower than the VF threshold, and even lower than a threshold for myocytes excitation.

Holden et al [5] used the results of the simulations in the experiments with bare guinea pigs' hearts in order to estimate the safety margin of Taser. A 3D realistic human body model, which is referred as Dstl BooleanMan [6], was used. There were 12 tissues represented: fat, muscle, skeleton, brain (grey matter), heart, intestines, kidneys, liver, lung (inflated), pancreas, spinal cord and stomach. Their electromagnetic properties were set for 120 kHz according to the Gabriels' data for the dielectric properties of human tissues. Darts were modeled as two cuboids. The 120 kHz sine-wave with a peak voltage of around 300 V and duration of $120 \mu\text{s}$ was applied as the darts boundary conditions. The simulating was performed based on the transmission line matrix method.

The current density distribution around the heart area was analysed. The peak absolute current density found around the heart was 0.11 mA/mm^2 . The electric current of this density did not cause a VF when applied to a bare guinea pig's heart. A safety margin of 60-fold was

defined for Taser X26 in the experiments with guinea pigs.

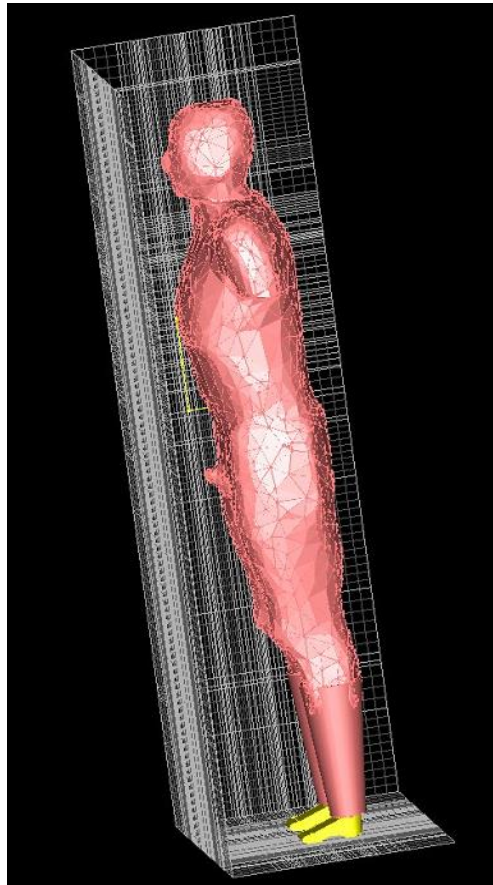


Figure 4-5 Dstl BooleanMan [6]

Leitgeb et al [7-10] derived a VF threshold for a single Taser impulse based on the cellular excitation threshold current density. They assessed the probability of VF after a Taser application taking into account the ventricular volume exposed to the currents with the threshold density.

In their studies a detailed anatomical model NORMAN (see Chapter 2) was used. This model includes 35 different tissues. The Taser impulse was approximated as a sine wave with a frequency of 18.4 Hz. The dielectric properties of the tissues were set for this frequency according to the Gabriel's data. The finite integration method was used to perform the calculations.

They could not exclude the risk of VF after a Taser application [10]. They estimated the probability of VF to be between 5% and 30% [7], depending on the dart-to-heart distance [7] and on the individual characteristics of a person [8].

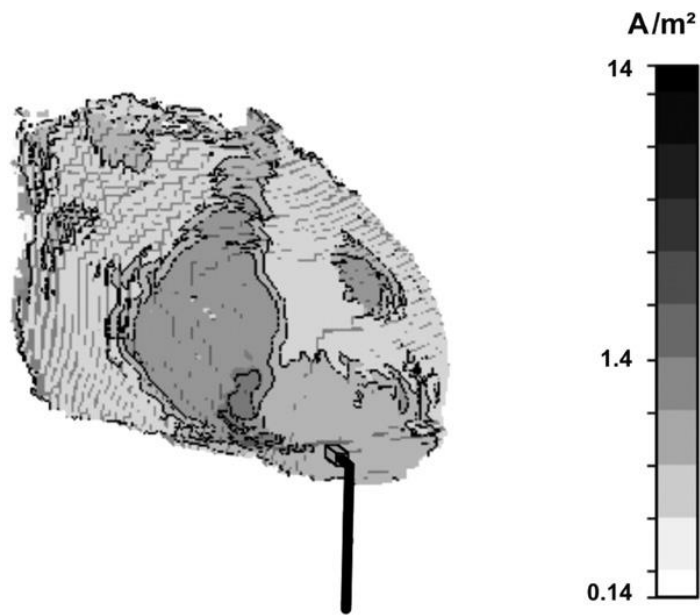


Figure 4-6 Current density distribution on the heart [10]

They also assessed the possibility of Taser interference with implanted cardiac pacemakers. They concluded that Taser is able to induce interference voltages, which may cause irreversible functional changes or damage of an implanted cardiac pacemaker, when applied in a contact mode on the upper part of the body (both frontal and dorsal) [9]. On the contrary, in a dart mode, it was found irrelevant [8]. However, it was found possible that a transient interference and capturing can take place [8].

There were other studies investigating the effects of Taser's current on heart and muscles with the help of modelling.

Mayhew [11], Singh [12] and Kwatra [13] performed an analysis of the effects of electric current produced by EID using an anatomical model of the human torso provided by the Naval Health Research Center Detachment. The model is based on the Visible Human Project (see Chapter 2) and represents 10 tissues.

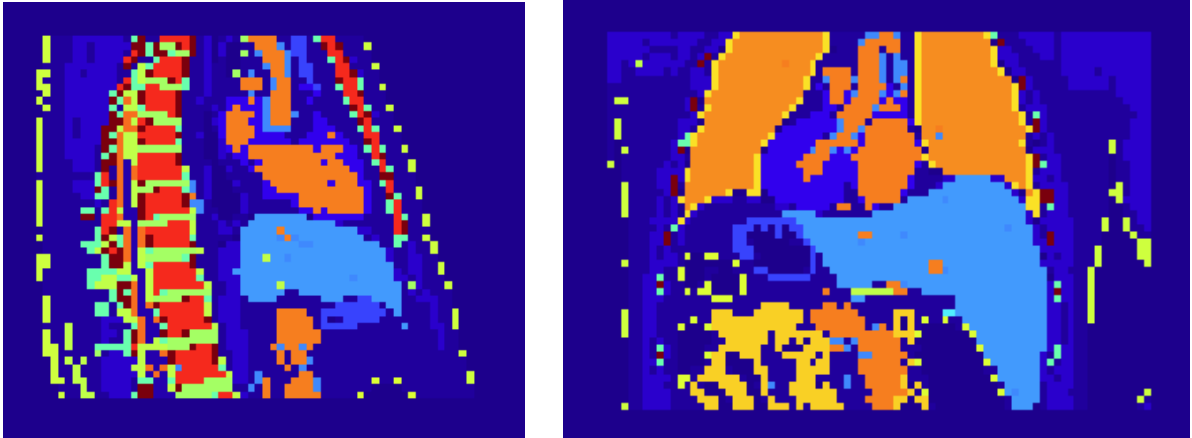


Figure 4-7 Vertical cross-section of model: torso seen from the side and from the front [11]

The fundamental frequency of the Taser impulse was selected as 120 kHz. The dielectric properties of the tissues were set for this frequency according to the Gabriel's data. The Taser impulse was modeled as a Gaussian pulse.

The average current density in the heart was estimated as 0.0662 mA/mm^2 for an excitation current of 3 A. No conclusion about the Taser's safety was stated.

Additionally the analysis of the sensitivity to different parameters was performed: darts separation, darts penetration depth (also imitating different clothing thickness), variation of dielectric parameters of tissues (including dry and wet skin).

Panescu et al [14] investigated the effects of Taser impulses on muscles in order to evaluate its neuromuscular activation efficiency. A 3D FEM model with dimensions of 150 mm x 50 mm x 20 mm (see fig. 4-8) was designed.

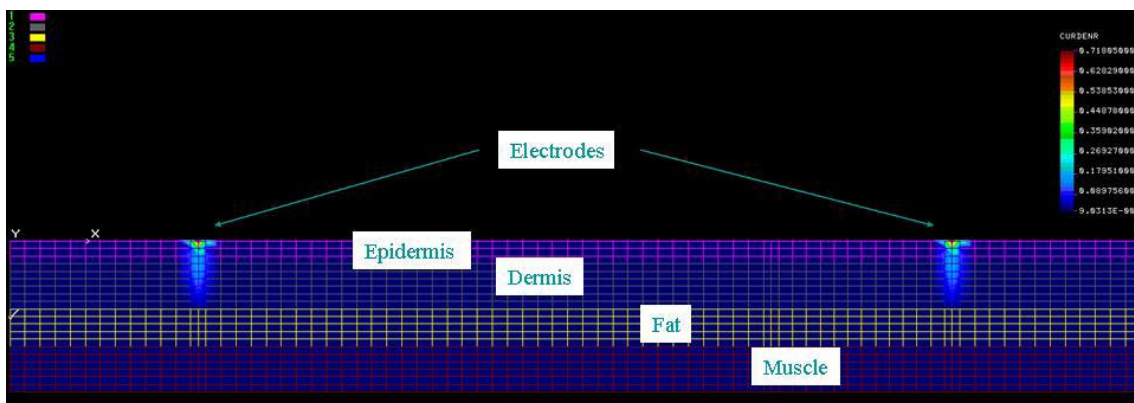


Figure 4-8 Three-dimensional FEM model representing four human body tissues and two darts [14]

There were four tissues represented: epidermis, dermis, fat and muscle. The following resistivities were set for the tissues: epidermis – 10 kOhm·m, dermis – 5 Ohm·m, fat – 22 Ohm·m, muscle – 5 Ohm·m. The darts were designed as two cylinders 9 mm long and 2 mm in diameter. They were separated at 100 mm distance. The voltage boundary conditions were set for the darts, performing the voltage source of 1000 V.

The analysis predicted for the muscle layer current density of 0.094 mA/mm² and field-strength of 470 V/m. It was admitted that these values exceed the thresholds for neuromuscular activation, but are beyond the electroporation levels. It was concluded that Taser incapacitates subjects effectively and safe.

The main assumptions and the results of the modelling of these research groups are compiled in the table 4-1.

Table 4-1 Simulation results of different research groups in comparison

| Research group | Sun* | Stratbucker | Panescu+ | Holden ^o | Leitgeb | Mayhew | Kwarta Singh | Aronshtam |
|-----------------------|------------------|-------------|-----------|---------------------|----------------|------------|--------------|--------------------------------|
| Input parameters | | | | | | | | |
| I, A/ U,V | 1 10 | - 100 | - 1000 | - 300 | - - | 3.326 - | 3 - | Complex signal |
| f, kHz | 4.88/5 | - | 0.02 [15] | 8.3 | 0.0184 | 120 | 120 | Complex signal 8.3 - 500 |
| Z, Ohm | 300 | - | | 48 | 500- 11600 | | 100 | 500 - 600 |
| Gabriels' data | yes | no | no | yes | yes | yes | yes | yes |
| Results | | | | | | | | |
| E, V/m | - | 12 | 470 | - | - | - | - | 950 – 3500 |
| J, mA/mm ² | 0.162- 0.358 | 0.0027 | 0.094 | 0.11 | 7.73 | | 0.0662 | 0.133 – 2.31 |
| I, A | - | - | - | - | 0.000150 | 0.007695 | - | - |
| D, As/m ² | 0.021- 0.0465 | - | - | - | 0.002 – 0.1 | - | - | 0.002 – 0.02 |

* heart (23 to 33 mm from the skin) + 25 mm around heart area ^o muscles

The direct comparison of the results presented in the table 4.1 is not reasonable due to different initial conditions, e.g. signal magnitude and frequency, model geometry and dielectric properties of tissues.

However a brief qualitative analysis of the models shows the advantages of the simulation model developed in this study:

- a) Accurate reconstruction of the actual Taser impulse by a superposition of more than 60 harmonic signals in the Taser's spectrum;
- b) Availability of different model geometries (male/female, adult/ youth);
- c) Scalable model geometry;
- d) Full representation of a whole human body (more than 80 tissues);
- e) Use of the Gabriels' dielectric properties and possibility to vary them.

Moreover the developed model can be easily modified in the respect of input signals and completed with other non-lethal effects, e.g. kinetic impact (blunt trauma).

Such a model provides with a wide spectrum of research possibilities. One of them is the employment of the model for forensic post-accident investigations. The scalability of the geometry and a possibility to vary the dielectric properties of tissues (which change due to use of illegal substances) allow for an accurate reconstruction of an accident.

On the other hand, such a model is an effective tool in the developmental process. Beason et al [17] proposed to search for new signals to perform an effective and safe incapacitation. In the experiments with pigs they studied the influence of such parameters like pulse power, duration and repetition rate on the induced muscle contraction. The same investigation can be realized with the help of the simulation model.

However, as it was mentioned before, there is a need for a consensual safety standard for EIDs, which would allow for an accurate and secure decision about the feasibility of new signals.

5. Conclusions

The aim of this study was to understand what the requirements and restrictions for modern advanced non-lethal weapons are, and to offer an approach for a developmental procedure, that would compile knowledge and experience, and techniques from different fields.

After a deep investigation of the presently available and developed non-lethal technologies and weapons, it was concluded that the main shortcoming the traditional NLWs is their inadaptability to different or changing operational environment.

Therefore the essential characteristic of an advanced NLW is the ability to operate efficiently and safely in its whole spectrum of operational scenarios. A conceptual design approach was proposed of development of the advanced NLWs. The initial point of this concept is the analysis of operational scenarios, which provides the technical requirements and restrictions of the developed NLW. Then on the basis of knowledge about available non-lethal technologies and data acquisition systems (sensors plus signal-processing algorithms) a concept of the NLW is developed. The modern modelling and simulation tools allow ensuring the fulfilment of the requirements at this stage. In case of satisfactory results, a prototype is built and is then validated in the real tests. Finally, as soon as the tests show a proper outcome, the NLW is realised in its end-form.

These aspects were considered in the study on the example of electric incapacitating devices (EIDs), as these NLWs are widely used not only in the military, but also in the law enforcement operations, and are considered to be a very promising option to a lethal force.

A concept of an intelligent EID based on Taser X26 was proposed. An intelligent EID provides an effective darts-spread on the target for any distance within the operational range; adapts an output voltage (or power) to the target's bioimpedance and the repetition rate to the target's heart rate.

A great part of the study was devoted to the EID modelling and simulation, including the questions of validating and verification of the models and simulation techniques. A realistic 3D computer model was developed to study the effects of electric current on human body tissues. This model allows for investigation of an interaction between an EID and a person, and for analysis of the influence of different parameters, e.g. a displacement of the electrodes on the person's body, a penetration depth of the electrodes, and the gender peculiarities of the body etc.

The validation of the models and the simulation techniques, including the development of the

necessary toolset (computer models, measurement units), are considered in the present study too. The series of measurement on animal and human tissues both in-vivo and in-vitro were performed in order to verify the model's parameters (dielectric properties of tissues), and the correctness of the applied computational methods in the simulations.

The developed model has a great potential use for a number of applications, e.g. in forensic medicine. The model was used to perform a limited analysis of the possibility of Taser X26 to cause a ventricular fibrillation in an average person. A VF safety margin of 500% was calculated for a single Taser impulse, and a prolonged Taser application with duration of 25 seconds showed a 16% safety margin.

It was not possible to address all the aspects of the NLWs design in this study. However, an attempt was made to formulate a systematic approach for a development of new efficient live-saving non-lethal systems.

Summary

Non-lethal weapons by definition are not expected to be non-lethal; rather their specific purpose is to provide a significantly lower risk of lethality and irreversible damage. Having been available for at least 30 years by now, the NLWs are still technical immature: The limited operational range, no scalable effects, low selectivity, weak protection from abuse, and weather and counter-measures susceptibility often lead to a situation, when an engagement of an NLW is either not reasonable or ineffective, or would cause an undesired damage. All these cause a diverse attitude to the NLWs use both on the side of the armed forces and law enforcement, and among the civil society. So the demand for a new generation of NLWs has become obvious: a new type of advanced non-lethal weapons that provide a precise demanded outcome in a given operational scenario, ensuring the minimal risk of causing any residual damage.

In this study an attempt was made to understand what the requirements and restrictions for modern advanced non-lethal weapons are, and to offer an approach for a developmental procedure, that would compile knowledge and experience, as well as techniques from different fields.

A deep investigation of the presently available non-lethal technologies preceded the development of a new concept for a design procedure. The proposed procedure has consolidated the knowledge and experience from different fields: production, military science, law, artificial intelligence and medicine. The suggested procedure includes such aspects as derivation of the NLW's specifications from operational scenarios, development of the NLW's "intelligence", modelling and experimental proving of the developed NLW.

We investigated these aspects on the example of electric incapacitating devices. The non-lethal effect of the EIDs is based on the electric stimulation of a person by short high voltage impulses. The impulses cause a painful sensation and an uncontrolled contraction of skeletal muscles, and thus temporarily incapacitate a person during the stimulation. An EID delivers electric current through its electrodes (contact mode) or through two wired darts, which are shot into a person.

The EID's deployment reports were analysed to reveal the demands for an advanced EID. The two main requirements are the effective and safe employment in any circumstances. We have found a number of shortcomings of the available EIDs that affect both the safety and efficiency. So a concept of an "intelligent" EID was proposed. The concept contains the features that allow to eliminate the undesired patho-physiological changes in the persons

being exposed to an EID application, and at the same time to increase the efficiency of the NLW.

The EID's deployment reports and a number of researches devoted to the EID technology were studied in order to define the main technical characteristics of an advanced EID and to build an adequate simulation model for EID-human interaction. We proposed a concept of an intelligent EID based on Taser X26. Our concept EID provides for a more effective and safe deployment, due to following features: controlling of the distance to the target and the correction of the inter-dart angle for a better positioning on the body; controlling the amplitude of the electric output and correcting it according to the target's bioimpedance; controlling the EID's output repetition rate and correcting it according to the target's heart rate; and a possible reverse EID action as a defibrillator.

The modelling and simulation of the concept EID was a large part of the present study. We aimed to develop a validated simulation model for investigation of the EID's effects on human tissues and organs and for analysis of the influencing parameters. A number of physical and computer models were considered with respect to our purpose. We decided for a computational three-dimensional model based on realistic human models. The human models were a voxel phantom of an adult male and three non-voxel phantoms of one adult male, one adult female and one young female. The phantoms represented up to 80 different human tissues. The dielectric properties of the tissues were assigned according to the well-established Gabriel's databank. The EID output was represented similar to the shaped pulse of Taser X26. We decomposed it using Fourier transform into an array of 60 sine waves. Simulations were performed for every single sine excitation signal and their results were then superposed to obtain the effect of the total initial EID pulse.

The simulation model was validated with the help of a series of measurement on swine and human tissues. A special measurement unit was developed for this purpose. The model's parameters such as dielectric properties of tissues were verified in the in-vivo and in-vitro measurements. The applied computational method (FDTD) was validated by comparison of the measured and simulated results for a single tissue (liver).

The results of the simulations were used to analyse the factors that can influence the EID's safety and efficiency. Penetration depth appeared to be a significant parameter, since the conductivity of the current path changes depending on the thickness of the involved tissues. The position of the darts and their proximity to the heart are important with the respect to the EIDs effect on the heart. However, when both darts are not in the area directly above the

heart, their location is not meaningful. Frontal and dorsal EID applications cause significantly different reactions on the heart: the values of the electric field were approximately 2.5 (male) and 3.8 (female) lower for dorsal applications. Thus, the lowest impact on the heart occurs when an EID is applied on the back of the target.

We performed a limited safety analysis of the EID with respect to the risk of causing a ventricular fibrillation in an exposed person. Ventricular fibrillation is one of the most dangerous of the heart disorders that can lead to a death within 90 seconds, if the rhythm transforms into asystole. VF is characterized by disorganized contraction of the heart, when the ventricles rather tremble than contract. Such an activity prevents an effective blood circulation and can lead to a sudden cardiac death, which when not treated within ca. 5 min will lead to cerebral hypoxia and irreversible brain damage.

We adopted the VF threshold proposed by the International Electric Committee to perform the safety analysis. Two approaches were used. In the first one, the pulse with a voltage corresponding to the IEC VF threshold was applied in the simulation. In such a manner we obtained the VF thresholds for electric field magnitude, current and charge densities. However, it was found that only the charge density threshold could be utilised. It showed a safety margin of 500% for a single EID pulse. The second approach was based on the integral approximation of the delivered energy and allowed for evaluation of the effects of the prolonged EID application. It showed a 35% safety margin for a single EID pulse, and a 16% safety margin for a 25-s EID application. However, the accuracy of both approaches is not confirmed and so their results should be treated with caution.

The developed simulation model has a great potential use for many applications, e.g. in forensic medicine. However, there is a need for a consensual safety standard for EIDs, which would allow for an accurate and secure decision about the feasibility of new signals.

Thus the implementation of the advanced NLW design procedure was analysed on the example of an intelligent EID. This procedure provides a development of new efficient live-saving non-lethal systems, when supplied with the full spectrum of the necessary operational, technical and medical data, safety thresholds and norms.

Abstract

The aims of this study were to understand what the requirements and restrictions for modern advanced non-lethal weapons (NLW) are, and to offer an approach for a developmental procedure, that would compile knowledge and experience, as well as techniques from different fields.

After a deep investigation of the presently available non-lethal technologies a new concept for a design procedure was developed. The suggested procedure includes such aspects as derivation of the NLW's specifications from operational scenarios, development of the NLW's "intelligence", modelling and experimental proving of the developed NLW.

The main aspects of procedure implementation are discussed on the example of electric incapacitating devices (EIDs) with the focus on the safety of these devices. The analysis of the EID's application reports revealed a number of shortcomings of the available EIDs that affect both their safety and efficiency. A concept of an "intelligent" EID was described. The concept contains the features that allow to eliminate the undesired patho-physiological changes in the persons that underwent an EID application, and in the same time to increase the efficiency of the NLW. A great part of this research was devoted to the development of a simulation model for EID-human-interaction. The purpose of the model is the ability to investigate the effects of the EID on human tissues and organs. This provides a powerful tool both in the design process, and on the stage of operational employment, e.g. for forensic purposes. A realistic 3D computer model was developed to study the effects of the electric current produced by EID on humans, as well as to analyse the influence of different parameters on the EID application efficiency and safety. Both the process of model development and its verification are described.

The reasonability of the suggested design procedure and the role of different aspects are then discussed. In particular the practical forensic use of the model development is considered.

Zusammenfassung

Ziel dieser Studie war es die Randbedingungen und die Einschränkungen nicht-letaler Wirkmittel (NLW) zu verstehen. Aus einer Vielzahl gewonnener Einsatzerfahrungen und aus dem verfügbaren Expertenwissen sollte eine effektive Vorgehensweise für die Entwicklung moderner und fortschrittlicher nicht-letaler Wirkmittel abgeleitet werden.

Auf der Basis einer ausführlichen Literaturrecherche der gegenwärtig verfügbaren nicht-letalen Technologien wurde ein neuer Entwurfsablauf für fortschrittliche NLW erarbeitet. Dieser Entwurfsablauf beinhaltet die Ableitung von NLW-Spezifikationen aus den jeweiligen Anwendungsszenarien, die Entwicklung der geforderten Intelligenz des nicht-letalen Wirkmittels und die Überprüfung des entwickelten Konzepts in Simulationen und praktischen Tests.

Die wichtigsten Elemente des Entwurfsablaufs werden in dieser Studie am Beispiel einer fortschrittlichen Elektroschockwaffe (ESW) näher betrachtet, insbesondere wird auch die Frage der Sicherheit solcher Wirkmittel behandelt. Als Ergebnis der Analyse von unterschiedlichen Erfahrungsberichten beim Einsatz von ESW wird eine Reihe von Mängeln bei den verfügbaren Elektroschockwaffen diagnostiziert, die sowohl die Sicherheit, als auch die Effektivität der ESW beeinträchtigen. Um diese Mängel zu eliminieren wird eine fortschrittliche ESW vorgeschlagen. Diese ermöglicht es unerwünschte pathophysiologische Veränderungen bei einer Zielperson nach einer ESW-Anwendung zu vermeiden, wobei gleichzeitig auch die Effizienz einer solchen Anwendung gesteigert werden kann.

Die Entwicklung eines Simulationsmodells für die Interaktion zwischen ESW und Zielperson wird in der Studie ausführlich beschrieben. Die besondere Aufgabe des Modells ist es, die Wirkung einer ESW auf die Gewebe und die Organe eines Menschen bestimmen zu können. Das entwickelte Simulationsmodell stellt ein vielseitiges Instrument sowohl in der Entwicklungsphase, als auch bei der Anwendung von ESW, z. B. für forensische Nachuntersuchungen dar. Mit Hilfe dieses dreidimensionalen Rechenmodells lassen sich sowohl die Wirkungen elektrischer Impulse von ESW auf Menschen untersuchen als auch die Einflüsse unterschiedlicher Parameter auf die Sicherheit einer ESW analysieren.

In der Studie werden sowohl der Entwicklungsprozess für das Simulationsmodell, als auch dessen Verifikation beschrieben. Es werden die Sinnfälligkeit und Angemessenheit des vorgeschlagenen Entwurfsablaufs begründet und die Bedeutung unterschiedlicher Teilaspekte diskutiert. Im Besonderen wird auch die praktische forensische Anwendung von Simulationsmodellen betrachtet.

References

Chapter 1

1. The Human Effects of Non-lethal Technologies. The final report of NATO RTO-TR-HFM-073. 2006
2. Directive Subject: Policy for Non-Lethal Weapons, DODD 3000.3. Department of Defense. 1996
3. Scott Richard L. Conflict Without Casualties: Non-Lethal Weapons in Irregular Warfare. Thesis. Naval Postgraduate School, Monterey. 2007
4. An Assessment of Non-Lethal Weapons Science and Technology. Committee for an Assessment of Non-Lethal Weapons Science and Technology/ Naval Studies Board/ Division on Engineering and Physical Sciences. 2003.
5. Smoke operations. Field Manual No. 3-50. Headquarters Department of the Army Washington DC. 1990. <http://www.fas.org/irp/doddir/army/fm3-50.pdf>
6. Lakoski J.M., Bosseau Murray W., Kenny J.M. The advantages and Limitations of Calmatives for Use as a Non-Lethal Technique. The Pennsylvania State University. 2000.
7. Sutherland R. G. Chemical and Biochemical Non-lethal Weapons. Political and Technical Aspects. SIPRI, 2008.
8. Stocker H., Lt.-Col. Dick J., Berube G. Non-Lethal Weapons. Opportunities for R&D. Technical memorandum. Defence Research and Development Canada. 2004

Chapter 2

1. Aronshtam Y., Tränkler H.-R. Systematischer Entwurf fortschrittlicher nichtletaler Wirkmittel AP1. Internal report. 2010
2. Non-Lethal Weapons and Future Peace Enforcement Operations, RTO-TR-SAS-040, Nov. 2004, (Operational Scenarios, Combined Technologies). <http://www.rta.nato.int/Pubs/RDP.asp?RDP=RTO-TR-SAS-040>
3. NATO SAS-035 Measures of Effectiveness Framework. 2003
4. Bestel J., Clement F., and Sorine M.. A Biomechanical Model of Muscle Contraction.
5. Hyashibe M., Poignet P., Guiraud D.et al. Nonlinear identification of skeletal muscle dynamics with Sigma-Point Kalman Filter for model-based FES. (<http://www.lirmm.fr/~hayashibe/icra08.pdf>)
6. A Hodgkin-Huxley model (http://en.wikipedia.org/wiki/Hodgkin%E2%80%93Huxley_model)
7. Field Plotting Using Teledeltos Paper. Aston University Department of Electronic Engineering and Applied Physics.
8. Allen P.H.G. Field mapping with conducting paper. Phys. Educ. (1968) 3
9. Prutchi D., Norris M. Design and development of medical electronic instrumentation: A Practical Perspective of the Design, Construction, and Test of Medical Devices. 2004.

10. Guy A.W. Analysis of electromagnetic fields induced in biological tissue by thermographic studies on equivalent phantom models. *IEEE Trans Microwave Theory Tech MTT* (1971) 19:189-217
11. Chou C.-K. Formulas for Preparing Phantom Muscle Tissue at Various Radiofrequencies. 1984
12. Cheung A.Y., Koopman D.W. Experimental development of simulated biomaterials for dosimetry studies of hazardous microwave radiation. *IEEE Trans. Microw. Theory Tech.* (1976) 24: 669–73
13. Bini M.G. et al. The polyacrylamide as a phantom material for electromagnetic hyperthermia studies. *IEEE Trans. Biomed. Eng.* (1984) 31: 317–22
14. Andreuccetti D. Use of polyacrylamide as a tissue-equivalent material in the microwave range. *Bioelectromagnetics* (1988) 9 (4): 373–379
15. Surowiec et al. Utilization of a multilayer polyacrylamide phantom for evaluation of hyperthermia applicators. *Int. J. Hyperthermia* (1992) 8: 795–807
16. McCann et al. Feasibility of salvage interstitial microwave thermal therapy for prostate carcinoma following failed brachytherapy: studies in a tissue equivalent phantom. *Phys. Med. Biol.* (2003) 48: 1041–52
17. Sunaga et al. Development of a dielectric equivalent gel for better impedance matching for human skin. *Bioelectromagnetics* (2003) 24: 214–17
18. Legendijk P.N. Hyperthermia dough: a fat and bone equivalent phantom to test microwave/radiofrequency hyperthermia heating systems. *Phys. Med. Biol.* (1985) 30: 709–12
19. Robinson M. J. et al. New materials for dielectric simulation of tissues. *Phys. Med. Biol.* (1991) 36: 1565–71
20. Nikawa et al. Soft and dry phantom modelling material using silicone rubber with carbon fibre. *IEEE Trans. Microw. Theory Tech.* (1996) 44: 1949–53
21. Youngs et al. Design of solid broadband human tissue simulant materials. *IEE Proc.-Sci. Meas. Technol.* (2002) 149: 232–8
22. Chang et al. A conductive plastic for simulating biological tissue at microwave frequencies. *IEEE Trans. Electromagn. Compat.* (2000) 42: 76–81
23. Lazebnik M., Madsen E. L., Frank G. R., Hagness S. C. Tissue-mimicking phantom materials for narrowband and ultrawide-band microwave applications. 2005.
24. Wegmüller M., Olszewska J., Oberle M., Fröhlich J. Solid Phantoms to Verify Channel Models of the Human Body. 2007.
25. Lemosquet A., de Carlani L. et. al. Voxel anthropomorphic phantoms: review of models used for ionising radiation dosimetry. *Radioprotection* (2003) 38(4) (<http://www.radioprotection.org/index.php?option=article&access=standard&Itemid=129&url=/articles/radiopro/pdf/2003/04/Lemosquet.pdf>)
26. <http://www.comsol.com/showroom/gallery/497/http://www.comsol.com/showroom/gallery/497/>
27. Xu X.G., Chao T.C., Bozkurt A. VIP-Man: an image-based whole-body adult male model constructed from colour photographs of the visible human project for multi-particle Monte Carlo calculations. *Health Phys.* (2000) 78: 476-486.

28. Sachse F.B., Werner C.D., Meyer-Waarden K., Dossel O. Development of a human body model for numerical calculation of electrical fields. *Comperi. Med. /mcig. Gruph.* (2000) 24: 165- 171.
29. Aldridge J.S., Rechwerdt P.J., Roche T.R. A proposal for a standard electronic anthropomorphic phantom for radiotherapy. *Med. Phys.* (1999) 26: 1901- 1903.
30. Zankl M., Wittman A. The adult male voxel "Golem" segmented from whole body CT patient data. *Radiat. Environ. Biophys.* (2001) 27: 153- 164
31. Zubal I.G., Harrell C.K., Smith E.O., Kattner Z., Gindi G., Hoffer P.B. Computerized three-dimensional segmented human anatomy. *Med. Phys.* (1994) 21: 299-302.
32. Jones D.G. A realistic anthropomorphic phantom for calculation organ doses arising from external photon radiation. *Radiat. Protect. Dosimetry* (1997) 72 (1): 21-29
33. Saito K., Wittmann A., Koga S. et al. Construction of a computed tomographic phantom for a Japanese male adult and dose calculation System *Radiat. Environ. Biophys.* (2001) 40: 69-76
34. Petoussi-Hens N., Zankl M. Voxel anthropomorphic models as a tool for internal dosimetry. *Radiat. Prot. Dos.* (1998) 79: 4 15-4 18.
35. Caon M., Bibbo G., Pattison J. An EGS4-ready tomographic computational model of a fourteen year-old female torso for calculating organ doses from CT examinations. *Phys. Med. Biol.* (1999) 44: 2213-2225
36. http://www.nlm.nih.gov/pubs/factsheets/visible_human.html
37. Nescolarde L. Whole-body and thoracic bioimpedance measurement: Hypertension and hyperhydration in hemodialysis patients. *Proceedings of the 29th Annual International Conference of the IEEE EMBS* (2007), pp. 3593–3596
38. Basic Anatomical and Physiological Data for Use in Radiological Protection Reference Values. ICRP Publication 89. *Ann. ICRP* 32 (3-4), 2002
39. Dimbylow P. J. The development of realistic voxel phantoms for electromagnetic field dosimetry *Proc. Voxel Phantom development* (1996): 1–7
40. http://www.itis.ethz.ch/index/index_humanmodels.html
41. Gabriel C. and Gabriel S. Compilation of the Dielectric Properties of Body Tissues at RF and Microwave Frequencies (<http://www.brooks.af.mil/AFRL/HED/hedr/reports/dielectric/home.html>)
42. Gabriel C. "Compilation of the dielectric properties of body tissues at RF and microwave frequencies", Report N.AL/OE-TR- 1996-0037, Occupational and environmental health directorate, Radiofrequency Radiation Division, Brooks Air Force Base, Texas (USA), June 1996.
43. Gabriel C., Gabriel S. and Corthout E. The dielectric properties of biological tissues: I. Literature survey. *Phys. Med. Biol.* (1996) 41: 2231-2249.
44. Gabriel S., Lau R.W. and Gabriel C. The dielectric properties of biological tissues: II. Measurements in the frequency range 10 Hz to 20 GHz. *Phys. Med. Biol.* (1996) 41: 2251-2269.
45. Gabriel S., Lau R.W. and Gabriel C. The dielectric properties of biological tissues: III. Parametric models for the dielectric spectrum of tissues. *Phys. Med. Biol.* (1996) 41: 2271-2293.

46. The Electrical Conductivity of Tissues. The Biomedical Engineering Handbook: Second Edition. B.J. Roth. 2002. (http://www.cmu.edu.cn/jcyxy/upl_files/20081122184243806.pdf)
47. Gielen F. L. H., Wallinga-de Jonge W., and Boon K.L. Electrical conductivity of skeletal muscle tissue: Experimental results from different muscles in vivo. 1984. (<http://www.springerlink.com/content/8g3513123202001g/fulltext.pdf>)
48. Hirata A, Yamazaki K., Hamada S., Kamimura Y., Tarao H., Wake K., Suzuki Y., Hayashi N. and Fujiwara O. Intercomparison of induced fields in Japanese male model for ELF magnetic field exposures: effect of different computational methods and codes. Radiation Protection Dosimetry (2010)138 (3:) 237-244
49. Lehmann H., Pollara L., Spichtig S., Kühn S. and Wolf M. Head exposure system for a human provocation study to assess the possible influence of UMTS-like electromagnetic fields on cerebral circulation using near-infrared imaging. Bioelectromagnetism (2011) 33: 124-133
50. www.comsol.com
51. Zurek S. http://en.wikipedia.org/wiki/File:Example_of_2D_mesh.png
52. Johnson S.G. <http://upload.wikimedia.org/wikipedia/commons/thumb/d/d3/Yee-cube.svg/300px-Yee-cube.svg.png>

Chapter 3

1. <http://www.security-discount.com/products/de/Elektroschocker/PTB-Elektroschocker-200000-Volt-zugelassen-in-DE-Inkl-Batterie-Spray.html>
2. Soft Kill. R. Langreth. Popular Science 245, (4), 1994.
3. <http://www.jaycor.com/eme/watcan.htm>
4. <http://web.archive.org/web/20040626083201/>
5. http://de.wikipedia.org/wiki/Wireless_eXtended_Range_Electronic_Projectile
6. <http://www.taser.com/>
7. <http://www.taser.com/products/law-enforcement/taser-x26-eed>
8. Kroll M. 2008 Physiology and pathology of TASER® electronic control devices. Journal of Forensic and Legal Medicine. J For Leg Med 16(4): 173–177
9. TASER® X26E Series Electronic Control Device Specification (Law Enforcement X26). 2007. <http://www.extremetactical.com/taser/x26LE%20spec%20sheet.pdf>
10. MacDonald JM, Kaminski RJ, Smith MR. 2009 The effect of less-lethal weapons on injuries in police use-of-force events. Amer J Pub Health 99:1-7
11. <http://www.taser.com/research-and-safety/field-use-and-statistics>
12. Statistical analysis of deaths following police Taser use Amnesty International AMR 51/013/2012 15.02.2012
13. <http://www.amnesty.org/en/news/usa-stricter-limits-urged-deaths-following-police-taser-use-reach-500-2012-02-15>
14. The U.S. Army Center for Health Promotion and Preventive Medicine’s Position on whether TASER® Electro Muscular Incapacitation Launched Electro Stun Weapons are

Safe to use on U.S. Army Military and Civilian Personnel during Training. Memorandum for U.S. Army Armament Research, Development and Engineering Center 2005

15. Verwendung von Elektroschockwaffen durch deutsche Sicherheitskräfte. Antwort der Bundesregierung auf die Kleine Anfrage der Abgeordneten Ulla Jelpke, Wolfgang Neskovic, Heike Hänsel, weiterer Abgeordneter und der Fraktion DIE LINKE. Drucksache 16/11806. 13.02.2009 <http://dip21.bundestag.de/dip21/btd/16/119/1611961.pdf>

16. Strom als Waffe. A. von Tils. In Y Das Magazin der Bundeswehr. 2009 (6). http://www.y-punkt.de/portal/poc/ypunkt?uri=ci:bw.bwde_ypunkt.aktuell.forschung_technik&de.conet.contentintegrator.portlet.current.id=01DB131000000001|7T3BJE889INFO

17. <http://amnesty.org/en/news-and-updates/report/tasers-potentially-lethal-and-easy-abuse-20081216>

18. Taser Loses 1st Product-Liability Suit; Jury Awards \$6Million. Margaret Cronin Fisk. 07.06.2008 <http://www.bloomberg.com/apps/news?pid=newsarchive&refer=us&sid=aYJitFRQLpZk>

19. "Less than lethal?" The use of stun gun weapons in US Law Enforcement. Amnesty International. 2008

20. Electroacupuncture-induced analgesia in a rat model of ankle sprain pain is mediated by spinal alpha-adrenoceptors. Sung Tae Koo, Kyu Sang Lim, Kyungsoon Chung, Hyunsu Ju, Jin Mo Chung. International Association for the Study of Pain. 2007.

21. <http://www.openradiology.org/zosirws/survey/bone%20metastasis%20radiofrequency/technique>

22. Advanced Taser® M18/M18L Operating Manual. <http://www.stungunweapon.com/taser-m18-manual.html>

23. <http://taser.com/products/law-enforcement/taser-x2#safety>

24. Measurement data registered during the volunteer research in Taser Training Center in Scottsdale, USA in 2009. Obtained from M. Kroll on a private request.

25. Sun H., Haemmerich D., Rahko P.S., Webster J.G. 2010 Estimating the probability that the Taser directly causes human ventricular fibrillation. *JMedEngTech* 4(3): 178-191.

26. Sun H., Webster J.G. 2007 Estimating neuromuscular stimulation within the human torso with TASER stimulus, *Phys. Med. Biol.* 52 (21) 6401–6411.

27. Kroll M.W., Physiology and pathology of Taser1 electronic devices, *J. Forensic Legal Med.* 16 (4) (2009) 173–177.

28. Stratbucker R.A., Kroll M.W., McDaniel W., Panescu D., Cardiac current density distribution by electrical pulses from TASER devices, *Conf. Proc. IEEE Eng. Med. Biol. Soc.* 1 (2006) 6305–6307.

29. Nanthakumar K., Masse S., Umapathy K., Panescu D., Sevaptsidis E., Waxman M., Cardiac stimulation with high voltage discharge from stun guns, *CMAJ* 178 (11) (2008) 1451–1457.

30. Baldwin D.E., Nagarakanti R., Hardy S.P., Jain N., Borne D.M., England A.R., Nix E.D., Daniels C.L., Abide Jr. W.P., Glancy D.L. 2010 Myocardial infarction after taser exposure, *J. La. State Med. Soc.* 162 (5): 291–295.

31. Multerer S., Bekenbosch J.W., Das B., Johnsrude C., Atrial fibrillation after taser exposure in a previously healthy adolescent, *Pediatr. Emerg. Care* 25 (12) (2009) 851–853.

32. Naunheim R.S., Treastler M., Aubin C. 2010 Ventricular fibrillation in a man shot with a Taser, *Emerg. Med. J.* 27 (8):645–646.
33. Kroll M.W., Ho J.D., Panescu D. et al. 2007 Potential errors in autopsy reports of custodial deaths temporally associated with electronic control devices: a cardiovascular perspective, in: *American Academy of Forensic Science Annual Conference*, San Antonio, Texas, February 19–27, 2007.
34. Dawes D.M., Ho J.D., Re: Myocardial infarction after taser exposure, *J. La. State Med. Soc.* 162 (5) (2010) 291–295
35. Ho J.D., Dawes D.M., Reardon R.F., Strote S.R., Kunz S.N., Nelson R.S. et al. 2011 Human cardiovascular effects of a new generation conducted electrical weapon, *Forensic Sci. Int.* 204 (1–3): 50–57.
36. Walter R.J., Dennis A.J., Valentino D.J., Margeta B., Nagy K.K., Bokhari F., Wiley D.E., Joseph K.T., Roberts R.R.. 2008 TASER X26 discharges in swine produce potentially fatal ventricular arrhythmias, *Acad. Emerg. Med.* 15 (1) 66–73.
37. Leitgeb N., Niedermayr F., Loos G. and Neubauer R. 2011 Cardiac fibrillation risk of TASER X-26 dart mode application. *Wien Med Wochenschr* 161/23–24: 571–577.
38. Leitgeb N., Niedermayr F., Loos G. and Neubauer R. 2010 Numerically simulated cardiac exposure to electric current densities induced by TASER X-26 pulses in adult men. *Phys. Med. Biol.* 55: 6187–6195.
39. Zipes D. P. 2012 Sudden cardiac arrest and death following application of shocks from a Taser Electronic Control Device. *AHA Circulation* 125:2417-2422
40. Levine S.D., Sloane C., Chan T.; et al. Cardiac monitoring of subjects exposed to the Taser (abstr 187) 2005 Paper presented at: Annual meeting of the Society of Academic Emergency Medicine; May 22–25; New York, NY.
41. Effects of current on human beings and livestock – Part 1: General aspects. TS 60479-1, IEC: 2005.
42. Wiggers CJ, Wégria R. 1940 Ventricular fibrillation due to single, localized induction and condenser shocks applied during the vulnerable phase of ventricular systole. *Am J Physiol.* 128:500-505.
43. Han J., Dreifus L.S., Likoff W. 1973 Ventricular vulnerability to fibrillation. *Cardiac Arrhythmias.* pp. 87–95.
44. Chattipakorn N., Shinlapawittayatorn K., and Chattipakorn S. 2005. Electrophysiological Mechanisms of Ventricular Fibrillation Induction. *Indian Pacing Electrophysiol J.* 5(1): 43–50.
45. Lakkireddy D., Wallick D., Ryschon K., Chung M.K., Butany J., Martin D., Saliba W., Kowalewski W., Natale A., Tchou P. 2006 Effects of cocaine intoxication on the threshold for stun gun induction of ventricular fibrillation. *JAmColCard* 48(4): 805-811
46. AED Plus Biphasic Waveform. ZOLL Medical Corporation. 2008. www.zoll.com
47. Despa F., Basati S., Zhen-Du Zhang, D'Andrea J., Reilly J.P., Bodnar E.N., Lee R.C. 2009 Electromuscular incapacitation results from stimulation of spinal reflexes. *Bioelectromagnetics* 30(5): 411-421.
48. http://www.itis.ethz.ch/index/index_humanmodels.html

49. Lee J., Keun Seo J., Je Woo E. 2007 Mathematical framework for current density imaging due to discharge of electro-muscular disruption devices. *Numerical Analysis ESAIM: Mathematical Modelling and Numerical Analysis* 41 : 447-459
50. PSDB Evaluation of Taser Device. T. Donnelly, K. Douse, M. Gardner, and D. Wilkinson. 2002. <http://www.lawanddemocracy.org/pdf/psdb09-02.pdf>
51. <http://www.home.agilent.com/agilent/product.jsp?nid=-34376.739734.00&lc=ger&cc=DE>
52. Agilent U2531A Impedance Measurement Application. Internal instruction. M. Rist. 2010.
53. Hanna Instruments conductivity solution 1413 uS/cm HI 70031.
54. Calculation of the dielectric properties of body tissues (based on Gabriel databank). 2010 <http://niremf.ifac.cnr.it/tissprop/htmlclie/htmlclie.htm>
55. Efficacy and Safety of Electrical Stun Devices. The Potomac Institute for Policy Studies. 2008.
56. Ergebnisse von Forschungsarbeiten und statistischen Untersuchungen des Instituts zur Erforschung elektrischer Unfälle. D. Kieback. *Elektrotechnik und Informationstechnik*. 106. Jahrgang. Heft 1. 1989.
57. Definition of terms related to cardiac rhythm. WHO/ISFC Task Force. Robles de Medina E.O., Bernard R., Coumel P. et al. *Eur J Cardiol* 8 (2): 127-44. 1978
58. Wirkungen des elektrischen Stroms auf Menschen und Nutztiere. Lehrbuch der Elektropathologie. G. Biegelmeier. 1986. VDE Verlag GmbH. ISBN-10: 800714523, ISBN-13: 978-3800714520
59. Principles of applied biomedical instrumentation. L. Geddes, L. Baker. 1975. ISBN: 0-471-29496-9.
60. Damage, damage number. J. Mark. Internal report. 2008
61. Therapeutic indices for transthoracic defibrillator shocks: Effective, damaging, and lethal electrical doses. Babbs C.F., M.D., M.S., Ph.D, Tacker W.A., M.D., Ph.D., Van Vleet J.F., D.V.M., Ph.D., Bourland J.D., E.E., Ph.D., Geddes L.A., M.E., Ph.D. *American Heart Journal*, 99: 734-738. 1980.

Chapter 4

1. Sun H., Webster J. Models of ventricular fibrillation probability and neuromuscular stimulation after TASER® use in humans. A dissertation submitted in partial fulfillment of the requirements for the degree of Doctor of Philosophy (Electrical Engineering) at the University of Wisconsin at Madison 2007.
2. Wu J.Y., Sun H., O'Rourke A. P., Huebner S. M., Rahko P. S., Will J. A. and Webster J. G. 2007 Taser dart-to-heart distance that causes ventricular fibrillation in pigs *IEEE Trans. Biomed. Eng.* 54(3):503-8
3. MacLeod R. S., Johnson C. R. and Ershler P. R. 1991 Construction of an inhomogeneous model of the human torso for use in computational electrocardiography *Proc. Annu. Int. Conf. IEEE Eng. Med. Biol. Soc.* 13(2): 688-9.

4. Stratbucker R.A., Kroll M.W., McDaniel W., Panescu D. 2006 Cardiac Current Density Distribution by Electrical Pulses from TASER devices Proc. 28th IEEE EMBS Annu. Int. Conf. New York City, USA, Aug 30-Sept 3.
5. Holden S. J., Sheridan R. D., Coffey T. J., Scaramuzza R. A., Diamantopoulos P. 2007 Electromagnetic modeling of current flow in the heart from TASER devices and the risk of cardiac dysrhythmias. *Phys. Med. Biol.* 52: 7193–7209.
6. Diamantopoulos P. and Holden S. J. 2002 Three dimensional computer modelling of the human anatomy IV World Congress of Biomechanics, Calgary, Alberta, Canada, 4–9 August 2002.
7. Leitgeb N., Niedermayr F., Loos G. and Neubauer R. 2011 Cardiac fibrillation risk of TASER X-26 dart mode application. *Wien Med Wochenschr* 161/23–24: 571–577.
8. Leitgeb N., Niedermayr F. and Neubauer R. 2012 Interference of implanted cardiac pacemakers with TASER X26 dart mode application. *Biomed Tech* 57:201–206.
9. Leitgeb N., Niedermayr F., Loos G. and Neubauer R. 2012 Risk of Pacemaker Patients by TASER X26 Contact Mode Application. *Journal of Electromagnetic Analysis and Applications* 4: 96-100
10. Leitgeb N., Niedermayr F., Loos G. and Neubauer R. 2010 Numerically simulated cardiac exposure to electric current densities induced by TASER X-26 pulses in adult men. *Phys. Med. Biol.* 55: 6187–6195.
11. Mayhew R.L.S. 2010 Finite-Difference Time-Domain Analysis of Currents from a Human Electro-Muscular Incapacitation Device. A thesis submitted to the Graduate Faculty of North Carolina State University in partial fulfillment of the requirements for the degree of Master of Science Electrical Engineering Raleigh, North Carolina.
12. Singh V. et al. 2010 Computation of Induced Current Densities in the Human Body at Low Frequencies Due to Contact Electrodes Using the ADI-FDTD Method. *IEEE Transactions on Electromagnetic Compatibility.* 99: 1-8.
13. Kwatra N. 2009 Computation of Recruitment Volumes in the Human Body due to External Electric or Magnetic Stimulation using ADI-FDTD Method. MS thesis. North Carolina State University.
14. Panescu D., Kroll M. W., Efimov I. R., Sweeney J. D. 2006 Finite Element Modeling of Electric Field Effects of TASER Devices on Nerve and Muscle. Proceedings of the 28th IEEE EMBS Annual International Conference New York City, USA.
15. Panescu D., Webster J. G. 1994 A nonlinear finite element model of the electrode-electrolyte skin system *IEEE Trans. Biomed. Eng.* 41(7): 681–687.
16. Sun H., Wu J.-Y., Abdallah R., and Webster J. G. 2005 Electromuscular incapacitating device safety Proc. IFMBE 11(1) 3rd EMBE Conference, Prague.

Abbreviations

| | |
|----------|---|
| 3D | – three-dimensional |
| A | – Ampere |
| AC | – alternate electric current |
| AED | – automated external defibrillator |
| CED | – conducted energy devices |
| CEW | – conducted energy weapon |
| CS | – 2-chlorobenzalmalononitrile, a riot control agent, named after Ben Corson (C) and Roger Stoughton (S) |
| CN | – Phenacyl chloride, a riot control agent |
| DC | – direct electric current |
| ECG | – electrocardiogram |
| EID | – electric incapacitating device |
| Hz | – Hertz |
| IEC | – The International Electrotechnical Commission |
| J | – Joule |
| NLT | – non-lethal technology |
| NLW | – non-lethal weapon |
| OC | – oleoresin capsicum |
| V | – Volt |
| VF | – ventricular fibrillation |
| <i>D</i> | – Charge density |
| <i>E</i> | – Electric field strength |
| <i>J</i> | – Electric current density |
| <i>I</i> | – Magnitude of electric current |
| <i>U</i> | – Voltage |

Acknowledgments

This study is a result of my activities at the Institut für Technik Intelligenter Systeme (ITIS, Universität der Bundeswehr München) and at the Institut für Rechtsmedizin (Ludwig-Maximilians Universität München) in the frame of the projects supported by the Wehrtechnische Dienststelle für Schutz und Sondertechnik (WTD 52, Oberjettenberg).

I would like to express my heartfelt gratitude to Prof. Dr. Hans-Rolf Tränkler, Dr. Oliver Peschel, Dr. Sebastian Kunz and TRDir. Franz Wolf for their support and supervision.

Danksagung

Diese Studie entstand im Rahmen meiner Tätigkeit als wissenschaftliche Mitarbeiterin am Institut für Technik Intelligenter Systeme (ITIS) an der Universität der Bundeswehr München und am Institut für Rechtsmedizin der Ludwig-Maximilians Universität München in Projekten gefördert durch die Wehrtechnische Dienststelle für Schutz und Sondertechnik in Oberjettenberg.

Ich bedanke mich ganz herzlich bei Herrn Prof. Dr.-Ing. Hans-Rolf Tränkler, Herrn PD Dr. med. Oliver Peschel, Herrn Dr. med. Sebastian Kunz und Herrn TRDir Franz Wolf für die Betreuung und Unterstützung.

Appendix 1 Multi-simulation tool

The code is written in Python.

```
import SEMCAD
import Tool

class MultiSimSetupTool(Tool.ExtensionTool):
    def CreateEMMultiSims(self):
        for i in range(1, 60):
            sim = SEMCAD.simulations.GetSimulation(i)
            sim.ComputeVoxels()
            sim.WriteSolverInputFile()

            SEMCAD.SaveProject()

    def GetName(self):
        return "Multi-Simulation Setup"

    def GetCategory(self):
        return "Simulation"

    def GetCategoryMenu(self):
        return "Simulation"

    def Start(self):
        self.CreateEMMultiSims()

    def Stop(self):
        self.Exit()

    def HasPickList(self):
        return False

    def CanBack(self):
        return False

    def CanNext(self):
        if self.state == 0:
            return True
        else:
            return False

    def CanDone(self):
        if self.state == 1 or self.state == -1:
            return True
        else:
            return False

Tool.Register("MultiSimSetup", MultiSimSetupTool)
```

Appendix 2 Measurement data for the dielectric properties of organic tissues

1. Animal tissues

The animal tissues were obtained from a 4 months old swine. The measurements were performed within 2 hours after its slaughter.

1.1. Heart

Electrodes: 2 mm diameter, inter-electrode distance 60 mm.

| Freq, Hz | Mag, Ohm | Phase, rad | Re, Ohm | Im, Ohm |
|----------|----------|------------|---------|---------|
| 100 | 1167.00 | -1.57 | 1166.67 | -31.90 |
| 150 | 1163.33 | -2.29 | 1162.67 | -46.47 |
| 200 | 1159.00 | -2.97 | 1157.67 | -60.00 |
| 350 | 1143.33 | -4.77 | 1139.33 | -94.99 |
| 500 | 1126.00 | -6.29 | 1119.67 | -123.40 |
| 750 | 1096.33 | -8.38 | 1084.67 | -159.70 |
| 1100 | 1055.67 | -10.57 | 1038.00 | -193.67 |
| 1650 | 998.97 | -12.98 | 973.53 | -224.30 |
| 2450 | 932.00 | -15.10 | 899.80 | -242.77 |
| 3650 | 858.17 | -16.69 | 822.03 | -246.50 |
| 5450 | 784.27 | -17.61 | 747.53 | -237.27 |
| 8150 | 716.73 | -17.77 | 682.53 | -218.73 |
| 12150 | 658.10 | -17.64 | 627.10 | -199.50 |
| 18150 | 608.20 | -17.20 | 581.03 | -179.83 |
| 27050 | 563.53 | -17.03 | 538.83 | -165.03 |
| 40350 | 524.70 | -16.95 | 501.93 | -152.97 |
| 60250 | 489.13 | -16.40 | 469.23 | -138.17 |
| 89850 | 453.17 | -16.98 | 433.37 | -132.30 |
| 134100 | 418.50 | -16.60 | 401.10 | -119.57 |
| 200000 | 389.02 | -17.60 | 370.67 | -117.57 |

1.2. Liver

a) Electrodes: 2 mm diameter, inter-electrode distance 60 mm.

| Freq, Hz | Mag, Ohm | Phase, rad | Re, Ohm | Im, Ohm |
|----------|----------|------------|---------|---------|
| 100 | 3043.50 | -0.74 | 3043.00 | -39.52 |
| 150 | 3039.50 | -1.32 | 3038.50 | -70.08 |
| 200 | 3034.00 | -1.82 | 3033.00 | -96.60 |
| 350 | 3014.00 | -3.23 | 3009.50 | -169.70 |
| 500 | 2989.00 | -4.41 | 2980.50 | -229.65 |
| 750 | 2942.50 | -6.20 | 2925.50 | -317.80 |
| 1100 | 2876.00 | -8.06 | 2847.50 | -403.10 |
| 1650 | 2775.00 | -10.53 | 2728.50 | -507.15 |
| 2450 | 2646.50 | -13.19 | 2577.00 | -603.80 |
| 3650 | 2495.00 | -15.97 | 2398.00 | -686.10 |
| 5450 | 2315.50 | -19.04 | 2189.00 | -755.25 |
| 8150 | 2115.00 | -22.52 | 1953.50 | -809.95 |
| 12150 | 1902.50 | -25.97 | 1710.50 | -833.15 |
| 18150 | 1688.00 | -29.14 | 1474.50 | -822.00 |
| 27050 | 1451.00 | -32.96 | 1218.00 | -789.45 |
| 40350 | 1243.50 | -34.90 | 1019.75 | -710.65 |
| 60250 | 1047.00 | -35.91 | 848.10 | -613.80 |
| 89850 | 874.15 | -37.85 | 689.75 | -535.95 |
| 134100 | 736.80 | -38.38 | 576.70 | -456.70 |
| 200000 | 600.43 | -39.30 | 463.24 | -378.28 |

b) Electrodes: needle electrodes 0.5 mm diameter, 80 mm inter-electrode distance.

| Freq, Hz | Mag, Ohm | Phase, rad | Re, Ohm | Im, Ohm |
|----------|----------|------------|---------|---------|
| 100 | 1072.50 | -0.96 | 1072.50 | -17.97 |
| 150 | 1070.50 | -1.38 | 1070.50 | -25.75 |
| 200 | 1068.50 | -1.77 | 1068.00 | -33.00 |
| 300 | 1063.50 | -2.43 | 1062.50 | -45.14 |
| 450 | 1056.00 | -3.40 | 1054.00 | -62.69 |
| 600 | 1048.50 | -4.27 | 1045.50 | -77.96 |
| 900 | 1032.50 | -5.67 | 1027.50 | -101.95 |
| 1250 | 1015.50 | -7.06 | 1008.00 | -124.90 |
| 1850 | 986.60 | -9.12 | 974.05 | -156.35 |
| 2650 | 952.45 | -11.30 | 933.95 | -186.60 |
| 3800 | 909.20 | -13.83 | 882.85 | -217.35 |
| 5450 | 861.85 | -16.04 | 828.30 | -238.05 |
| 7850 | 804.25 | -19.24 | 759.35 | -265.00 |
| 11300 | 743.80 | -21.83 | 690.45 | -276.55 |
| 16250 | 676.75 | -25.41 | 611.30 | -290.35 |
| 23350 | 605.25 | -28.65 | 531.15 | -290.20 |
| 33600 | 534.60 | -31.49 | 455.90 | -279.20 |
| 48350 | 474.00 | -32.83 | 398.20 | -256.70 |
| 69500 | 405.25 | -37.46 | 321.65 | -246.45 |
| 100000 | 351.45 | -37.42 | 278.98 | -213.12 |

c) Electrodes: needle electrodes 0.5 mm diameter, 60 mm inter-electrode distance.

| Freq, Hz | Mag, Ohm | Phase, rad | Re, Ohm | Im, Ohm |
|----------|----------|------------|---------|---------|
| 100 | 694.55 | -1.05 | 694.40 | -12.78 |
| 150 | 692.85 | -1.55 | 692.65 | -18.80 |
| 200 | 690.95 | -1.88 | 690.55 | -22.65 |
| 300 | 685.55 | -2.46 | 684.90 | -29.44 |
| 450 | 681.50 | -3.57 | 680.15 | -42.45 |
| 600 | 677.65 | -4.50 | 675.55 | -53.16 |
| 900 | 668.05 | -6.08 | 664.30 | -70.76 |
| 1250 | 654.60 | -7.55 | 648.90 | -86.01 |
| 1850 | 635.60 | -9.58 | 626.75 | -105.75 |
| 2650 | 611.05 | -11.77 | 598.15 | -124.65 |
| 3800 | 585.70 | -13.94 | 568.45 | -141.05 |
| 5450 | 549.25 | -16.81 | 525.80 | -158.85 |
| 7850 | 511.35 | -19.73 | 481.30 | -172.65 |
| 11300 | 473.10 | -22.04 | 438.50 | -177.45 |
| 16250 | 432.75 | -24.21 | 394.70 | -177.45 |
| 23350 | 385.50 | -28.17 | 339.80 | -181.95 |
| 33600 | 342.50 | -30.31 | 295.60 | -172.70 |
| 48350 | 299.95 | -32.89 | 251.80 | -162.70 |
| 69500 | 253.55 | -36.37 | 204.15 | -150.35 |
| 100000 | 218.64 | -36.87 | 174.88 | -131.03 |

d) Electrodes: needle electrodes 0.5 mm diameter, 40 mm inter-electrode distance.

| Freq, Hz | Mag, Ohm | Phase, rad | Re, Ohm | Im, Ohm |
|----------|----------|------------|---------|---------|
| 100 | 427.40 | -1.00 | 427.30 | -7.45 |
| 150 | 426.70 | -1.37 | 426.60 | -10.19 |
| 200 | 426.10 | -1.72 | 425.90 | -12.77 |
| 300 | 424.40 | -2.42 | 424.00 | -17.92 |
| 450 | 421.50 | -3.37 | 420.80 | -24.80 |
| 600 | 418.40 | -4.20 | 417.30 | -30.67 |
| 900 | 412.10 | -5.74 | 410.00 | -41.19 |
| 1250 | 404.60 | -7.15 | 401.50 | -50.37 |
| 1850 | 392.50 | -9.13 | 387.50 | -62.28 |
| 2650 | 378.20 | -11.08 | 371.20 | -72.72 |
| 3800 | 361.00 | -13.17 | 351.50 | -82.23 |
| 5450 | 341.00 | -15.32 | 328.90 | -90.08 |
| 7850 | 318.60 | -17.51 | 303.90 | -95.88 |
| 11300 | 294.30 | -19.67 | 277.10 | -99.08 |
| 16250 | 268.70 | -21.57 | 249.90 | -98.82 |
| 23350 | 240.90 | -23.09 | 221.60 | -94.47 |
| 33600 | 213.80 | -24.18 | 195.10 | -87.60 |
| 48350 | 186.80 | -24.02 | 170.60 | -76.04 |
| 69500 | 163.20 | -21.92 | 151.40 | -60.94 |
| 100000 | 137.72 | -16.85 | 131.83 | -39.92 |

1.3. Lungs

Electrodes: 2 mm diameter, inter-electrode distance 60 mm.

| Freq, Hz | Mag, Ohm | Phase, rad | Re, Ohm | Im, Ohm |
|----------|----------|------------|---------|----------|
| 100 | 4093.00 | -1.30 | 4092.00 | -92.59 |
| 150 | 4072.00 | -1.71 | 4070.00 | -121.45 |
| 200 | 4052.50 | -2.05 | 4050.50 | -145.15 |
| 350 | 4004.50 | -2.85 | 3999.50 | -199.10 |
| 500 | 3962.50 | -3.48 | 3954.50 | -240.25 |
| 750 | 3901.50 | -4.31 | 3890.50 | -293.15 |
| 1100 | 3829.50 | -5.23 | 3813.50 | -348.70 |
| 1650 | 3737.50 | -6.18 | 3715.50 | -402.25 |
| 2450 | 3635.50 | -7.09 | 3607.50 | -448.80 |
| 3650 | 3518.50 | -8.35 | 3481.00 | -510.85 |
| 5450 | 3393.00 | -9.38 | 3348.00 | -552.85 |
| 8150 | 3259.50 | -10.82 | 3201.50 | -611.85 |
| 12150 | 3117.00 | -12.61 | 3042.00 | -680.45 |
| 18150 | 2964.00 | -14.44 | 2870.00 | -739.15 |
| 27050 | 2806.50 | -16.66 | 2688.50 | -804.30 |
| 40350 | 2630.50 | -20.24 | 2468.00 | -910.25 |
| 60250 | 2434.50 | -24.17 | 2220.50 | -996.80 |
| 89850 | 2224.00 | -28.21 | 1958.00 | -1052.10 |
| 134100 | 1920.50 | -31.60 | 1633.00 | -1001.10 |
| 200000 | 1658.00 | -45.04 | 1165.42 | -1175.20 |

1.4. Muscle

Electrodes: needle electrodes 0.5 mm diameter, 80 mm inter-electrode distance.

| Freq, Hz | Mag, Ohm | Phase, rad | Re, Ohm | Im, Ohm |
|----------|----------|------------|---------|---------|
| 100 | 882.20 | -3.02 | 881.00 | -46.46 |
| 150 | 871.95 | -3.65 | 870.20 | -55.54 |
| 200 | 863.35 | -4.23 | 860.95 | -63.63 |
| 300 | 848.90 | -5.13 | 845.50 | -75.87 |
| 450 | 830.70 | -6.21 | 825.80 | -89.91 |
| 600 | 816.05 | -7.09 | 809.80 | -100.75 |
| 900 | 793.00 | -8.57 | 784.15 | -118.10 |
| 1250 | 771.10 | -9.96 | 759.55 | -133.35 |
| 1850 | 738.90 | -11.98 | 722.80 | -153.35 |
| 2650 | 703.60 | -14.03 | 682.65 | -170.60 |
| 3800 | 661.95 | -16.18 | 635.75 | -184.40 |
| 5450 | 615.35 | -18.10 | 584.90 | -191.15 |
| 7850 | 563.30 | -20.00 | 529.30 | -192.65 |
| 11300 | 512.85 | -20.80 | 479.40 | -182.05 |
| 16250 | 463.85 | -21.85 | 430.55 | -172.60 |
| 23350 | 419.80 | -21.42 | 390.80 | -153.30 |
| 33600 | 383.70 | -21.00 | 358.25 | -137.50 |
| 48350 | 353.80 | -20.22 | 332.00 | -122.20 |
| 69500 | 322.85 | -19.25 | 304.75 | -106.30 |
| 100000 | 301.45 | -18.15 | 286.34 | -93.91 |

1.5. Fat

Electrodes: 2 mm diameter, inter-electrode distance 60 mm.

| Freq, Hz | Mag, Ohm | Phase, rad | Re, Ohm | Im, Ohm |
|----------|----------|------------|---------|---------|
| 100 | 1137.00 | -0.28 | 1137.00 | -5.52 |
| 150 | 1136.00 | -0.39 | 1136.00 | -7.76 |
| 200 | 1134.50 | -0.50 | 1134.50 | -9.86 |
| 300 | 1132.50 | -0.68 | 1132.50 | -13.44 |
| 450 | 1129.50 | -0.88 | 1129.50 | -17.42 |
| 600 | 1126.50 | -1.06 | 1126.50 | -20.82 |
| 900 | 1120.00 | -1.32 | 1119.50 | -25.75 |
| 1250 | 1112.50 | -1.50 | 1112.50 | -29.07 |
| 1850 | 1103.00 | -1.60 | 1102.50 | -30.89 |
| 2650 | 1093.50 | -1.61 | 1093.50 | -30.76 |
| 3800 | 1084.50 | -1.49 | 1084.50 | -28.24 |
| 5450 | 1077.50 | -1.37 | 1077.00 | -25.74 |
| 7850 | 1071.50 | -1.13 | 1071.50 | -21.07 |
| 11300 | 1067.00 | -1.08 | 1067.00 | -20.19 |
| 16250 | 1063.00 | -0.73 | 1063.00 | -13.47 |
| 23350 | 1060.00 | -0.43 | 1060.00 | -7.95 |
| 33600 | 1056.00 | -0.23 | 1056.00 | -4.26 |
| 48350 | 1055.50 | -0.50 | 1055.50 | -9.21 |
| 69500 | 1043.00 | 0.29 | 1043.00 | 5.23 |
| 100000 | 1016.92 | 0.90 | 1016.50 | 15.91 |

1.6. Tongue

Electrodes: 2 mm diameter, inter-electrode distance 60 mm.

| Freq, Hz | Mag, Ohm | Phase, rad | Re, Ohm | Im, Ohm |
|-----------|----------|------------|---------|---------|
| 100,00 | 391.97 | -0.11 | 391.97 | -0.75 |
| 150,00 | 391.87 | -0.14 | 391.87 | -0.98 |
| 200,00 | 391.80 | -0.18 | 391.77 | -1.24 |
| 350,00 | 391.57 | -0.28 | 391.57 | -1.95 |
| 500,00 | 391.20 | -0.36 | 391.20 | -2.45 |
| 750,00 | 390.70 | -0.49 | 390.70 | -3.36 |
| 1100,00 | 390.07 | -0.61 | 390.03 | -4.16 |
| 1650,00 | 389.27 | -0.79 | 389.27 | -5.34 |
| 2450,00 | 388.33 | -1.00 | 388.23 | -6.81 |
| 3650,00 | 387.00 | -1.31 | 386.90 | -8.88 |
| 5450,00 | 385.43 | -1.66 | 385.30 | -11.17 |
| 8150,00 | 383.67 | -2.07 | 383.40 | -13.83 |
| 12150,00 | 381.33 | -2.89 | 380.83 | -19.19 |
| 18150,00 | 378.27 | -3.27 | 377.67 | -21.56 |
| 27050,00 | 374.47 | -4.97 | 373.03 | -32.43 |
| 40350,00 | 370.00 | -6.51 | 367.53 | -41.97 |
| 60250,00 | 362.00 | -7.60 | 358.77 | -47.84 |
| 89850,00 | 351.90 | -9.71 | 346.70 | -59.29 |
| 134100,00 | 346.07 | -13.30 | 336.60 | -79.29 |
| 200000,00 | 331.44 | -20.13 | 310.09 | -114.56 |

2. Human tissue

2.1. Liver

The measurements were performed on a liver of a male person, 47 years old, forensic autopsy within 24 hrs after death, death after a fall from a roof.

a) Electrodes: 0.5 mm diameter, inter-electrode distance 20 mm.

| Freq, Hz | Mag, Ohm | Phase, rad | Re, Ohm | Im, Ohm |
|----------|----------|------------|---------|---------|
| 100 | 514.70 | -0.73 | 514.60 | -6.55 |
| 150 | 513.70 | -0.99 | 513.60 | -8.91 |
| 200 | 512.30 | -1.23 | 512.20 | -11.02 |
| 300 | 510.60 | -1.70 | 510.40 | -15.12 |
| 450 | 507.90 | -2.30 | 507.50 | -20.35 |
| 600 | 505.30 | -2.83 | 504.70 | -24.95 |
| 900 | 500.50 | -3.80 | 499.40 | -33.17 |
| 1250 | 495.40 | -4.80 | 493.70 | -41.49 |
| 1850 | 487.10 | -6.27 | 484.10 | -53.23 |
| 2650 | 476.70 | -7.87 | 472.20 | -65.25 |
| 3800 | 463.10 | -9.84 | 456.30 | -79.13 |
| 5450 | 446.30 | -11.95 | 436.60 | -92.37 |
| 7850 | 424.60 | -14.54 | 411.00 | -106.60 |
| 11300 | 398.80 | -17.18 | 381.00 | -117.80 |
| 16250 | 367.80 | -20.09 | 345.40 | -126.30 |
| 23350 | 333.00 | -22.43 | 307.80 | -127.10 |
| 33600 | 292.60 | -24.33 | 266.70 | -120.60 |
| 48350 | 256.00 | -25.58 | 230.90 | -110.60 |
| 69500 | 220.90 | -23.77 | 202.20 | -89.04 |
| 100000 | 184.60 | -20.09 | 173.37 | -63.40 |

b) Electrodes: 0.5 mm diameter, inter-electrode distance 80 mm.

| Freq, Hz | Mag, Ohm | Phase, rad | Re, Ohm | Im, Ohm |
|----------|----------|------------|---------|---------|
| 100 | 2269.00 | -0.74 | 2269.00 | -29.18 |
| 150 | 2264.50 | -0.98 | 2264.00 | -38.55 |
| 200 | 2260.00 | -1.27 | 2260.00 | -50.22 |
| 300 | 2252.00 | -1.70 | 2251.00 | -66.65 |
| 450 | 2241.50 | -2.31 | 2239.50 | -90.41 |
| 600 | 2229.50 | -2.74 | 2227.00 | -106.60 |
| 900 | 2208.00 | -3.75 | 2203.00 | -144.55 |
| 1250 | 2188.50 | -4.83 | 2180.50 | -184.30 |
| 1850 | 2156.00 | -6.20 | 2143.00 | -232.90 |
| 2650 | 2114.00 | -7.96 | 2094.00 | -292.65 |
| 3800 | 2056.00 | -10.08 | 2024.50 | -359.95 |
| 5450 | 1984.50 | -12.72 | 1936.00 | -436.85 |
| 7850 | 1903.50 | -14.61 | 1841.50 | -480.10 |
| 11300 | 1785.00 | -18.29 | 1695.00 | -560.25 |
| 16250 | 1654.50 | -22.15 | 1532.50 | -623.85 |
| 23350 | 1498.50 | -26.70 | 1339.00 | -673.20 |
| 33600 | 1336.50 | -31.40 | 1141.00 | -696.35 |
| 48350 | 1150.50 | -34.73 | 945.20 | -655.10 |
| 69500 | 1011.10 | -35.53 | 822.70 | -585.80 |
| 100000 | 860.53 | -36.67 | 689.84 | -512.31 |

2.2. Liver

The measurements were performed on a liver of a female child, 7 months old, 7.4 kg, forensic autopsy within 12 hrs after death, reason of death unclear/suspect of an infection.

a) Electrodes: 0.5 mm diameter, inter-electrode distance 20 mm.

| Freq, Hz | Mag, Ohm | Phase, rad | Re, Ohm | Im, Ohm |
|----------|----------|------------|---------|---------|
| 100 | 83.67 | -0.93 | 83.66 | -1.37 |
| 150 | 83.58 | -0.78 | 83.57 | -1.13 |
| 200 | 83.61 | -0.78 | 83.60 | -1.14 |
| 300 | 83.59 | -0.92 | 83.58 | -1.35 |
| 450 | 83.48 | -1.11 | 83.46 | -1.62 |
| 600 | 83.37 | -1.33 | 83.35 | -1.94 |
| 900 | 83.14 | -1.79 | 83.09 | -2.59 |
| 1250 | 82.85 | -2.31 | 82.78 | -3.33 |
| 1850 | 82.32 | -3.05 | 82.20 | -4.38 |
| 2650 | 81.71 | -3.74 | 81.54 | -5.32 |
| 3800 | 80.76 | -4.71 | 80.49 | -6.63 |
| 5450 | 79.48 | -6.35 | 79.00 | -8.79 |
| 7850 | 77.83 | -7.74 | 77.12 | -10.49 |
| 11300 | 75.97 | -9.17 | 75.00 | -12.11 |
| 16250 | 73.69 | -11.25 | 72.28 | -14.38 |
| 23350 | 69.64 | -15.17 | 67.21 | -18.22 |
| 33600 | 66.00 | -17.60 | 62.90 | -19.94 |
| 48350 | 61.41 | -19.03 | 58.05 | -20.03 |
| 69500 | 55.46 | -22.91 | 51.08 | -21.57 |
| 100000 | 48.27 | -24.27 | 43.98 | -19.80 |

b) Electrodes: 0.5 mm diameter, inter-electrode distance 40 mm.

| Freq, Hz | Mag, Ohm | Phase, rad | Re, Ohm | Im, Ohm |
|----------|----------|------------|---------|---------|
| 100 | 178.77 | -0.72 | 178.77 | -2.25 |
| 150 | 178.67 | -0.69 | 178.67 | -2.14 |
| 200 | 178.60 | -0.79 | 178.57 | -2.46 |
| 300 | 178.50 | -0.88 | 178.47 | -2.73 |
| 450 | 178.20 | -1.20 | 178.13 | -3.72 |
| 600 | 177.80 | -1.43 | 177.73 | -4.44 |
| 900 | 177.13 | -1.92 | 177.03 | -5.94 |
| 1250 | 176.43 | -2.29 | 176.30 | -7.04 |
| 1850 | 175.20 | -3.10 | 175.00 | -9.48 |
| 2650 | 173.73 | -3.96 | 173.33 | -11.98 |
| 3800 | 171.63 | -5.13 | 170.97 | -15.34 |
| 5450 | 169.10 | -6.20 | 168.13 | -18.26 |
| 7850 | 165.77 | -7.95 | 164.20 | -22.92 |
| 11300 | 161.90 | -9.47 | 159.70 | -26.63 |
| 16250 | 155.80 | -12.88 | 151.87 | -34.73 |
| 23350 | 149.53 | -15.07 | 144.37 | -38.87 |
| 33600 | 140.57 | -18.95 | 132.93 | -45.64 |
| 48350 | 128.63 | -21.86 | 119.37 | -47.88 |
| 69500 | 115.67 | -26.18 | 103.80 | -51.03 |
| 100000 | 103.21 | -28.83 | 90.33 | -49.75 |

c) Electrodes: 0.5 mm diameter, inter-electrode distance 60 mm.

| Freq, Hz | Mag, Ohm | Phase, rad | Re, Ohm | Im, Ohm |
|----------|----------|------------|---------|---------|
| 100 | 308.17 | -0.47 | 308.13 | -2.53 |
| 150 | 307.83 | -0.48 | 307.83 | -2.57 |
| 200 | 307.77 | -0.44 | 307.77 | -2.34 |
| 300 | 307.57 | -0.75 | 307.50 | -4.02 |
| 450 | 307.17 | -1.01 | 307.10 | -5.42 |
| 600 | 306.70 | -1.19 | 306.60 | -6.36 |
| 900 | 306.30 | -1.73 | 306.17 | -9.23 |
| 1250 | 305.50 | -2.19 | 305.30 | -11.67 |
| 1850 | 303.07 | -3.12 | 302.67 | -16.51 |
| 2650 | 300.70 | -4.06 | 299.97 | -21.30 |
| 3800 | 296.67 | -5.20 | 295.43 | -26.91 |
| 5450 | 292.30 | -6.44 | 290.47 | -32.78 |
| 7850 | 285.73 | -8.57 | 282.53 | -42.56 |
| 11300 | 278.03 | -10.61 | 273.27 | -51.17 |
| 16250 | 268.97 | -12.25 | 262.83 | -57.07 |
| 23350 | 254.80 | -16.64 | 244.13 | -72.97 |
| 33600 | 239.67 | -20.07 | 225.07 | -82.22 |
| 48350 | 218.87 | -23.75 | 200.27 | -88.05 |
| 69500 | 196.53 | -27.24 | 174.70 | -89.73 |
| 100000 | 174.27 | -30.42 | 150.24 | -88.08 |

d) Electrodes: 0.5 mm diameter, inter-electrode distance 80 mm.

| Freq, Hz | Mag, Ohm | Phase, rad | Re, Ohm | Im, Ohm |
|----------|----------|------------|---------|---------|
| 100 | 505.30 | -0.10 | 505.30 | -0.91 |
| 150 | 504.97 | -0.16 | 504.97 | -1.43 |
| 200 | 505.43 | -0.30 | 505.43 | -2.65 |
| 300 | 505.57 | -0.49 | 505.57 | -4.34 |
| 450 | 505.53 | -0.79 | 505.50 | -7.01 |
| 600 | 505.20 | -1.11 | 505.10 | -9.78 |
| 900 | 504.60 | -1.65 | 504.37 | -14.55 |
| 1250 | 502.63 | -2.35 | 502.17 | -20.60 |
| 1850 | 499.40 | -3.23 | 498.60 | -28.13 |
| 2650 | 495.03 | -4.22 | 493.70 | -36.41 |
| 3800 | 488.83 | -5.35 | 486.70 | -45.54 |
| 5450 | 480.53 | -7.15 | 476.77 | -59.79 |
| 7850 | 469.93 | -8.99 | 464.17 | -73.40 |
| 11300 | 455.87 | -11.31 | 447.03 | -89.39 |
| 16250 | 438.13 | -14.38 | 424.37 | -108.77 |
| 23350 | 416.17 | -16.91 | 398.10 | -121.07 |
| 33600 | 386.13 | -21.26 | 359.83 | -140.03 |
| 48350 | 354.47 | -23.89 | 324.00 | -143.50 |
| 69500 | 314.40 | -27.68 | 278.27 | -145.87 |
| 100000 | 275.34 | -31.79 | 233.88 | -144.77 |

2.3. Muscle

The measurements were performed on a muscle tissue of a male person, 50 years old, forensic autopsy within 24 hrs after death, death after a car accident.

a) Electrodes: 0.5 mm diameter, inter-electrode distance 80 mm.

| Freq, Hz | Mag, Ohm | Phase, rad | Re, Ohm | Im, Ohm |
|----------|----------|------------|---------|---------|
| 100 | 152.40 | -0.13 | 152.40 | -0.35 |
| 150 | 152.23 | -0.44 | 152.23 | -1.18 |
| 200 | 152.10 | -0.67 | 152.07 | -1.78 |
| 300 | 151.53 | -0.98 | 151.47 | -2.59 |
| 450 | 150.70 | -1.28 | 150.63 | -3.36 |
| 600 | 149.93 | -1.43 | 149.90 | -3.75 |
| 900 | 148.90 | -1.59 | 148.87 | -4.14 |
| 1250 | 148.07 | -1.69 | 147.97 | -4.36 |
| 1850 | 147.03 | -1.82 | 147.00 | -4.68 |
| 2650 | 146.27 | -1.99 | 146.17 | -5.09 |
| 3800 | 145.40 | -2.27 | 145.27 | -5.76 |
| 5450 | 144.43 | -2.63 | 144.27 | -6.61 |
| 7850 | 143.27 | -3.23 | 143.07 | -8.07 |
| 11300 | 141.77 | -3.94 | 141.43 | -9.73 |
| 16250 | 139.70 | -4.99 | 139.17 | -12.14 |
| 23350 | 137.13 | -5.76 | 136.47 | -13.76 |
| 33600 | 133.87 | -7.30 | 132.80 | -17.02 |
| 48350 | 130.03 | -7.93 | 128.80 | -17.94 |
| 69500 | 125.20 | -9.85 | 123.33 | -21.42 |
| 100000 | 118.60 | -10.78 | 116.48 | -22.17 |